SUPPLEMENT TO THE FINAL REPORT

SYSTEMS ANALYSIS OF CHEMICALS AND ENERGY RECOVERY IN SULFATE PULPING

PROJECT 2893

SEPTEMBER 15, 1971 - SEPTEMBER 14, 1972

Prepared by

PROJECT STAFF

Graduate Students - Purdue University

Peter M. Chase

Edgar F. Jacobi

Laxmi K. Rastogi

Clifford C. Smith

Staff Member - Institute of Paper Chemistry

Dr. Robert A. Holm

Staff Members - Purdue University

Dr. Antti J. Koivo

Dr. Theodore J. Williams

Report 4

Institute of Paper Chemistry

Report 50

Purdue Laboratory for Applied Industrial Control

Division of Industrial and Environmental Systems

The Institute of Paper Chemistry

Appleton, Wisconsin 54911

Purdue Laboratory for Applied Industrial Control

Schools of Engineering

Purdue University

West Lafayette, Indiana 47907

FOREWORD

This Report serves as a Supplement to the Final Report for the Project Period for Project 2893 of the Institute of Paper Chemistry along with Purdue University entitled, Systems Analysis of Chemicals and Energy Recovery in Sulfate Pulping (Report 3, Institute of Paper Chemistry and Report 45, Purdue Laboratory for Applied Industrial Control, dated September 14, 1971). As such it closes the reporting of research under this Project except for the thesis reports of the Purdue University graduate students involved and any subsequent reports of the Institute concerning the "dynamics and control of brown stock washers."

This Report discusses several important topics on which research had not been completed at the time of the above-mentioned Report. This includes the characteristics of "pure water" washes for Kamyr digesters; the possibility of oscillatory responses for multiple-effect, black-liquor evaporators along with a method for its control; a more complete model and control system for the causticizing and liquor preparation area; and further work on the kiln. This is now complete and reported herein.

We wish again to thank the sixteen sponsoring companies of the project and particularly their representatives who attended our several reporting meetings and who guided our efforts through this extended period of the research.

Robert A. Holm, Director
Division of Industrial and
Environmental Systems
Institute of Paper Chemistry

Theodore J. Williams, Director
Purdue Laboratory for Applied
Industrial Control
Purdue University

TABLE OF CONTENTS

LIST OF TABLES

LIST OF FIGURES

CONCLUSIONS

As stated in the FOREWORD, the present report supplements and completes the work of the Final Report for the Project Period of Project 2893 of the Institute of Paper Chemistry entitled, Systems Analysis of Chemicals and Energy Recovery in Sulfate Pulping. This work was carried out jointly by the Institute and by Purdue University. The results reported here thus are added to those already recorded and do not change any of those already presented in other ways.

The present work has developed the following additional conclusions and results:

1. A mechanism has been postulated to explain the oscillations which occur on some multiple-effect, black-liquor evaporators. It is based on the very large changes in fluid viscosity and hence heat transfer coefficients which occur in such systems due to temperature and composition variations.

2. A feedback control loop included in the control system for multiple-effect evaporators proposed in the earlier report has been shown to correct for the oscillations when they occur.

3. The mathematical model for the causticizing and liquor preparation section begun in the previous reporting period has been completed, and the necessary control system for it has been devised.

4. The use of clean water as a washing fluid in the Kamyr digester has shown in simulation its capability to reduce chemical

loss and decrease evaporator load at the same time. The details of method and gains are presented in the text.

As previously, these results have been obtained from computer simulations based on data obtained from the several plants of the project sponsors. As stated earlier, this work would benefit greatly by being carried out on data from a single complete mill. Only in this latter way can the exact total dollar savings possible from the proposals developed by this research program be evaluated.

SECTION I

INTRODUCTION

Project 2893, Systems Analysis of Chemicals and Energy Recovery in Sulfate Pulping, was developed by the Division of Industrial and Environmental Systems of the Institute of Paper Chemistry and the Purdue Laboratory for Applied Industrial Control of Purdue University during the winter of 1968-69. It was funded by sixteen of the nation's major paper companies during the summer of 1969. The work of the project has been mainly carried out by the graduate student staff of the Purdue Laboratory under the direction of the Laboratory's professorial staff with the help of several of the technical staff of the Institute. The students' work is recorded in this Report and its preceding companion volume, the Final Report for the Project Period, dated September 14, 1972.

Work on this project which was carried out by the Institute staff on their premises has been reported in separate Institute reports. These have been concerned mainly with the brown stock washers.

The work of each of the Purdue students has or will culminate in the preparation of his graduate thesis. These are published as separate reports by the Purdue Laboratory for Applied Industrial Control and distributed to the program-sponsoring companies. The present reports present all of the important findings of the research. The individual reports will present more details of these, plus the pertinent computer programs involved, etc.

SECTION II

A DYNAMIC MATHEMATICAL MODEL OF THE WASH ZONE OF THE KAMYR DIGESTER AND THE EFFECT OF A CLEAN WATER WASH

COUNTERCURRENT DIFFUSION WASHING

Washing (the separation of dissolved solids from the cooked chips), by means of a flow of relatively solids-free liquor countercurrent to the descending pulped chip mass in a Kamyr digester, has become an increasingly popular industrial practice. It is the purpose of this Section to provide an adequate mathematical description of the phenomena associated with this process for the purpose of aiding its automatic control, optimization, and design.

This manner of washing is often referred to as "diffusion washing" in that it is supposed that the dissolved solids contained in the liquid associated with the pulp (that which is within the fiber itself) diffuses to the free-flowing countercurrent liquor of lower solids concentration. Fick's second law of diffusion describes this type of mass transport and analyses and experiments have been carried out to elucidate the form and parameters of such a solution [1,2]. However, such a description, although phenomenologically quite plausible, is mathematically difficult to solve analytically or to compute by digital means except for the linear dynamic or the steady state cases. This is because of the introduction of the spatial variable of chip dimension and the resulting partial differential equations present.

A simpler, yet analgous description, is proposed here which eliminates the chip dimension as a variable and thus has the advantage of being computable in both the non-linear and dynamic form.

THE PROPOSED MODEL

In the diffusion model the driving force for mass transfer is the second spatial derivative of concentration. This has boundary conditions requiring the concentration at the maximum chip dimension to be equal to that of the free liquor volume. In the spatial dimension of wash zone length, a two point boundary condition is placed on: (1) the entering chip liquor concentration at z = 0; and (2) the entering wash liquor concentration at z = L. By mass balance the remainder of the description is evolved (see Figure 1).

The proposed model replaces the second spatial derivative of concentration as a driving force within the chip with a single difference between average concentration within the chip and that in the free liquor. When combined with the required mass balance and input boundary conditions, this description can be written as follows:

$$\frac{V_d}{L}\frac{\partial x_d}{\partial t} + v_d \frac{\partial x_d}{\partial z} = -\frac{kA}{L}(x_d - x_u) \qquad (1)$$

$$\frac{V_u}{L}\frac{\partial x_u}{\partial t} + v_u \frac{\partial x_u}{\partial z} = -\frac{kA}{L}(x_d - x_u) \qquad (2)$$

given $x_d(0)$ and $x_u(L)$

where

$x_d(z,t)$ = entrapped downflow dissolved solids concentration, lbs/ft^3

$x_u(z,t)$ = free upflow dissolved solids concentration, lbs/ft^3

v_d = entrapped downflow liquid flow rate, ft^3/hr

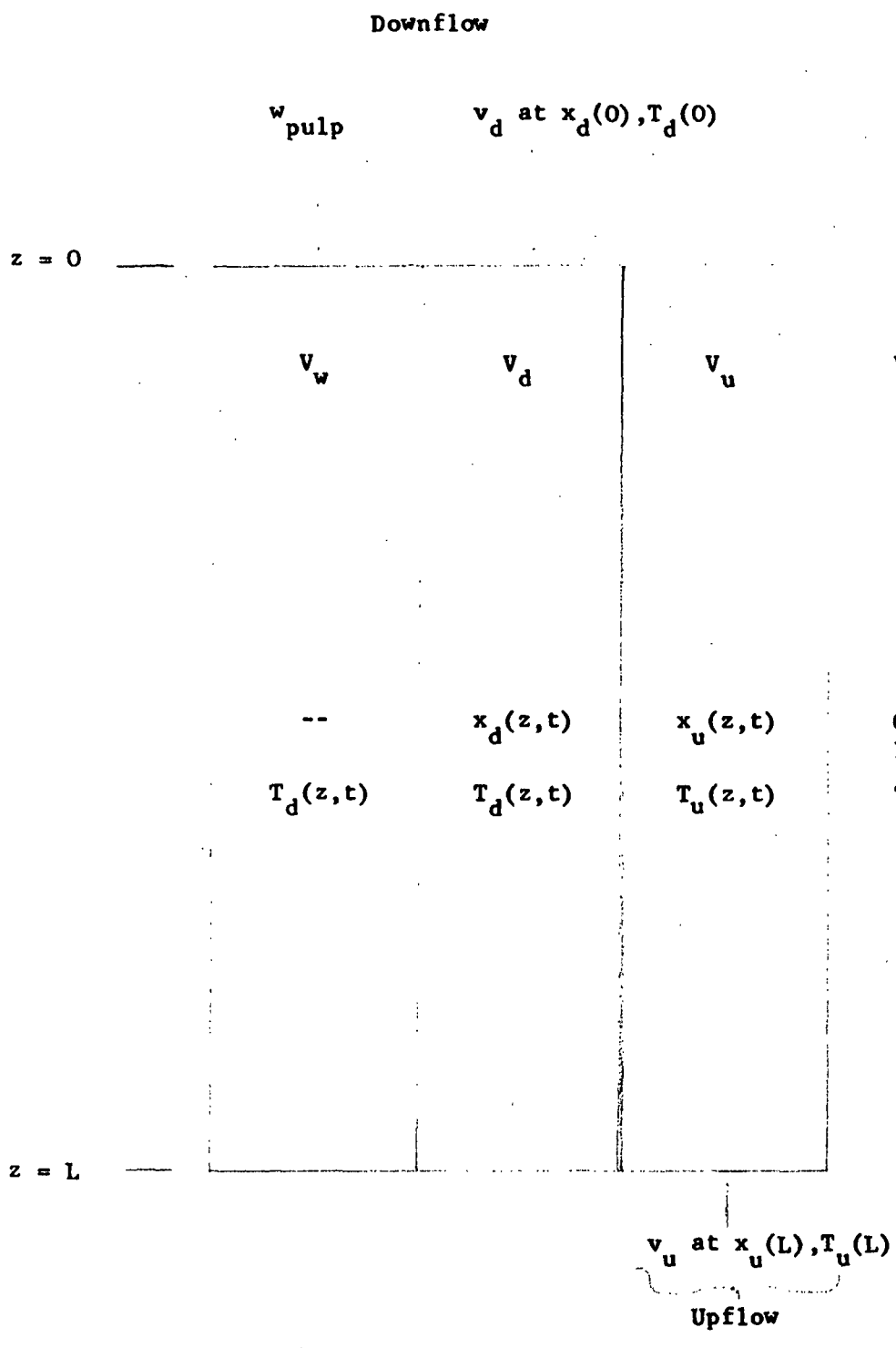

FIGURE 1

DISTRIBUTED MODEL OF WASH ZONE

v_u = free upflow liquid flow rate, ft^3/hr

V_d = total entrapped liquid volume, ft^3

V_u = total free liquid volume, ft^3

k = mass transfer coefficient, $\frac{lbs}{hr(lb/ft^3)ft^2}$

A = mass transfer area, ft^2

L = length of wash zone, ft

For computation purposes Equations (1) and (2) can be discretized to a series of lumped sections (see Figure 2).

For n sections the equations are as follows,

$$\frac{dx_{d_i}}{dt} = -\frac{kA}{V_d}(x_{d_i}-x_{u_i}) - \frac{v_d}{V_d/n}(x_{d_{i-1}}-x_{d_i}) \qquad i = 1,2,\ldots,n \qquad (3)$$

$$\frac{dx_{u_i}}{dt} = -\frac{kA}{V_u}(x_{d_i}-x_{u_i}) - \frac{v_u}{V_u/n}(x_{u_{i+1}}-x_{u_i}) \qquad i = 1,2,\ldots,n \qquad (4)$$

where $x_{d_0} = x_d(0)$

$x_{u_{n+1}} = x_u(L)$

The energy balance between the two flows can also be described by energy diffusion.

Taking the same approach as in the mass transfer case to obtain the distributed equations,

$$\frac{\rho_d V_d c_{p_d}}{L}\frac{\partial T_d}{\partial t} + \rho_d v_d c_{p_d}\frac{\partial T_d}{\partial z} = -\frac{k_e A_e}{L}(T_d-T_u) \qquad (5)$$

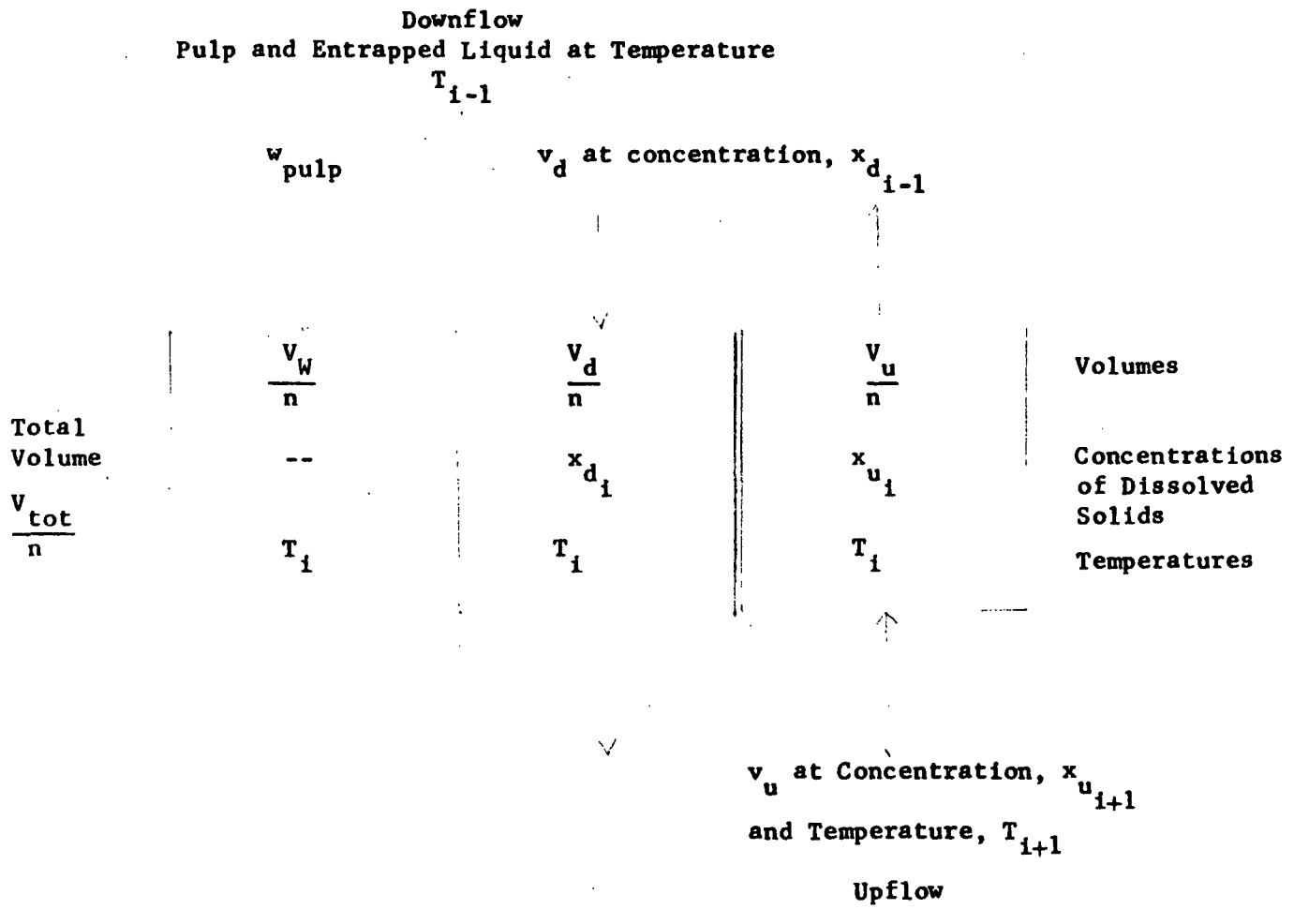

FIGURE 2

I^{TH} ELEMENT OF DISCRETIZED MODEL

$$\frac{\rho_u V_u c_{p_u}}{L}\frac{\partial T_u}{\partial t} + \rho_u v_u c_{p_u}\frac{\partial T_u}{\partial z} = -\frac{k_e A_e}{L}(T_d - T_u) \qquad (6)$$

given $T_d(0)$ and $T_u(L)$ as boundary conditions, and

where

$T_d(z,t)$ = temperature of combined pulp and entrapped liquid, ^oF

$T_u(z,t)$ = temperature of upflow liquid, ^oF

$\rho_d c_{p_d}$ = heat capacity of combined downflow, $\frac{BTU}{ft^3\ ^oF}$

$\rho_u c_{p_u}$ = heat capacity of upflow, $\frac{BTU}{ft^3\ ^oF}$

k_e = heat transfer coefficient, $\frac{BTU}{hr\ ^oF\ ft^2}$

A_e = heat transfer area, ft^2

If it is assumed that there will be negligible temperature differences between liquid and pulp within a section ($k_e A_e$ is very high relative to energy capacity flow), a discretized energy balance can be written as follows

$$\frac{dT_i}{dt} = \frac{\left[\rho_\ell c_{p_\ell} v_d + (x_{d_{i-1}} v_d + w_{pulp}) c_{p_w}\right] T_{i-1} + (\rho_\ell c_{p_\ell} + x_{u_{i+1}} c_{p_w}) v_u T_{i+1}}{\rho_\ell c_{p_\ell}\frac{(V_u+V_d)}{n} + (x_{d_i}\frac{V_d}{n} + x_{u_i}\frac{V_u}{n} + \frac{W_{pulp}}{n})\, c_{p_w}}$$

$$i = 1,2,\ldots,n \qquad (7)$$

where

$T_0 = T_d(0)$

$T_{n+1} = T_u(L)$

and

ρ_ℓ = density of liquid, lbs/ft^3

c_{p_ℓ} = heat capacity of liquid, $\frac{BTU}{lb\ ^oF}$

w_{pulp} = pulp mass flow rate, lbs/hr

W_{pulp} = total pulp mass in wash zone, lbs

c_{p_w} = heat capacity of pulp and dissolved solids, $\frac{BTU}{lb\ ^oF}$

To provide a more comprehensive description and to provide a better means of validation against actual digester operation and design data, the model was expanded to include the quench zone. This was done by letting the first lumped section have not only free liquor inputs from the countercurrent upflow, but also cocurrent downflow at the same temperature and concentration conditions as the entrapped downflow (see Figure 3).

The equations for this new section replacing Equations 4 and 7 (for i = 1) are as follows:

$$\frac{dx_{u_1}}{dt} = -\frac{kA}{V_u}(x_{d_1}-x_{u_1}) - \frac{v_u}{V_{u/n}}(x_{u_2}-x_{u_1}) + \frac{(v_{tot}-v_d)}{V_{u/n}}(x_{d_0}-x_{u_1}) \tag{8}$$

$$\frac{dT_1}{dt} = \frac{[\rho_\ell c_{p_\ell} v_{tot} + (x_{d_0} v_{tot} + w_{pulp}) c_{p_w}]\, T_0 + (\rho_\ell c_{p_\ell} + x_{u_2} c_{p_w}) v_u T_2}{\rho_\ell c_{p_\ell} \frac{(V_u+V_d)}{n} + (x_{d_1}\frac{V_d}{n} + x_{u_1}\frac{V_u}{n} + \frac{W_{pulp}}{n})} \tag{9}$$

where, v_{tot} = total liquid volumetric feed rate to digester top, ft^3/hr.

The extraction per cent solids (before flashing) is given by the relation:

$$x_{ext} = \frac{x_{u_1}}{x_{u_1}+\rho_\ell} \tag{10}$$

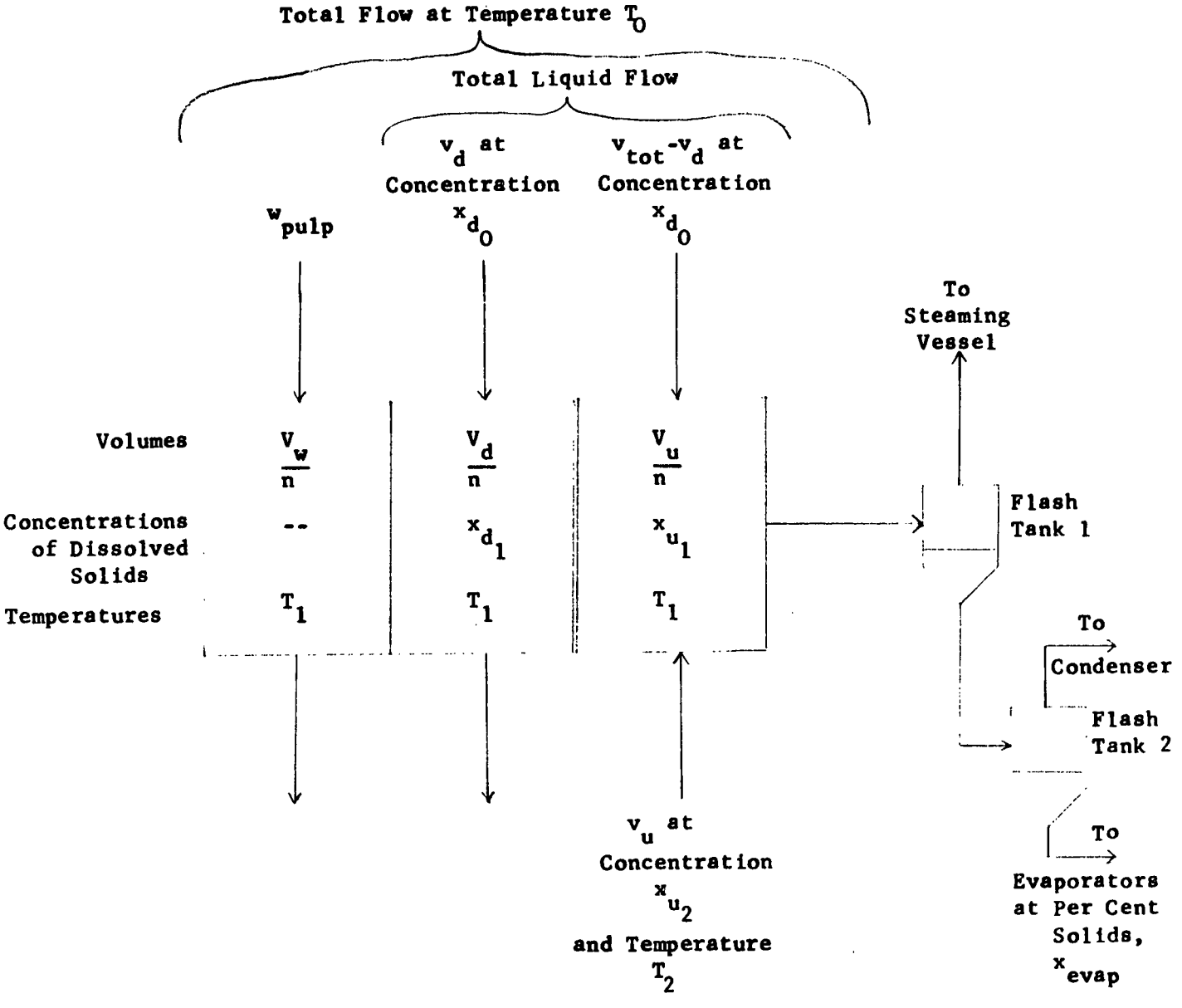

FIGURE 3

QUENCH ZONE ELEMENT OF DISCRETIZED MODEL

The flashing of the extraction flow first to the steaming vessel conditions and then finally to atmospheric conditions for feeding to the evaporators is given by the relationships;

$$x_{flash_1} = \frac{x_{ext}}{1 - \left[c_{p_w} x_{ext} + c_{p_\ell}(1-x_{ext})\right](T_1 - T_{sv})/H_{vap_{sv}}} \tag{11}$$

$$x_{evap} = \frac{x_{flash_1}}{1 - \left[c_{p_w} x_{flash_1} + c_{p_\ell}(1-x_{flash_1})\right](T_{sv} - 212)/969.7} \tag{12}$$

The total amount of solids per air dry ton of pulp as existing in the blow flow is calculated from the downflow exiting conditions, the given composition of the filtrate, and the blow line consistency as:

$$x_{S/ADT} = \frac{\left[w_{blwliq} - v_d(x_{d_n} + \rho_\ell)\right]x_{fil} + v_d x_{d_n}}{1.1\, w_{pulp}/2000} \tag{13}$$

where

w_{blwliq} = $(\frac{1.1}{c_{bl}} - 1)w_{pulp}$, blow liquor mass flow, lbs/hr

x_{fil} = solids content of filtrate, %/100

c_{bl} = consistency of pulp in blow line, $\frac{\text{lbs AD pulp}}{\text{lb flow}}$

where $H_{vap_{sv}}$ = heat of vaporization of steam at steaming vessel conditions, BTU/lb.

CALCULATION OF PARAMETERS

To estimate the mass of pulp that is contained in the washing zone, one can use the equation:

$$W_{pulp} = w^*_{pulp}\, t^*_R \tag{14}$$

where

w_{pulp} = pulp flow rate, lbs/hr

t_R = residence time, hr

and * denotes that the measurement of the variable was made under steady state conditions and will be referred to as the reference case.

It will be assumed that, in general, this mass will not change appreciably for any reason during the period of observation.

$$w^*_{pulp} = 60 \cdot V_{cm} \cdot S^*_{cm} \rho^*_{bd} Y^* \tag{15}$$

where

V_{cm} = chip meter volume, ft^3/revolution

S_{cm} = chip meter speed, RPM

ρ_{bd} = chip bulk density, $\frac{\text{lbs ODW}}{ft^3}$

Y = yield, %/100

Define the compaction factor, k_c, as

$$k_c = \frac{60 \cdot V_{cm} \cdot S^*_{cm} \cdot t^*_R}{V_{tot}} \tag{16}$$

This can be interpreted as the number of cubic feet needed to be fed to fill a cubic foot within the digester.

The volume occupied by pulp substance only is

$$V_W = \frac{W_{pulp}}{\rho_{ws}} \tag{17}$$

where

ρ_{ws} = density of pure wood pulp substance, lbs/ft^3

The entrapped volume of liquid can be calculated from a knowledge of the specific volume of water swollen pulp, $\frac{1}{\rho_w}$, and the specific volume of pure wood pulp substance, $\frac{1}{\rho_{ws}}$, as:

$$V_d = \left(\frac{1}{\rho_w} - \frac{1}{\rho_{ws}}\right) W_{pulp} \tag{18}$$

Let this volume of entrapped liquid be defined as the crictical moisture of pulp, m_{crit}, where:

$$m_{crit} = \frac{\rho_\ell \left(\frac{1}{\rho_w} - \frac{1}{\rho_{ws}}\right)}{1 + \rho_\ell \left(\frac{1}{\rho_w} - \frac{1}{\rho_{ws}}\right)} \tag{19}$$

also

$$\frac{1}{\rho_w} - \frac{1}{\rho_{ws}} = \frac{m_{crit}}{(1-m_{crit})} \frac{1}{\rho_\ell}$$

Thus, in terms of m_{crit}

$$V_d = \frac{m_{crit}}{(1-m_{crit})\rho_\ell} W_{pulp} \tag{20}$$

The remaining volume is thus the free or void volume,

$$V_u = V_{tot} - V_W - V_d \tag{21}$$

Flow rates, in terms of pulp flow rate, can be calculated as follows:

$$v_d = \left(\frac{1}{\rho_w} - \frac{1}{\rho_{ws}}\right) w_{pulp} \tag{22}$$

or

$$v_d = \left[\frac{m_{crit}}{\rho_\ell(1-m_{crit})}\right] w_{pulp} \tag{23}$$

and

$$v_u = v_d + \frac{\mathcal{D}_f\, w_{pulp}}{\rho_\ell} \tag{24}$$

where

$\mathcal{D}_f$ = dilution factor, $\frac{\text{lbs dilution of weak black liquor}}{\text{lb bone dry pulp}}$

Note: $v_u \geq 0$ for $\mathcal{D}_f \geq 0$.

In the steady state, Equations (1) and (2) are written

$$\frac{\partial x_d}{\partial z} = \frac{k'}{v_d}(x_d - x_u) \tag{25}$$

$$\frac{\partial x_u}{\partial z} = \frac{k'}{v_u}(x_d - x_u) \tag{26}$$

given

$$x_d(0) = x_{d_0} \text{ and } x_u(L) = x_{u_L}$$

where

$$k' = \frac{kA}{L}$$

Let

$$\Delta x = x_d - x_u$$

and

$$\alpha = k'\left(\frac{1}{v_d} - \frac{1}{v_u}\right)$$

Then

$$\frac{\partial}{\partial z}\Delta x = -\alpha\Delta x \tag{27}$$

and assuming k to be a constant

$$\Delta x(z) = [x_{d_0} - x_u(0)]\, e^{-\alpha z} \tag{28}$$

with $x_u(0)$ as yet unknown.

By conservation of mass

$$\int_0^L k'\Delta x\, dz = -v_u[x_{u_L} - x_u(0)] \tag{29}$$

Substituting from Equation 28 and integrating gives

$$\frac{k'[x_{d_o} - x_u(0)]}{\alpha}(1-e^{-\alpha L}) = -v_u[x_{u_L} - x_u(0)] \tag{30}$$

or

$$x_u(0) = \frac{\frac{k' x_{d_0}(1-e^{-\alpha L})}{\alpha} + v_u x_{u_L}}{\frac{k'(1-e^{-\alpha L})}{\alpha} + v_u} \tag{31}$$

Simplifying the above

$$x_u(0) = \frac{\beta x_{d_o} + x_{u_L}}{\beta+1} = x_{d_0} - \frac{x_{d_0} - x_{u_L}}{\beta+1} \tag{32}$$

where

$$\beta = \frac{1-e^{-\alpha L}}{\frac{v_u}{v_d} - 1}$$

Then substituting Equation 32 into 28

$$\Delta x(z) = \left[\frac{x_{d_0} - x_{u_L}}{\beta+1}\right] e^{-\alpha z} \tag{33}$$

Again by conservation of mass

$$x_d(z) = x_{d_0} - \frac{1}{v_d} \int_0^z k' \Delta x(\eta) d\eta \tag{34}$$

where η is the dummy integration variable.

Integrating and simplifying again

$$\frac{x_d(z)}{x_{d_0}} = 1 - \frac{(1 - \frac{x_{u_L}}{x_{d_0}})\ (1-e^{-\alpha z})}{1 - \frac{v_d}{v_u} e^{-\alpha L}} \tag{35}$$

From Equation 35, if $v_u \gg v_d$ and $x_{u_L} = 0$,

then

$$\frac{x_d(z)}{x_{d_0}} \approx e^{-\alpha z} \tag{36}$$

And since, $\alpha = k'(\frac{1}{v_d} - \frac{1}{v_u})$,

$$\frac{x_d(z)}{x_{d_0}} \approx e^{-\frac{k'}{v_d} z} \tag{37}$$

The same special case, i.e., ($v_u \gg v_d$, and $x_{u_L} = 0$), has been solved for the diffusion model [2].

$$\frac{x_d(z)}{x_{d_0}} = \frac{8}{\pi^2} \sum_{n=1}^{\infty} \frac{1}{(2n-1)^2} \exp\left[-(2n-1)^2 \pi^2 \frac{\mathscr{D}}{L_c^2} t\right] \tag{38}$$

where

L_c = chip thickness, ft

$\mathscr{D}$ = diffusion coefficient, $\frac{ft^2}{hr}$

For values of $\frac{\mathscr{D}}{L^2} t$ sufficiently large (say > 0.1), Equation 38 reduces to

$$\frac{x_d(t)}{x_{d_0}} \approx \frac{8}{\pi^2} e^{-\frac{\pi^2 \mathscr{D}}{L_c^2} t} \tag{39}$$

By making the observation that

$$z = \frac{v_d L}{V_d} t, \text{ and } k' = \frac{kA}{L}$$

Equation 37 becomes

$$\frac{x_d(t)}{x_{d_0}} = e^{-\frac{kA}{V_d} t} \tag{40}$$

with the obvious time constant association of

$$\frac{kA}{V_d} = \frac{\pi^2 \mathscr{D}}{L_c^2} \tag{41}$$

An effort was made to calculate the mass transfer coefficient by a means other than that of an equivalence to the diffusion model. An analysis was made of the temperature dependence of mass transfer coefficients. From [6] the mass transfer coefficient is given by

$$k = j_D \, v/S_c^{1.5} \tag{42}$$

where

j_D - Colburn "j factor"

S_c = Schmidt number

v = linear velocity of flow

The Schmidt number has the form

$$S_c = \frac{\mu}{\rho \mathcal{D}} \tag{43}$$

where

μ = viscosity

ρ = density

$\mathcal{D}$ = diffusivity

and $\mathcal{D}$ and μ will both vary with temperature.

Using the expression

$$\frac{\mathcal{D}_1}{\mathcal{D}_2} = \frac{T_1}{T_2} \frac{\mu_2}{\mu_1}$$

or

$$\mathcal{D}_2 = \frac{T_2 \mu_1 \mathcal{D}_1}{T_1 \mu_2} \tag{44}$$

where $T_{1,2}$ are temperatures in ^{o}K.

The temperature dependence of, k, can be calculated from tabular values of μ, $\mathcal{L}$, ρ, etc. (See Table I and Figure 4.)

This temperature dependence was approximated by piecewise linear segments and was used in the simulation. It will be noted that the temperature dependence of the mass transfer coefficient is strong. It will be noted that in the case of the diffusion model the dependence is exponential.

TABLE I

VALUES USED TO ESTABLISH TEMPERATURE

DEPENDENCE OF MASS TRANSFER COEFFICIENT

j_D = 0.012

v = 300 ft/hr

T_1 = 293°K

μ_1 = 1.005 centipoise

$\mathcal{D}_1$ = 5.84×10^{-5} $\frac{ft^2}{hr}$

k	T(°F)	μ, viscosity, $\frac{lbs\ sec}{ft^2}$	Specific gravity, S.G.
1.74×10^{-3}	100	142.0	0.993
0.335×10^{-2}	150	89.1	0.980
0.835×10^{-2}	200	67.7	0.962
0.259×10^{-1}	250	47.6	0.940
0.537×10^{-1}	300	38.2	0.919
0.975×10^{-1}	350	31.8	0.890

$$k = \frac{j_D v}{S_c^{1.5}}, \quad \frac{lb}{hr\ lb/ft^3\ ft^2}$$

where $S_c = \frac{(2.39)(0.00479)\mu}{(62.4)(SG)(\mathcal{D})}$

where $\mathcal{D} = T_k \mu_1 \mathcal{D}_1 / [T_1 (0.00479) \mu]$

where $T_k = [(T-32)/1.8] + 273$

Note: Values are taken from [6].

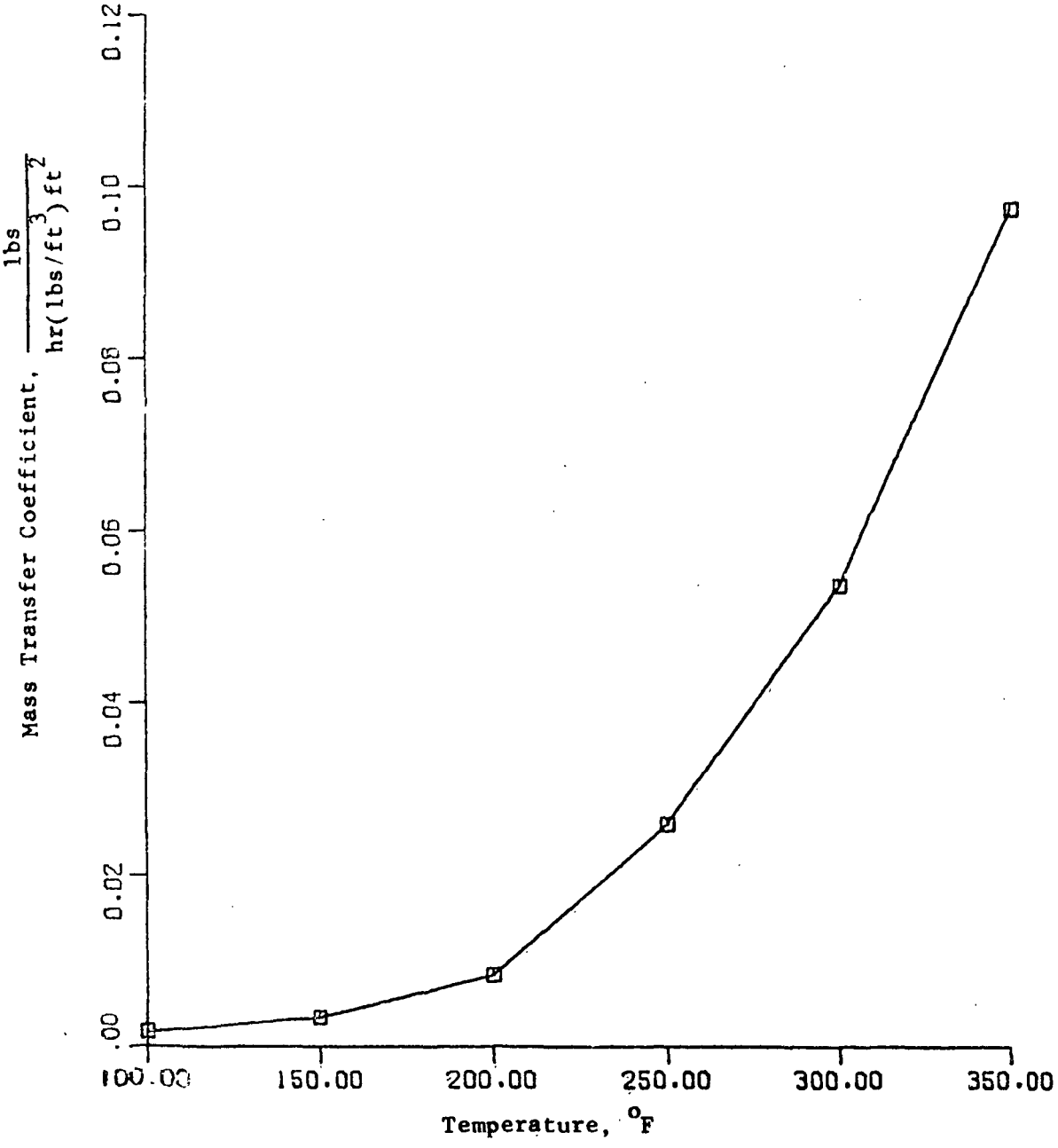

FIGURE 4

TEMPERATURE DEPENDENCE OF MASS TRANSFER COEFFICIENT

SIMULATION PARAMETERS

Two digesters, one at each of two different reference production rates, were studied with the simulation used in this study. Johnsson [5] also provided data on washing in the steady state for two different production rates. A typical modern digester was also simulated in our study. The values used are summarized in Table II.

TABLE II

PARAMETERS USED IN SIMULATIONS

Variable	Description	Units	Johnsson Low Production Case	Johnsson High Production Case	Typical Modern Digester
A	Mass Transfer Area	ft^2	20(6615)	20(6350)	20(43504)
c_{bl}	Consistency on Blow Line	---	0.1	0.1	0.1
c_{p_ℓ}	Heat Capacity of Liquid	$\frac{BTU}{lb\ ^oF}$	1.0	1.0	1.0
c_{p_w}	Heat Capacity of Wood and Solids	$\frac{BTU}{lb\ ^oF}$	0.35	0.35	0.35
f	Dilution Factor	lbs dilution/ lb bd pulp	2.62	2.04	3.3
k	Mass Transfer Coefficient	$\frac{lbs}{hr(\frac{lb}{ft^3})\ ft^2}$	---	---	---
k_c	Compaction Factor	---	2.5	2.5	2.22
L	Wash Zone Length	ft	49.2	49.2	76.4
m_{crit}	Critical Moisture	%/100	0.65	0.65	0.65
n	Number of Discretized Sections	---	20	20	20
t_R^*	Residence Time	hr	2.08	1.33	4.22
S_w	Specific Surface of Wood Chip	ft^2/ft^3	47.25	47.25	47.25
$H_{vap_{sv}}$	Heat of Vaporization of Steam at T_{sv}	BTU/lb	941	941	941

TABLE II (Continued)

Variable	Description	Units	Johnsson Low Production Case	Johnsson High Production Case	Typical Modern Digester
T_i	Temperature of i^{th} Section	^oF	---	---	---
T_{sv}	Steaming Vessel Temperature	^oF	255	255	255
T_{d_0}	Temperature at End of Cook Zone	^oF	338	338	338.9
T_{u_L}	Temperature of Wash Liquor	^oF	266	266	265
v_d	Entrapped Liquid Volume Flow Rate	ft^3/hr	739.2	1108.8	2486
v_u	Countercurrent Liquid Flow Rate	ft^3/hr	1782	2327	6501
v_{tot}	Total Liquid Feed to Digester Top	ft^3/hr	2027.5	3122.8	8360
V_d	Entrapped Volume in Zone	ft^3	20(77)	20(73.9)	20(524.5)
V_u	Free Volume in Zone	ft^3	20(43.3)	20(57.4)	20(494.9)
V_{tot}	Total Volume of Zone	ft^3	2913	2913	23844
V_{pulp}	Volume Occupied by Pulp	ft^3	20(25.4)	20(24.4)	20(172.7)
w_{pulp}	Pulp Flow Rate	lbs/hr	24837	37256	83520
w^*_{pulp}	Reference Pulp Flow Rate	lbs/hr	24837	37256	83520
W_{pulp}	Mass of Pulp in Zone	lbs	20(2587.2)	20(2484.7)	20(17623)
x_{d_0}	Solids Concentration at End of Cook	lbs/ft^3	13.7	13.6	11.2
x_{u_L}	Solids Concentration of Wash Filtrate	lbs/ft^3	1.2	1.99	0.0

TABLE II (Continued)

Variable	Description	Units	Johnsson Low Production Case	Johnsson High Production Case	Typical Modern Digester
x_{u_i}	Entrapped Solids Concentration in i^{th} Sect.	lbs/ft^3	---	---	---
x_{d_i}	Free Solids Concentration in i^{th} Section	lbs/ft^3	---	---	---
Y^*	Yield	%/100	0.56	0.56	0.58
ρ_ℓ	Density of Liquid	lbs/ft^3	62.4	62.4	62.4
ρ_w	Density of Swollen Pulp	lbs/ft^3	25.4	25.4	25.4
ρ_{ws}	Density of Pure Wood Substance	lbs/ft^3	104	104	104
ρ_{log}	Density of Log	lbs/ft^3	33	33	33

Note 1: Volume of Johnsson's wash zone was estimated from his data on residence time.

Note 2: Value for ρ_{ws} is taken from [3].

Note 3: Value for m_{crit} is taken from [4].

SIMULATION RESULTS

Equations 5 and 6 show a temperature difference between upflow and downflow masses which forms the driving force for energy transfer between the flows. An attempt was made to validate the assumption that there was a negligible temperature difference between the flows at any given position by simulating the discretized equivalent to Equations 5 and 6 with estimates of k_e and A_e.

A_e was estimated by taking the specific surface of a 1/2" x 1" x 1/8" chip (S_w = 354 ft^2/ft^3) and multiplying by the estimated volume of wood (in chip form) contained in the zone. That latter volume is estimated by taking the oven dry wood equivalent of the pulp in the zone and dividing by the density of wood as a log, i.e.,

$$V_{chip} = \frac{k_c \rho_{bd} V_{tot}}{\rho_{log}} \tag{45}$$

Hence

$$A_e = S_w V_{chip} \tag{46}$$

For values of

k_c = 2.66

ρ_{bd} = 11.4 lbs/ft^3

ρ_{log} = 33 lbs/ft^3

V_{tot} = 19070 ft^3

and

A_e = 6.2 x 10^6 ft^2

Even for $k_e = 10 \frac{BTU}{hr\ ^oF\ ft^2}$ (a ridiculously low value), temperature differences of no more than 2^oF could be generated. It was, therefore, concluded that s single temperature would suffice, and hence Equation 7 would provide a suitable description of the temperature profile in the wash zone.

With the model form thus complete, both the high and low production cases of Johnsson were run to establish the necessary mass transfer area to fit his measured data. A summary of those runs are given in Table III. Concentration and temperature profiles are shown in Figures 5 and 6..

By comparing the mass transfer coefficient and the mass transfer area product which were found by fitting Johnsson's data [5] with the mass transfer coefficient as derived and the product given by the time constant association of Equation 41, it was found that they were in reasonable agreement.

After establishing the mass transfer area, a number of combinations of dilution factors, wash temperatures, and filtrate solids content were tried to determine the sensitivity of the blow line solids to each of these parameters. The results of these simulations are summarized in Table IV and shown graphically in Figure 7.

A typical modern digester has a much larger wash zone than that studied by Johnsson [5] with a correspondingly longer residence time. Such a typical modern digester was studied for the clean water wash case. Various dilution factors were tried. The results are summarized in Table V and shown graphically in Figure 8. Concentration and temperature profiles for $D_f = 3.3$ and $D_f = 0.5$ are shown in Figures 9 and 10.

TABLE III

FIT OF JOHNSSON'S [5] HIGH AND LOW PRODUCTION DATA

	Concentration within Chips at End of Wash (lbs/ft^3)	Extraction Solids(%)
Low Production Case		
Johnsson's Data	1.93	14.4
Model Calculation (S_w = 47.25)	1.55	14.5
Model Calculation (S_w = 32.5)	1.93	---
High Production Case		
Johnsson's Data	2.56	15.9
Model Calculation (S_w = 47.25)	2.96	15.5
Model Calculation (S_w = 61)	2.56	---

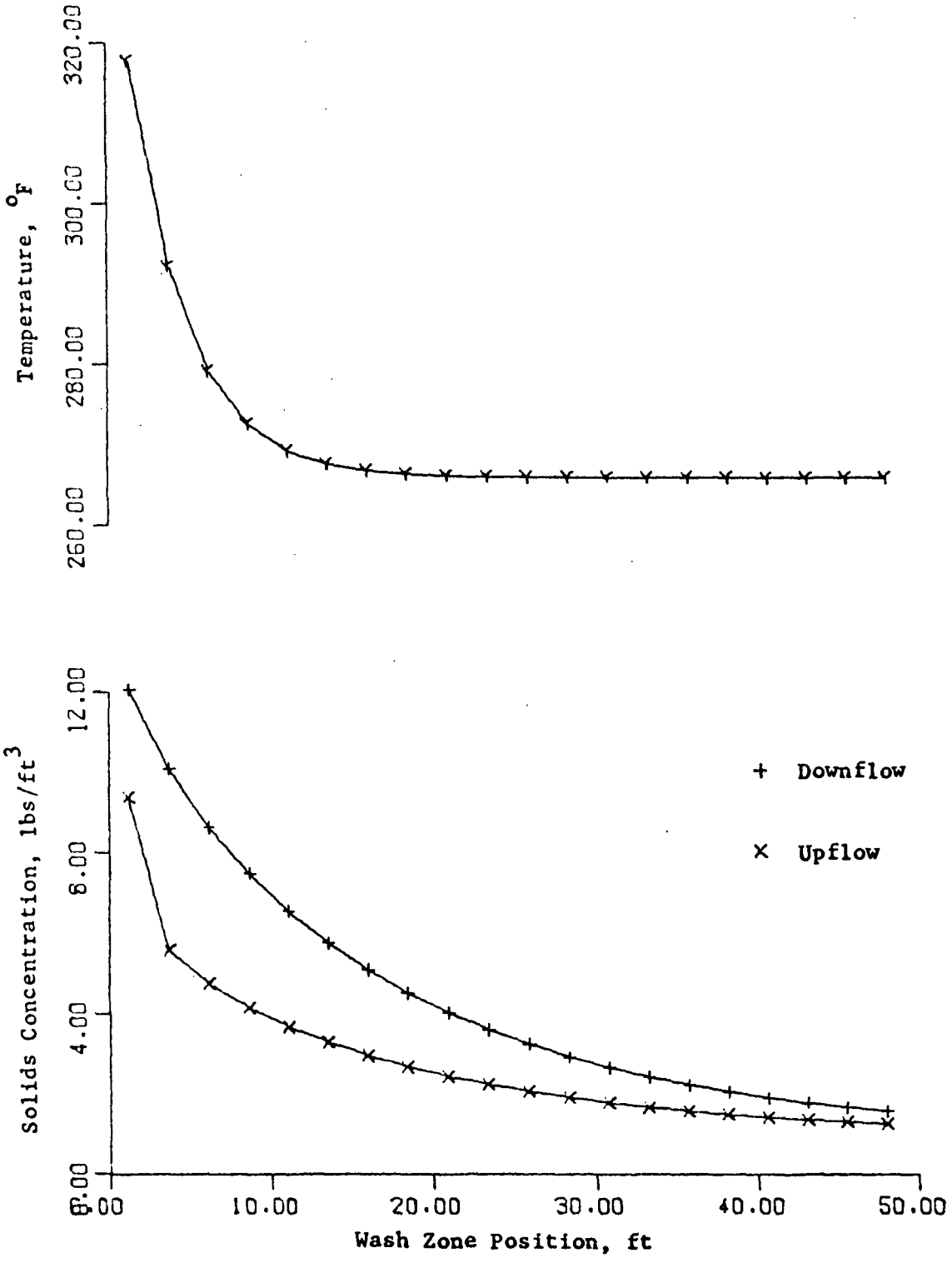

FIGURE 5

TEMPERATURE AND CONCENTRATION PROFILES

IN WASH ZONE FOR JOHNSSON'S LOW PRODUCTION CASE

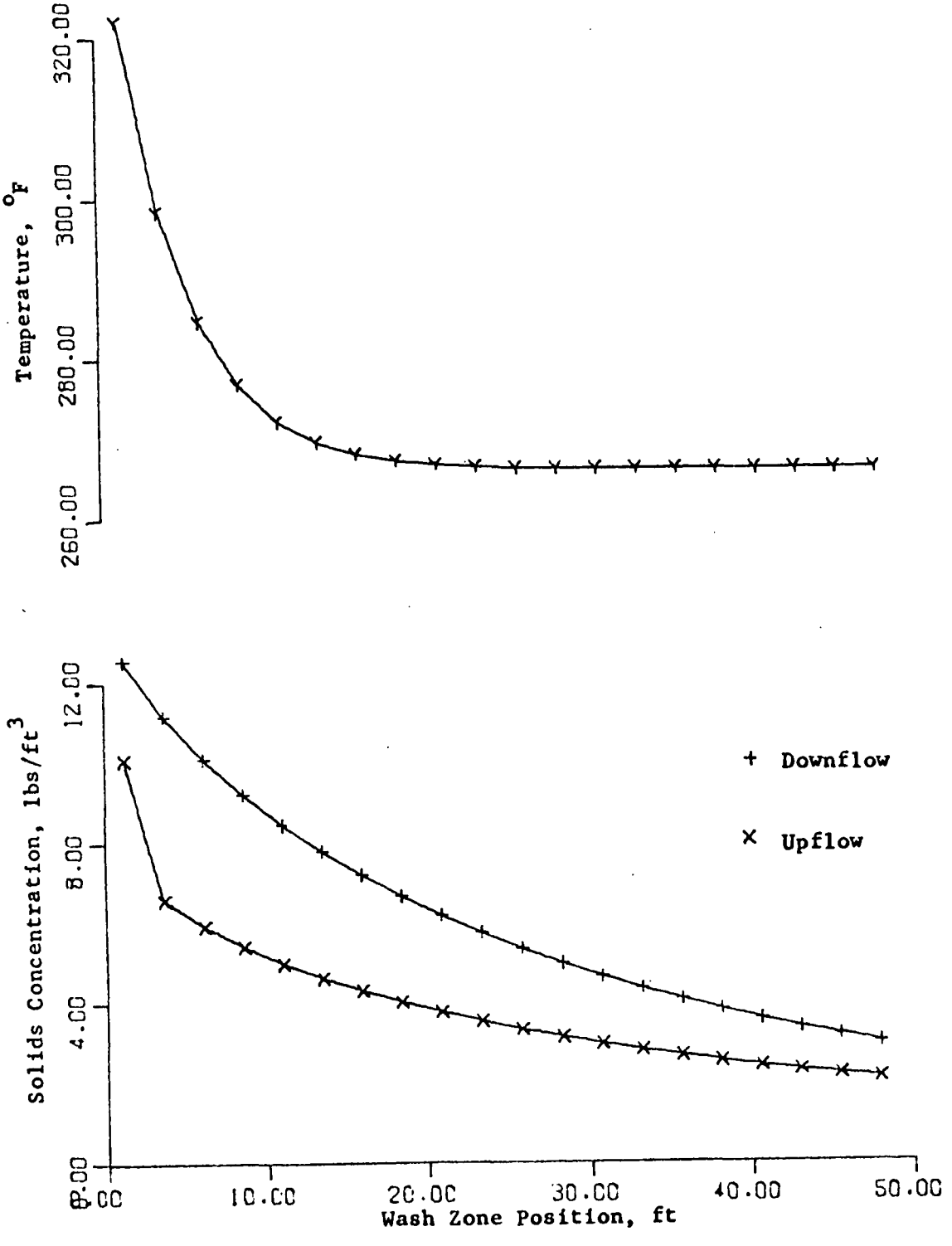

FIGURE 6

TEMPERATURE AND CONCENTRATION PROFILES

IN WASH ZONE FOR JOHNSSON'S HIGH PRODUCTION CASE

TABLE IV

BLOW LINE SOLIDS SENSITIVITY

	Dilution Factor, L_f	Wash Temp. T_{u_L}, ^oF	Filtrate Solids x_{u_L}, lb/ft^3	Blow Line Solids lbs/ADT	
	2.04	266	1.9	612	(160 Unwashed from Pulp)
Johnsson's High Production Case	1.0	266	0	74.4	
		275	0	66.8	
		284	0	58.3	
	2.04	266	0	59.0	
		275	0	47.4	
		284	0	38.2	
	2.5	266	0	53.9	
		275	0	42.1	
Low Production Case	2.62	266	1.2	362	(86.5 Unwashed from Pulp)
	2.62	266	0	19.6	

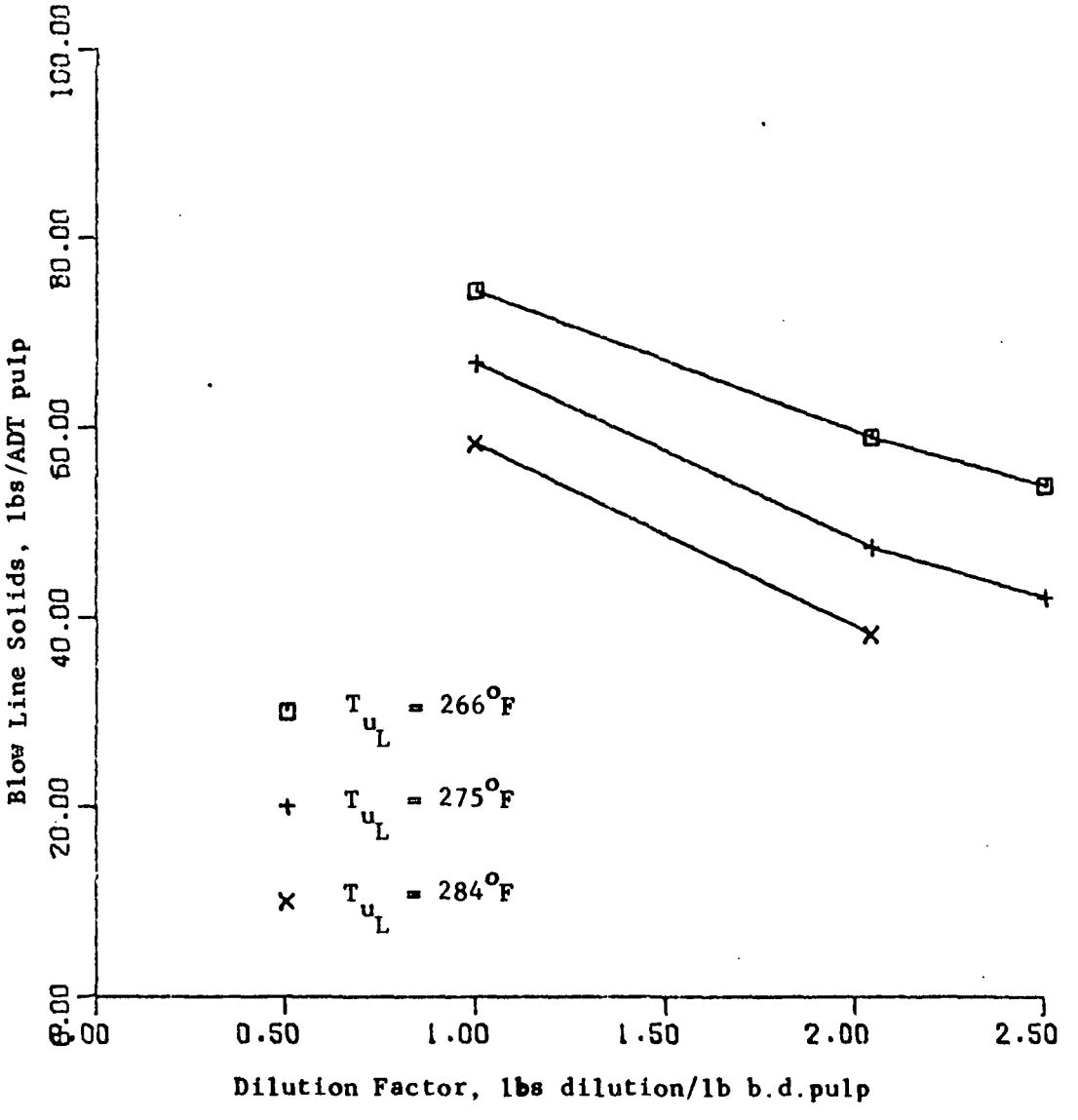

FIGURE 7

THE EFFECT OF DILUTION FACTOR AND WASH TEMPERATURE ON BLOW LINE SOLIDS FOR JOHNSSON'S HIGH PRODUCTION CASE WITH CLEAN WATER WASH

TABLE V

CLEAN WATER WASH FOR A TYPICAL MODERN DIGESTER

Dilution Factor	Blow Line Solids, lbs/ADT Pulp
3.3	1.53
3.0	1.82
2.0	3.75
1.0	10.2
0.5	19.1

Note: All run at $T_{u_L} = 265^{o}F$.

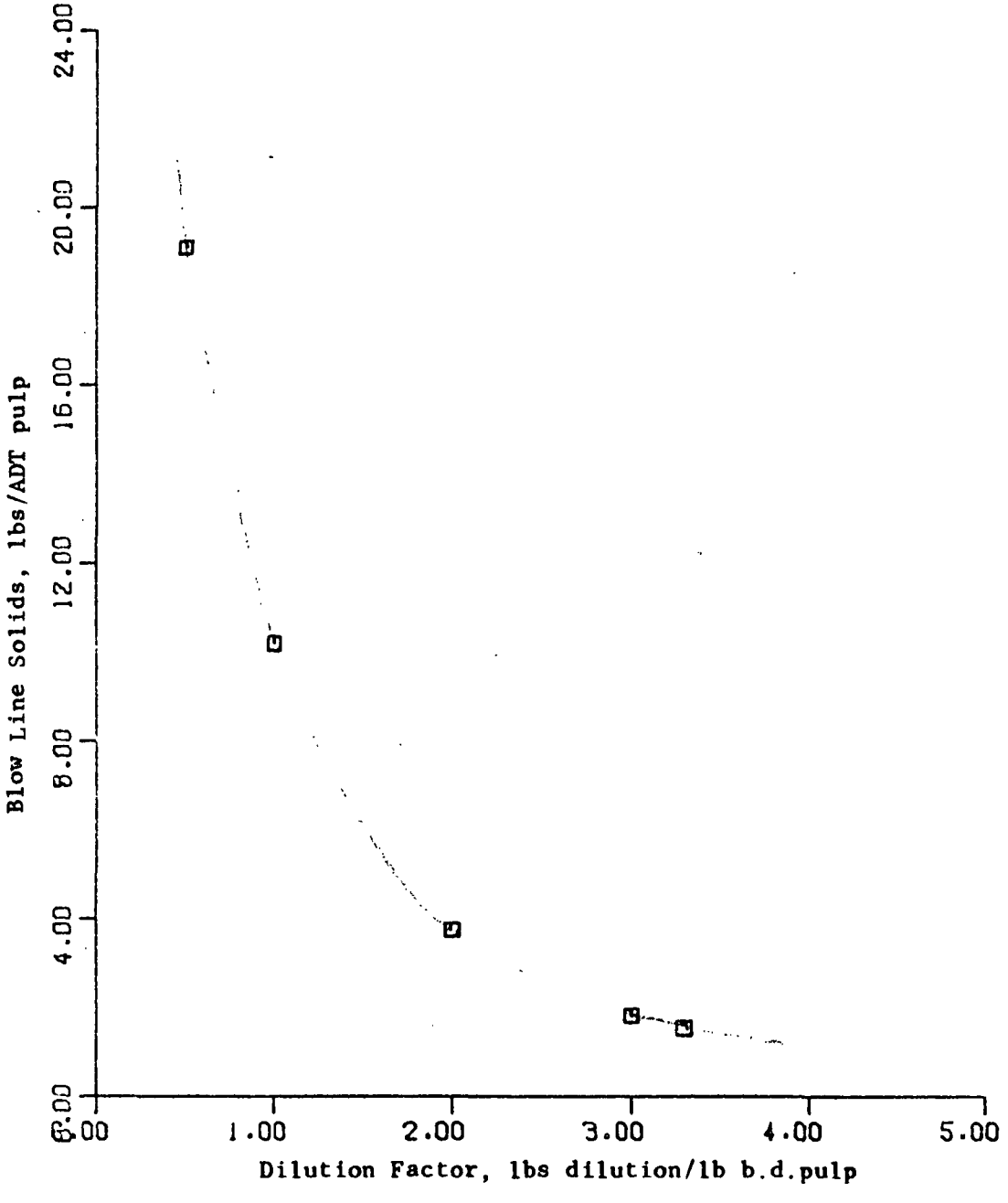

FIGURE 8

THE EFFECT OF DILUTION FACTOR ON BLOW LINE SOLIDS
FOR A TYPICAL MODERN DIGESTER WITH CLEAN WATER WASH

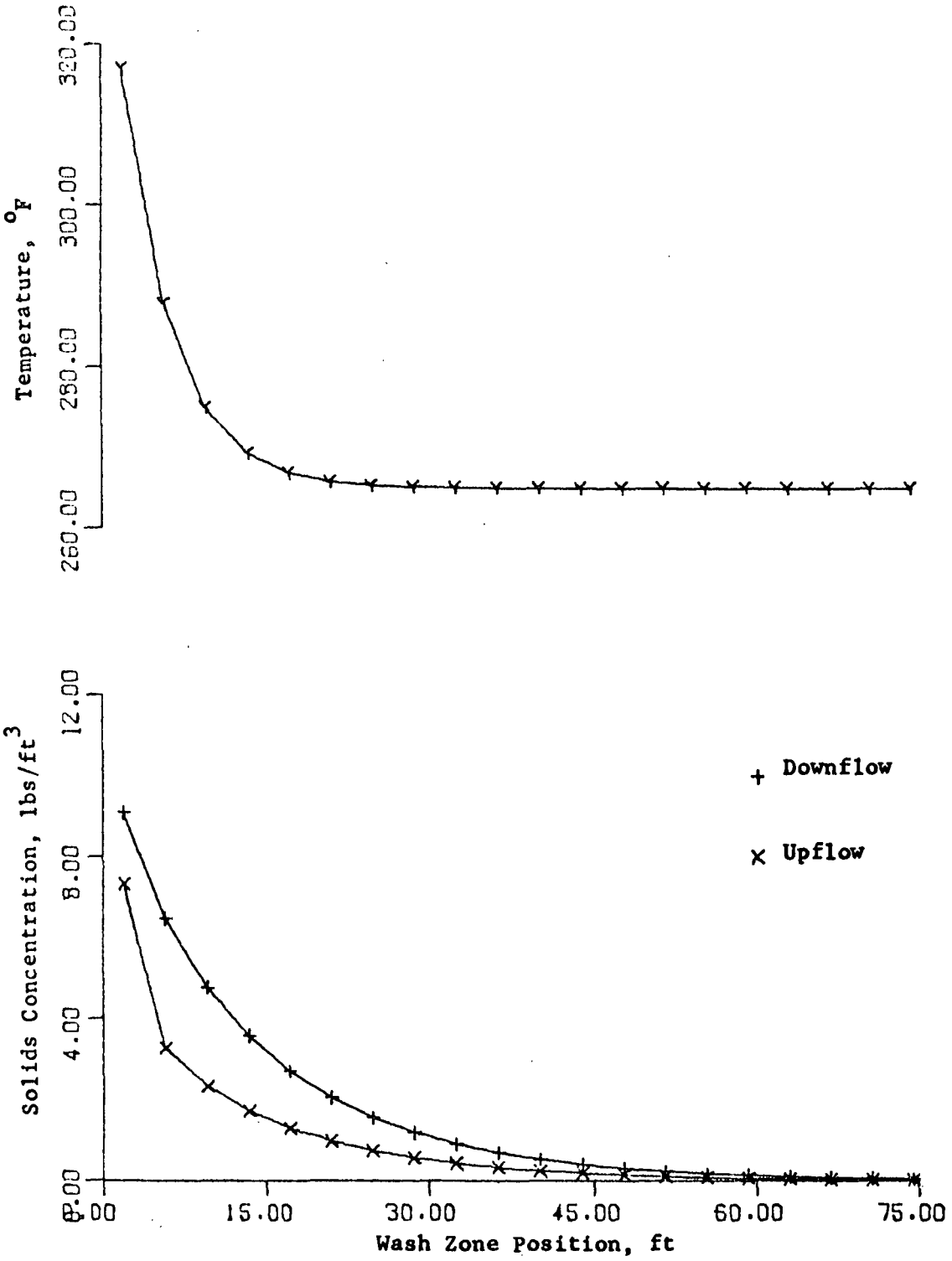

FIGURE 9

TEMPERATURE AND CONCENTRATION PROFILES FOR A TYPICAL MODERN DIGESTER WITH CLEAN WATER WASH DILUTION FACTOR = 3.3

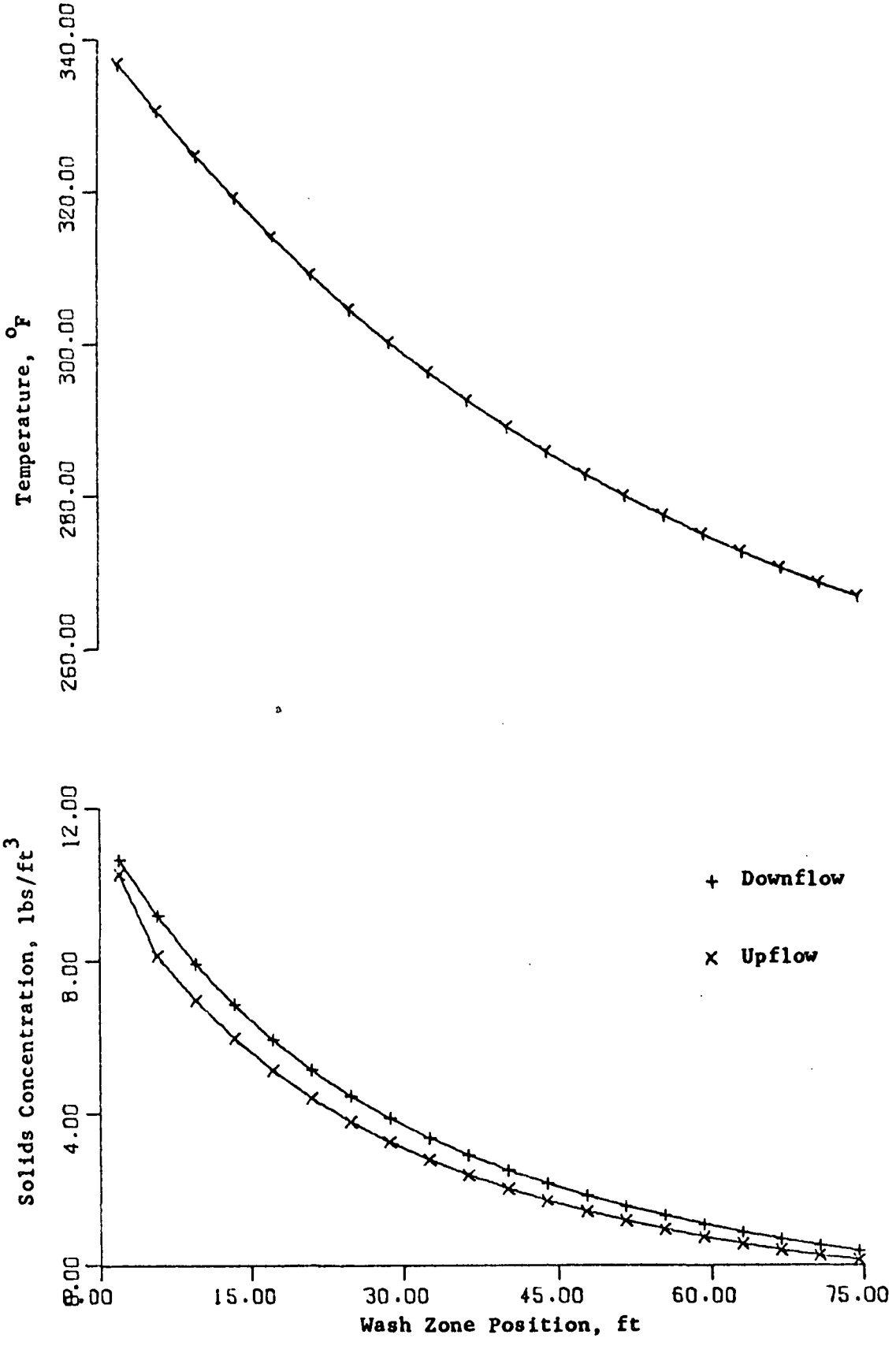

FIGURE 10

TEMPERATURE AND CONCENTRATION PROFILES FOR A TYPICAL MODERN DIGESTER WITH CLEAN WATER WASH

DILUTION FACTOR = 0.5

DISCUSSION OF RESULTS

It is clear that using clean water has a significant effect in reducing the unwashed solids exiting the digester. It is worthwhile noting that the "dirty" filtrate used in previous washing practice contributes approximately 75% of the solids leaving the digester with the pulp in the blow line. In addition to not returning solids to the washers, clean water wash also lowers the amount of the original solids which were in the unwashed pulp by 63% to 77% for Johnsson's cases, even though the residence time is rather short. For the much longer residence time of the typical modern digester, the results are even more dramatic. Typical design solids loss with brown stock washing and a dilution factor of 3.3 is 66 lbs/ADT. Clean water wash reduces it to 1.53 lbs/ADT with no brown stock washing. Even going to a dilution factor of 0.5, the losses from the digester are still only 29% of the design case using "dirty" water and brown stock washing.

The temperature dependence of the mass transfer coefficient is also apparent in that raising the wash temperature from 266^{o}F to 284^{o}F provides a 22%-35% reduction in unwashed solids.

ECONOMICS OF WASHING

A significant fraction of the total expense of Kraft pulp production is due to chemical loss because of incomplete washing. In bleachable pulps this chemical loss is further magnified by the bleaching chemical required to neutralize the unwashed chemicals and to bleach dissolved lignin left in the washed pulp. Current practice attributes to incomplete washing, 15-50 lbs of required chemical makeup (in the form of Na_2SO_4) per air dry ton of pulp produced. At 1.6¢/lb, this represents $0.24-$0.80/ADT. For a production capacity of 1000 ADT/day, this amounts to $72,000-$240,000/year in chemical loss due to incomplete washing alone.

For a 58% yield and a chemical charge of 0.194 lbs Active Alkali/lb oven dry wood, the above example represents a loss of 1.1%-3.6%. To maintain this level of performance, however, it is generally required to use 2-3 tons of water/ADT pulp during the operation of the vacuum drum washers. This water is the carrier of the recovered chemicals, and therefore is a dilution to the black liquor fed to the evaporators. Assuming a steam economy of 5.0 and an energy cost of $0.35/$10^6$ BTU, this represents an additional cost of $0.27-$0.40/ADT in energy to use wash water. In practice, the profitability of the Kraft recovery cycle depends in large part on obtaining a good balance between the cost of lost chemical and the energy cost necessary to recover that chemical.

An optimal balance, in the steady state, can be determined by matching the incremental cost of energy to recover chemicals by washing to the incremental savings in chemicals. By plotting the losses versus the dilution factor to achieve those losses (as in Figure 8), where the

slope of the curve represents the incremental savings, and the incremental energy cost is a linear function of dilution factor, a graphical matching of slopes can yield the optimal dilution factor.

For the typical modern digester and the above costs, the optimal dilution factor is approximately 0.5. At this dilution factor with the losses predicted, a savings over typical design values of 24 lbs Na_2SO_4 (salt cake) and $1.1X10^6$ BTU per air dry ton of pulp produced can be achieved. This represents $0.77/ADT.

CONCLUSIONS

Clean water wash cannot only reduce chemical loss by better washing, it can do it with less water and thus with lower energy costs. At the near optimal dilution factor of 0.5 for the typical modern digester, clean water wash represents 24 lbs Na_2SO_4 (salt cake) and $1.1X10^6$ BTU savings per air dry ton of pulp produced or $0.77/ADT over current designs.

For a typical design production rate of 1110 ADT/day and a 300-day production year, clean water wash can thus save $256,000/yr for a modern digester.

It is worth noting that, since the wash upflow is the source of energy removal for quenching, a lower dilution factor (see Figures 9 and 10) shows a distinctly higher temperature profile. This will result in "cooking" in the wash zone. The effects of this "extra" cooking, of course, can be computed and compensated for by an adjustment of the lower heater temperature.

REFERENCES CITED

1. McKibbins, S.W., "Application of Diffusion Theory to the Washing of Kraft Cooked Chips," TAPPI, 43, 10, 801-5 (October 1960).

2. Williams, D.A., McKibbins, S.W., and Riese, J.W., "Prediction of Countercurrent Diffusion Washer Efficiencies," TAPPI, 48, 9, 481-6, (September 1965)

3. Hermans, P.H., Contributions to the Physics of Cellulose Fibers, Elsevier, New York (1964).

4. Robertson, A.A., "The Physical Properties of Wet Webs, 1. Fiber-Water Association and Wet Web Behavior," TAPPI, 42, 12, 969-78 (December 1959).

5. Johnsson, L., Mathematical Models of the Kraft Cooking Process, Chalmers University of Technology, Department of Control Engineering, Report No. 11,(January 1970).

6. Handbook of Tables for Applied Engineering Science, Chemical Rubber Company, Cleveland, Ohio (1970).

SECTION III

OSCILLATORY RESPONSES IN MULTIPLE-EFFECT, BLACK LIQUOR EVAPORATORS AND THEIR CONTROL

INTRODUCTION

At the time of the presentation of the Final Report of the IPC-Purdue Project, Dr. Donald B. Brewster of Measurex, Inc. brought to our attention the fact that the strong black liquor concentration from a multi-effect evaporator system without a feedback controller from strong black liquor concentration has been known to oscillate with an amplitude of the order of 5% and with a period of about 10 to 15 minutes (similar oscillations have also been observed in a multi-effect evaporator system in Orange, Texas). A realistic dynamic model should also exhibit these same oscillations under these same operating conditions. Such a model may then lead to the answer of the questions--how and why do these oscillations arise? The oscillations can then be avoided by an improved design of an evaporator system, and/or attenuated by a good control scheme.

The model previously presented [11] has been modified to show this effect and the feedback controller in the control scheme is enough to counteract these oscillations.

THE EXISTENCE OF EVAPORATOR OSCILLATIONS

Reference [7] gives the response of the strong black liquor concentration of three multi-effect evaporators to step changes in the concentration of weak black liquor, in mass flow rate of weak black liquor, and in steam mass flow rate. These experimental results do not show any oscillations. Furthermore, a dynamic model derived on the basis of references [5], [12 - 14] cannot exhibit underdamped oscillations.

No reference has been found in the literature which mentions the control of oscillations in the concentration of strong black liquor from a multi-effect evaporator system. However, two references, [9] and [12], deal with pulsation of flows. Reference 9 describes a pulsation of flows observed through a Kestner one-tube evaporator (with internal diameter 15 mm and length 2.2 meters - this gives the length to diameter ratio about the same as that for the LTV evaporators used in Kraft paper mills) carrying water as the vaporizing fluid. Water enters the bottom of the tube at the same temperature as that in the upper boiling section. This reference also states that the amplitude of the oscillations could not be measured because of irregularities in the amplitudes, and that the pulse frequency varies both with the temperature difference between the heating steam and the water - water vapor mixture in the tube, Δt_{app}, and with the non-boiling section length in the tube. The range of frequencies 20 - 35/minute (for 20% - 70% non-boiling section length, and for $5^{o}C$ - $15^{o}C$ Δt_{app}) of flow oscillations is much higher than that required to produce a periodicity of 10-15 minutes in strong black liquor concentration from a sextuple evaporator system.

Reference [12] gives the pulsating temperature profiles observed in a pilot 4-tube climbing film evaporator. The authors found that these pulsations occur only under restricted conditions of liquor feed superheat (between $5^{o}C$ and $20^{o}C$) and of heat flux (less than 10 KW/m^2). In this pulsation, a pulse consists of two stages, the first, a slow building of a temperature pulse (i.e., the liquor temperature increases along the length of the tube with time); and second, a rapid collapse of the temperature pulse. In the first stage no flow of black liquor takes place out of the tube, and the liquor level slowly rises to the top of the tube. As soon as the liquor reaches the top of the tube, the second stage begins, i.e., the liquor in the tube and in the main liquor box flashes, and in the process ejects the liquid quickly out of the tube. The authors also give a simplified mathematical model of the building of the pulse.

However, since the liquid which is suddenly released forms a layer of liquid in the vapor space which opposes any further flashing of liquor in systems similar to the low pressure effects at Owens-Illinois plant at Orange, Texas, this mechanism does not seem to be the reason for the oscillations in strong black liquor concentration at that plant.

Figure 1 shows an analog record of strong black liquor concentration from a sextuple effect evaporator system at Owens-Illinois, Inc., Orange, Texas. The concentration shows a periodicity of about 10 minutes, and so does the flow rate of steam. The primary steam pressure remains almost constant throughout the duration of the record. Moreover, the other input variables such as mass flow rate, and the concentration of weak black liquor, and the vacuum in the last effect are not expected to cause these oscillations. Therefore, it follows that the evaporator system under these operating conditions behaves like an underdamped system.

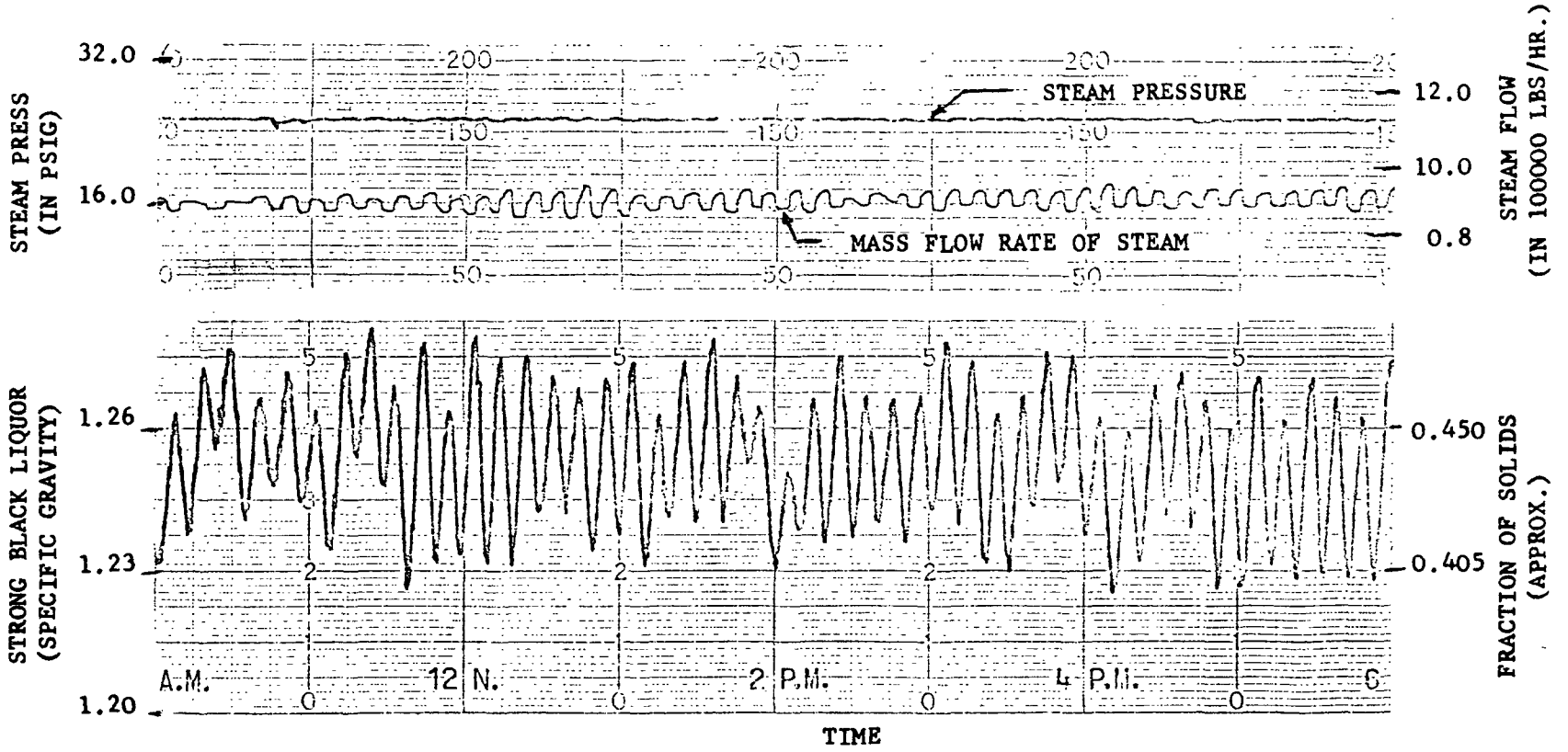

FIGURE 1

ANALOG RECORDS OF A SEXTUPLE-EFFECT EVAPORATOR SYSTEM

AT OWENS-ILLINOIS, INC., ORANGE, TEXAS

OSCILLATORY RESPONSE OF MULTI-EFFECT EVAPORATORS

OSCILLATORY DYNAMIC MODEL

The linear dynamic model [11] neglected:

1. Variations of heat transfer coefficient with black liquor temperature and concentration.

2. Variations in non-boiling section lengths.

3. Variations in the enthalpy of black liquor entering and leaving the main liquor box.

It is also known that the heat transfer coefficient of an evaporator increases with the increasing temperature of vaporizing liquor and with the decreasing concentrations of vaporizing liquor [1 - 4], and [10]. Now, if the temperature increases due to some disturbance, the heat transfer coefficient of an evaporator slowly increases, which in turn slowly increases the concentration of black liquor coming out the effect. The increased concentration will slowly decrease the heat transfer coefficient. However, since the vapors generated in an effect are fed to the next effect, and from the next to its next and so on in a series fashion, the increasing and decreasing heat transfer coefficients may produce oscillatory concentration of strong black liquor under some particular operating conditions of multi-effect evaporators.

The dynamic model in [11] was, therefore, modified to include the three above mentioned variations. Furthermore, because under an oscillatory condition, some of the variables may vary over a wider range than is

allowed for in a linearized model, a non-linear dynamic model is used for studying the oscillations in strong black liquor concentration.

MODIFICATIONS IN THE DYNAMIC MODEL

The linear dynamic model as given in [11] is overdamped, and will not show underdamped oscillations. In order to improve the dynamic model of multi-effect evaporator system given in [11], the following assumptions in that model are modified.

1. In [11], the non-boiling section length was assumed to be a constant for each effect. The non-boiling section length, L_N, in the actual evaporator varies depending upon the amount of sensible heat the liquor requires to reach the boiling point. The velocity of liquor in a non-boiling Section is small, about 4-6 ft/sec, thus the transport lag T_{DNBS} for the liquor to flow through the non-boiling section varies with the non-boiling section length L_N. At present the variation in L_N is included, but the variation in time delay T_{DNBS} is neglected. Since the variable L_N represents the physical non-boiling section length in an evaporator, the computed non-boiling section length is limited by the total tube length L_T (i.e., the whole tube length is a non-boiling section, and no evaporation takes place in that effect) and by 0.0 (i.e., the liquor enters the non-boiling section at a temperature higher than the boiling temperature, and flashing of liquor takes place -- part of its heat goes into evaporating liquor) as shown in Figure 2.

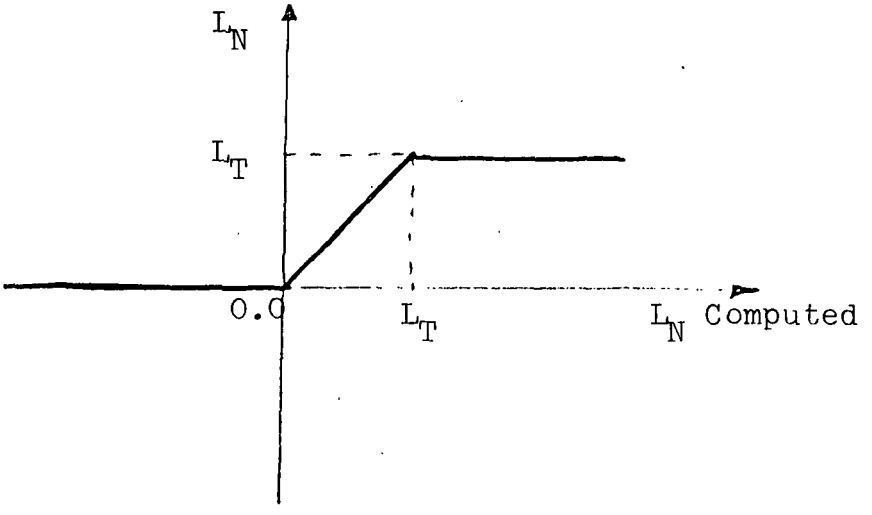

FIGURE 2

LIMITER CHARACTERISTIC FOR

NON-BOILING SECTION LENGTH, L_N

2. In [11], the heat transfer coefficient was assumed to be constant. However, the heat transfer coefficients as given by Sieder-Tate correlations [4], or by other correlations depend on the viscosity, μ, thermal conductivity, K, specific heat, C_p, velocity of liquor in tube V, etc. For example, the heat transfer coefficient of non-boiling section by Sieder-Tate. correlation is given by

$$U_N = 0.027 \frac{k}{D} \left(\frac{DV\rho}{\mu}\right)^{\frac{4}{5}} \left(\frac{C_p \mu}{k}\right)^{\frac{1}{3}} \left(\frac{\mu}{\mu_w}\right)^{\frac{1}{7}} \quad (1)$$

where

ρ = density of black liquor

μ_w = viscosity of black liquor at wall temperature

D = tube diameter

L = tube length

Viscosity, thermal conductivity, specific heat, and density of black liquor, all four depend on both the concentration of and the temperature of black liquor [4]. Their graphs are reproduced in Figures 3 and 4.

Similar results about the variation of heat transfer coefficients of sulfite liquor evaporators can be deduced from Figure 5 (reproduced from [1]) and Figure 6 (reproduced from [10]). Figure 5 shows that for liquor concentration in the range 45-50%, the heat transfer coefficient for a liquor temperature of 131°F lies below that for 211°F (indicating that heat transfer

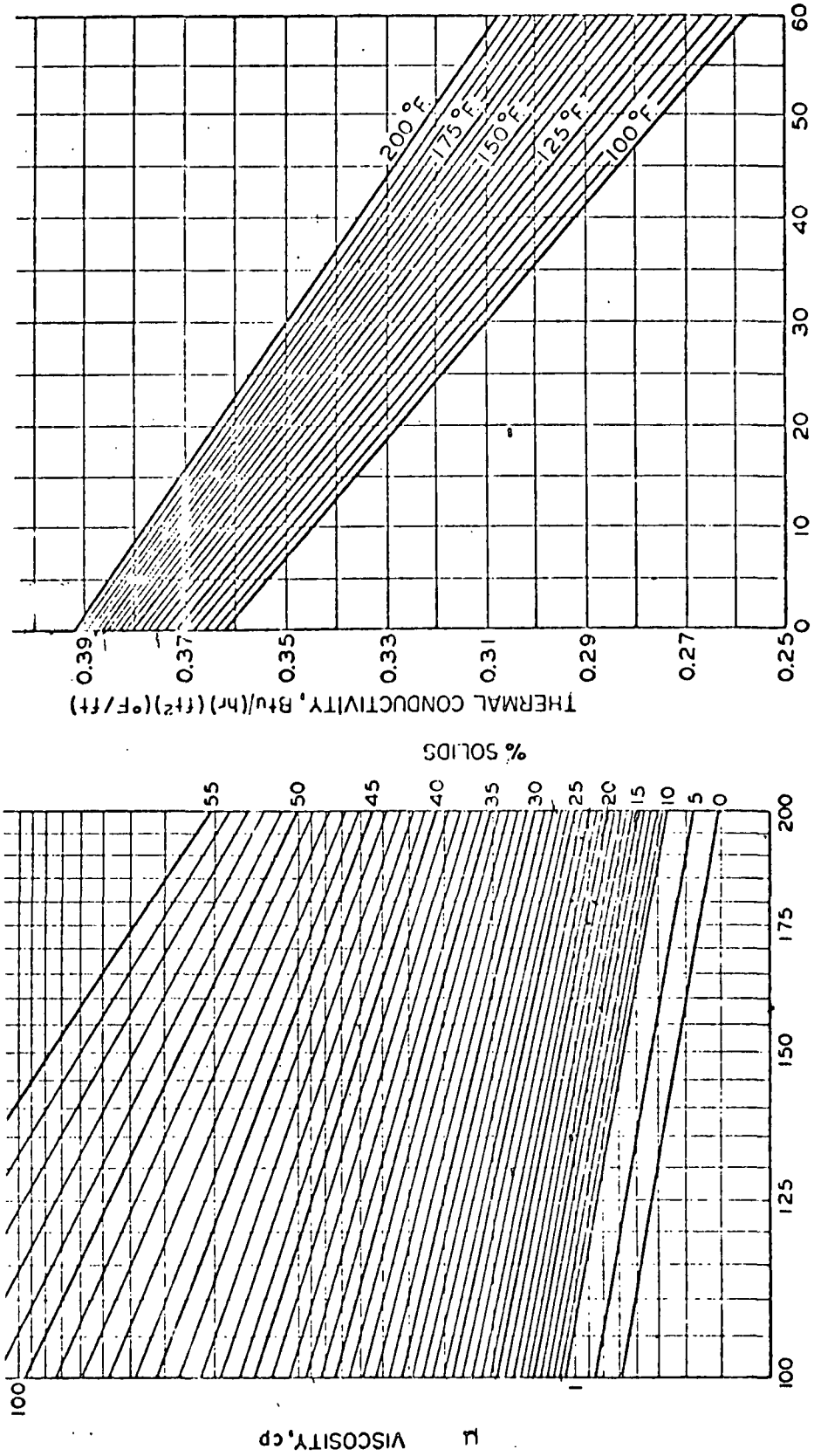

Thermal conductivity of a kraft black liquor.

Viscosity of a kraft black liquor.

(from Reference 4)

FIGURE 3

PROPERTIES OF BLACK LIQUOR

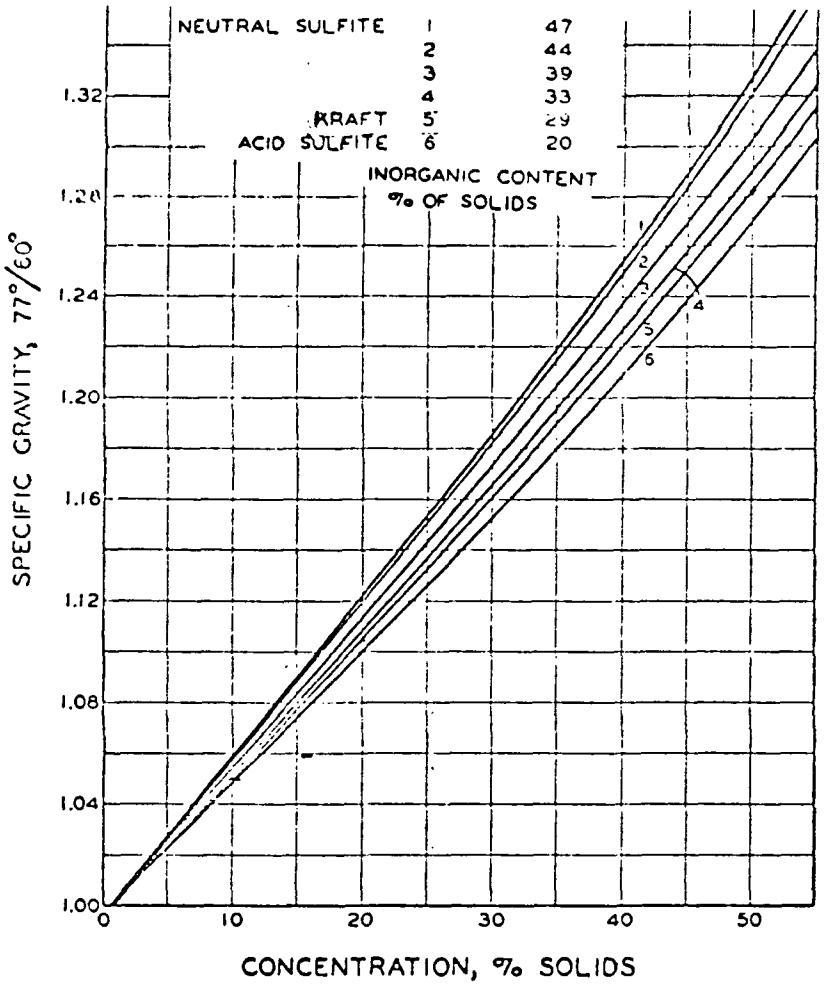

Specific gravity of spent liquors.

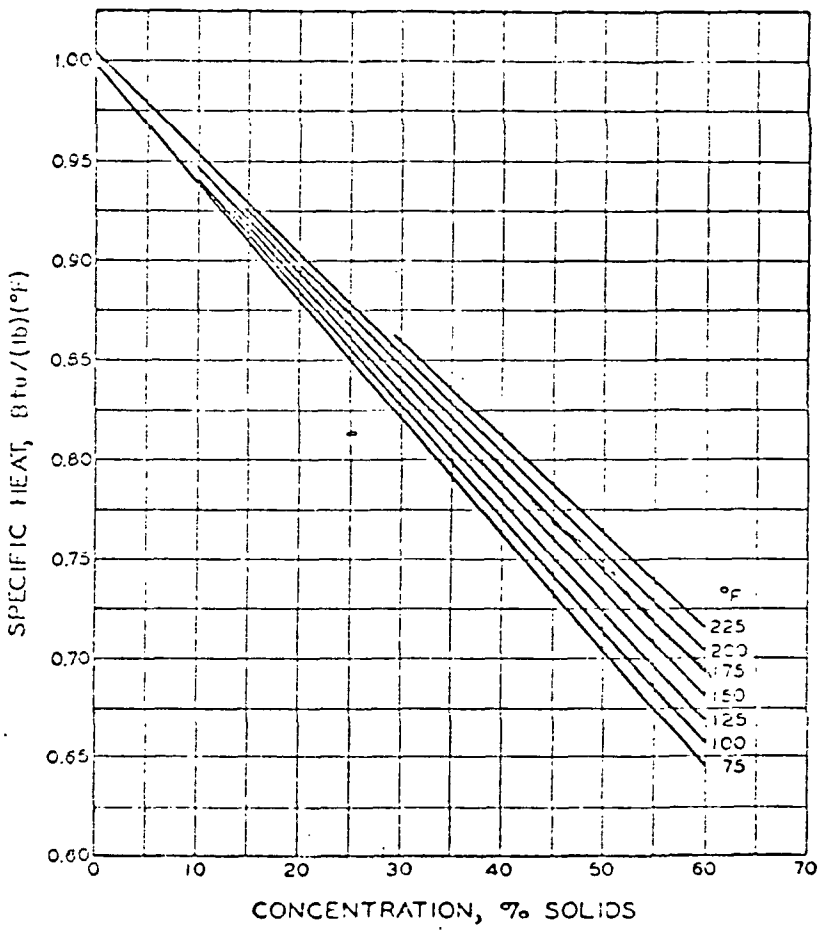

Specific heat of a kraft black liquor.

(from Reference 4)

FIGURE 4

PROPERTIES OF BLACK LIQUOR

211°F

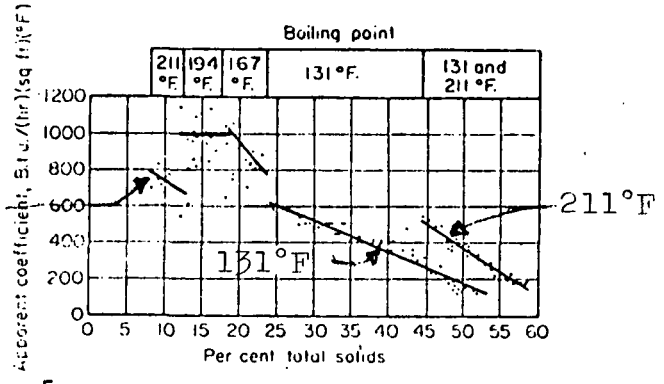

211°F

FIG. 5 Heat-transfer coefficients in evaporating sulfite liquor.

Operating Data for the Evaporation of Sulfite-pulp Liquor

¾ in. o.d., ⅝ in. i.d. nickel tubes 8 ft. 0 in. long

	First effect		Second effect	Third effect	Fourth effect
Liquor temperature, °F.	211	211	194	167	131
Temperature drop, °F.	20	36	20	25	45
% total solids	8–12	45–59	13–17	18–23	24–52
Approx. viscosity, centipoise	0.4 0.5	6–30	0.5	1–1.2	1.6–80
Avg. inlet velocity, ft./sec.	11.5	7.6	7.9	7.1	9.4
Avg. pressure drop, ft. H_2O	14.8	24.0	15.2	19.1	22.6

(from Reference **1**)

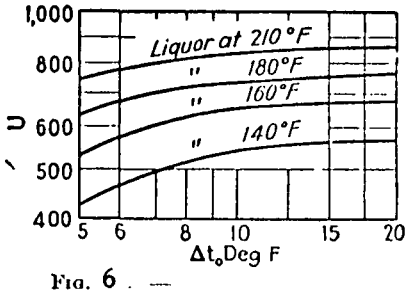

FIG. 6 — evaporation of water from sulphite liquor flowing in a slightly inclined steel tube (3 in. × 25 ft) jacketed by condensing steam.]

(from Reference **10**)

coefficient increases with increasing temperatures). Also, for a liquor temperature of 211°F, the heat transfer coefficient for 10% solids lies above that for 50% solids (i.e., heat transfer coefficient decreases with increasing concentrations). The conclusion that heat transfer coefficient increases with increasing sulphite liquor temperature is also indicated by Figure 6.

Since heat transfer varies as a function of black liquor temperature and its concentration, one can express the heat transfer coefficient, U_N, in the non-boiling section by

$$U_N = \bar{U}_N\left[1.0+\alpha_T(T_{BLO}-\bar{T}_{BLO}) + \alpha_C(C_{BL\ Out,MLB}-\bar{C}_{BLN})\right] \qquad (2)$$

and the heat transfer coefficient in the boiling section by

$$U_B = \bar{U}_B\left[1.0+\beta_T(T_{BLO}-\bar{T}_{BLO}) + \beta_C(C_{BLO}-\bar{C}_{BLO})\right] \qquad (3)$$

where overscore represents the steady state value. α_T and β_T represent fraction change of heat transfer coefficients per degree change of temperature in non-boiling and boiling sections. T_{BLO}, C_{BLO}, and C_{BLN} represent boiling temperature of liquor, concentration of strong black liquor leaving a vapor space, and concentration of weak black liquor entering main liquor box (MLB), respectively. Since the heat transfer coefficient increases with increasing black liquor temperature and decreases with increasing black liquor concentration, α_T and β_T take positive values, and α_C and β_C take negative values. In

addition, the computed linearized heat transfer coefficient values for large upsets may become too large to be realistic, or become negative. To avoid these possibilities, limiter characteristics (with positive upper and lower bounds) are included with Equations (2) and (3).

3. In [11], the model neglects the changes in the enthalpy of the liquor entering the main liquor box, and in the liquor leaving the main liquor box. The effect of main liquor box on the enthalpy is express by

$$\frac{dH^{i}_{BL\ Out,MLB}(t)}{dt} = \frac{\bar{\dot{M}}^{i}_{BLN}(t)}{\bar{\rho}^{i}_{BLN}\ V^{i}_{MLB\ eff}} \left[H^{i}_{BLN}(t) - H^{i}_{BL\ Out,MLB}(t)\right] \quad (4)$$

where $H_{BL\ Out,MLB}$, H_{BLN}, $\dot{M}_{BLN}$, and $V_{MLB\ eff}$ represent the enthalpy of liquor entering MLB, the mass flow rate of black liquor flowing in, and the effective volume for mixing in MLB respectively.

4. The sensible heat is transferred from the steam to the black liquor, as the liquor rises to the interface through the non-boiling section during the time interval T_{DNBS} (T_{DNBS} is assumed to be constant to simplify an iterative computation into a recursive computation, as given by Equation (5)). This heat transfer was approximated by a quasi-steady state energy balance (Equation (34) in [11]). In the modified model, computed non-boiling section length is obtained as

$$L^{i}_{N\ comp}(t) = \frac{\int_{t-T_{DNBS}}^{t} \dot{M}^{i}_{BLN}(t')dt'}{\int_{t-T_{DNBS}}^{t} U^{i}_{N}(t')D^{i}_{T}\{T^{i+1}_{STCH}(t') - T^{i}_{BLO}(t')\}dt'} \left[\right.$$

$$H^{i}_{BL,interface}(t) - H^{i}_{BL\ Out,MLB}(t-T_{DNBS}) \left. \right] \qquad (5)$$

where $H_{BL,interface}$ is the enthalpy of boiling black liquor. D_T is the area of heat transfer divided by L_T. T_{STCH} is the temperature in a steam chest. The value of non-boiling section is then computed according to Figure 2.

RESULTS OF DIGITAL COMPUTER SIMULATIONS FOR CONSOLIDATED PAPER, INC., WISCONSIN RAPIDS PLANT

The non-linear dynamic model included in [11] was modified to include Equations (2-5). The model was then set up for the sextuple effect evaporator system at Wisconsin Rapids, and the equations were solved on the CDC 1700 computer.

Simulations were carried out for various sets of values of parameters α_C and α_T ($\beta_C = \alpha_C$, and $\beta_T = \alpha_T$ for the results given in this section) as plotted in Figure 7. Parameter domain in which oscillations occur is approximately indicated by the cross-hatching.

Figure 8 shows the simulations of strong black liquor concentration correspondong to three sets of values of parameters lying on line AB, on which α_C remains unchanged, but the value of parameter α_T varies. The input to the system is a pulse of weak black liquor concentration which changes from 15% to 16% during the time interval 1.0 - 6.0 minutes. As the parameter α_T is increased, the strong black liquor concentration becomes more oscillatory, and becomes more underdamped.

Figure 9 shows simulations of strong black liquor concentration corresponding to four sets of values of parameters lying on line CD, on which the parameter α_T remains the same, but parameter α_C varies. The input pulse of the weak black liquor concentration is the same as for the previous figure; however, it is found that the period of strong black liquor concentration decreases as the magnitude of α_C increases.

Figure 10 shows the influence of non-boiling section time delays on the period of oscillations in strong black liquor concentration. Input

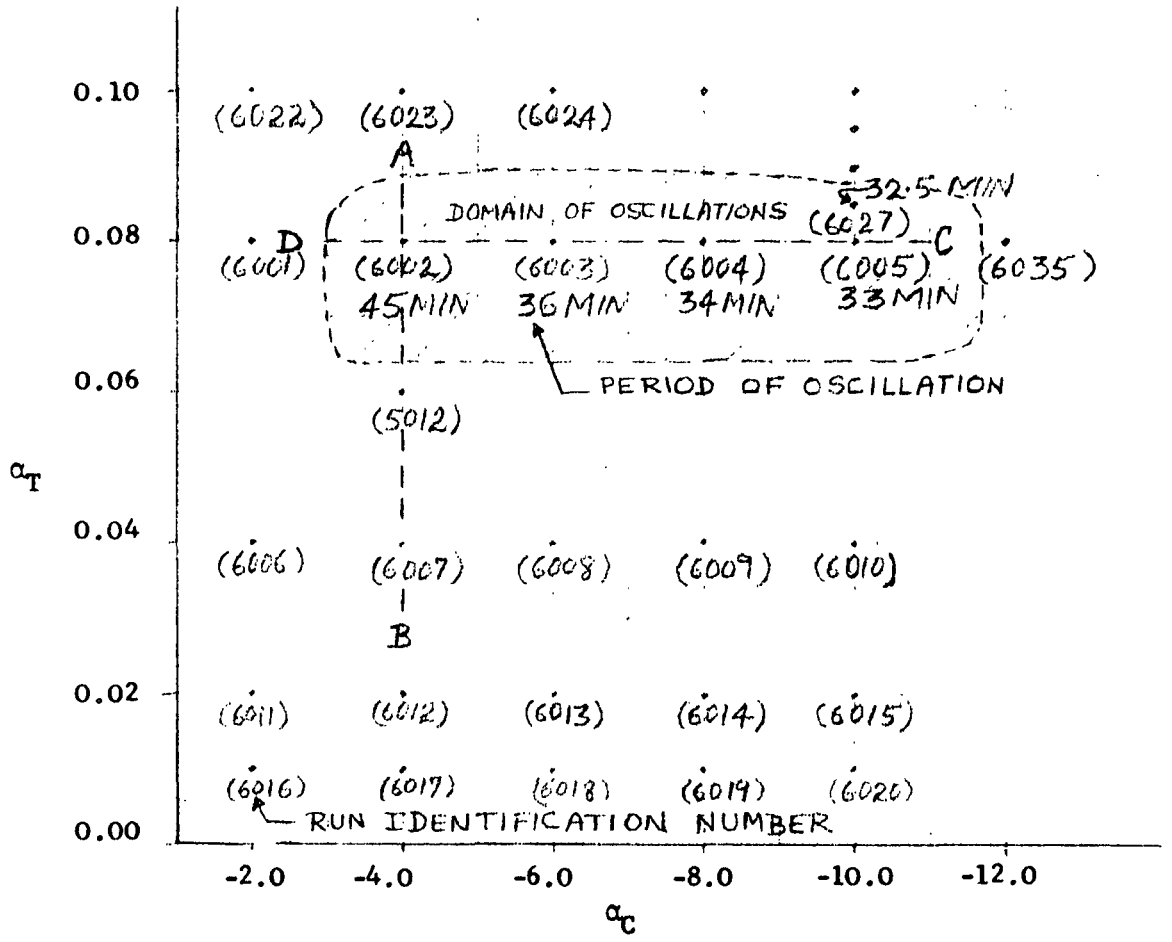

FIGURE 7

DOMAIN OF HEAT TRANSFER COEFFICIENT

PARAMETERS α_T AND α_C

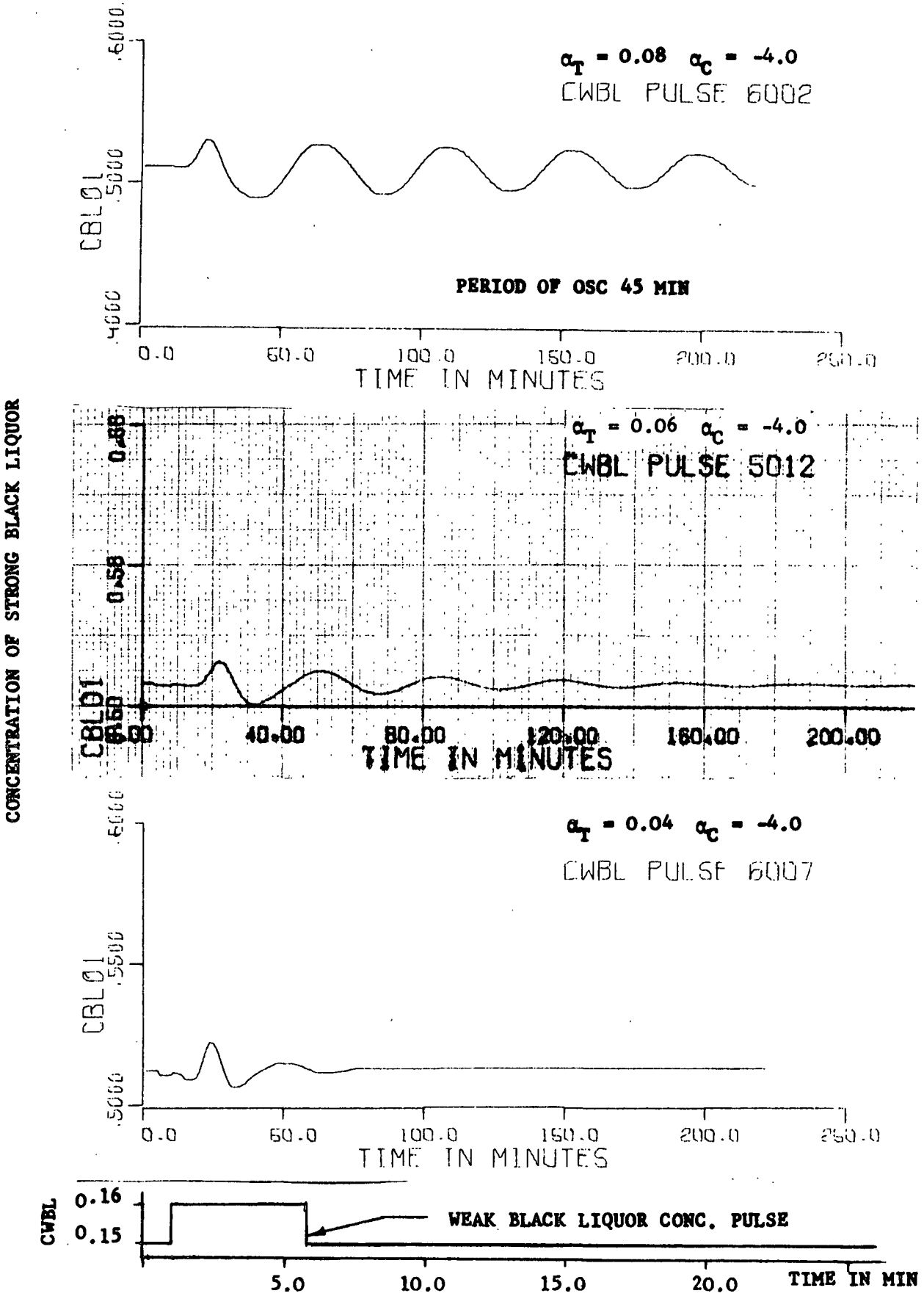

FIGURE 8

SIMULATIONS OF SYSTEM RESPONSE FOR DIFFERENT VALUES OF HEAT TRANSFER COEFF. PARAMETER α_T

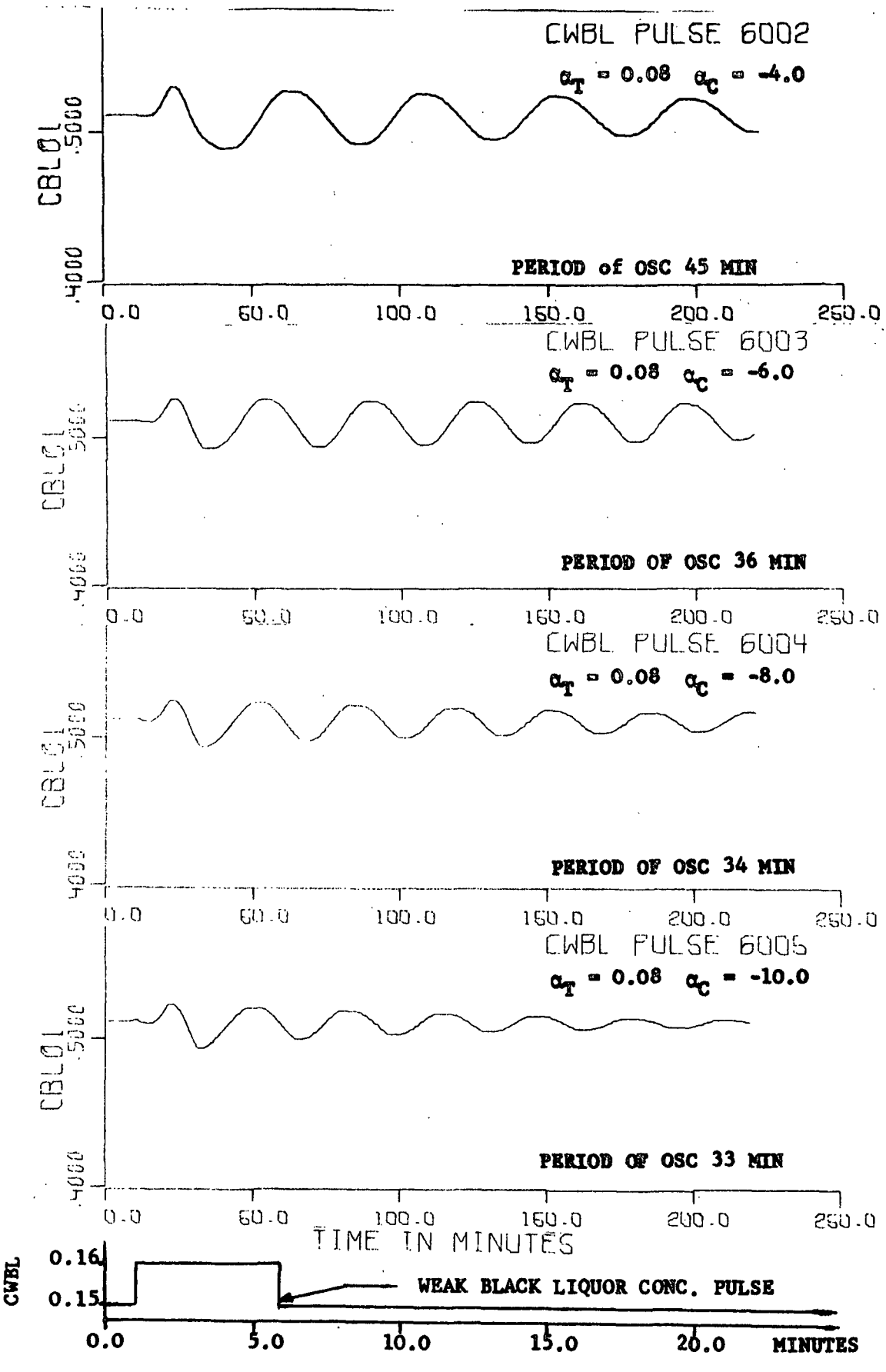

STRONG BLACK LIQUOR CONCENTRATION

FIGURE 9

SIMULATIONS OF SYSTEM RESPONSE FOR DIFFERENT VALUES OF HEAT TRANSFER COEFF. PARAMETER α_C

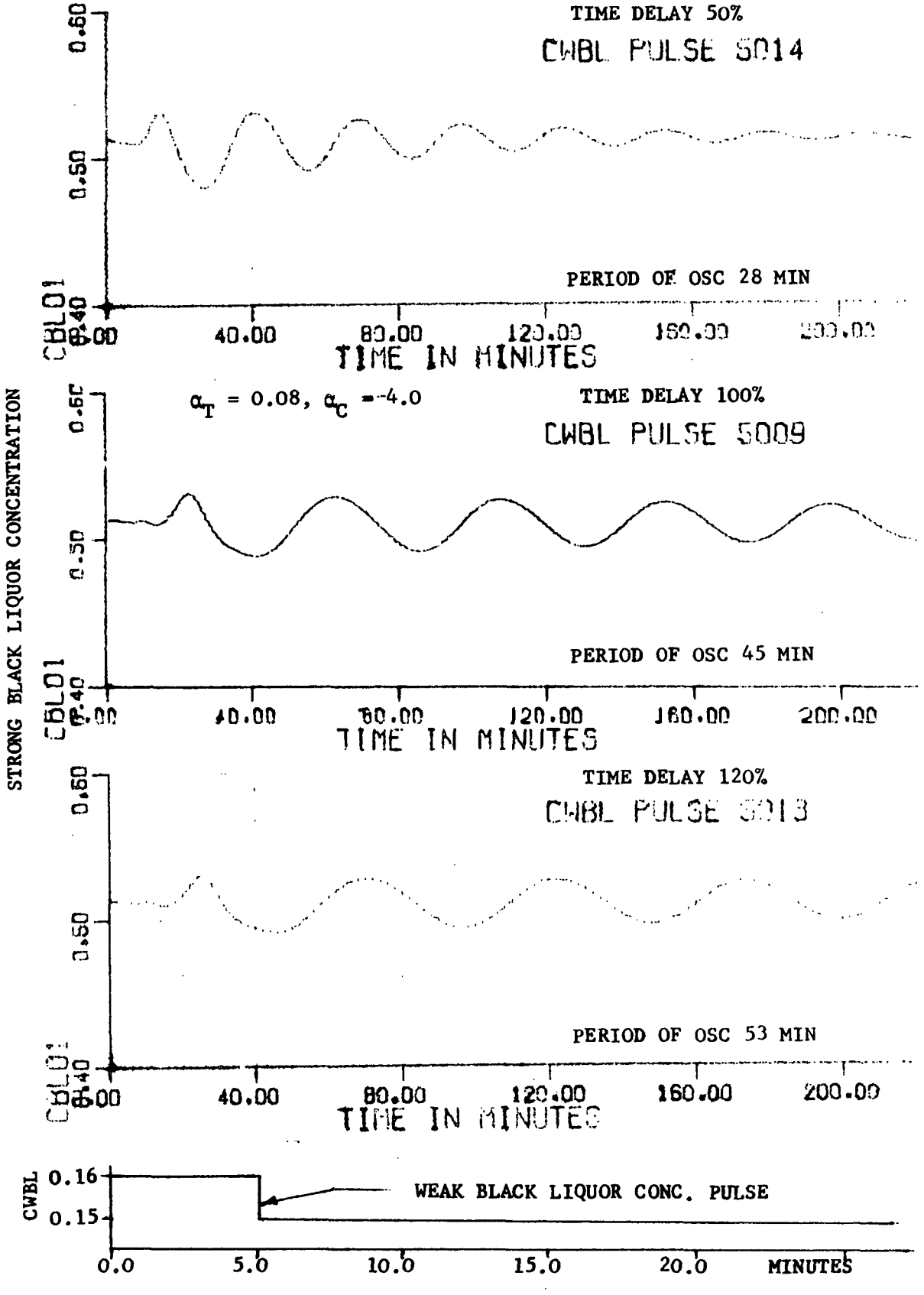

FIGURE 10

INFLUENCE OF NON-BOILING SECTION TIME DELAYS
ON THE PERIOD OF OSCILLATIONS

to the system is again a pulse of weak black liquor concentration which changes from 15% to 16% during the interval, 0.0-5.0 minutes. It is seen from Figure 10 that the period of oscillations in strong black liquor concentration increases with increasing values of time delays, and it decreases with the decreasing values of time delays. The time delays of approximately 1.0-5.0 minutes occur in non-boiling sections. The value of a time delay depends on the non-boiling section length, which in turn depends on the amount of sensible heat required by the liquor to reach the boiling temperature. If pre-heaters, and/or post-heaters are present, they would reduce the non-boiling section length. Therefore, it can be said that the period of oscillations is a function of both the operating conditions of the plant and the design of pre-heaters and post-heaters, etc.

Figure 11 shows that once a system oscillates for a disturbance of input for a set of parameters α_C and α_T, it oscillates also for other input disturbances. Pulse inputs applied are -0.1 psi in steam pressure, +1.0% in weak black liquor concentration, and $-30^{o}F$ in weak black liquor temperature. Since the system can oscillate even due to a very small pulse disturbance in steam pressure, the system is underdamped and usual disturbances present in the system will keep it oscillating as long as the operating conditions remain unchanged.

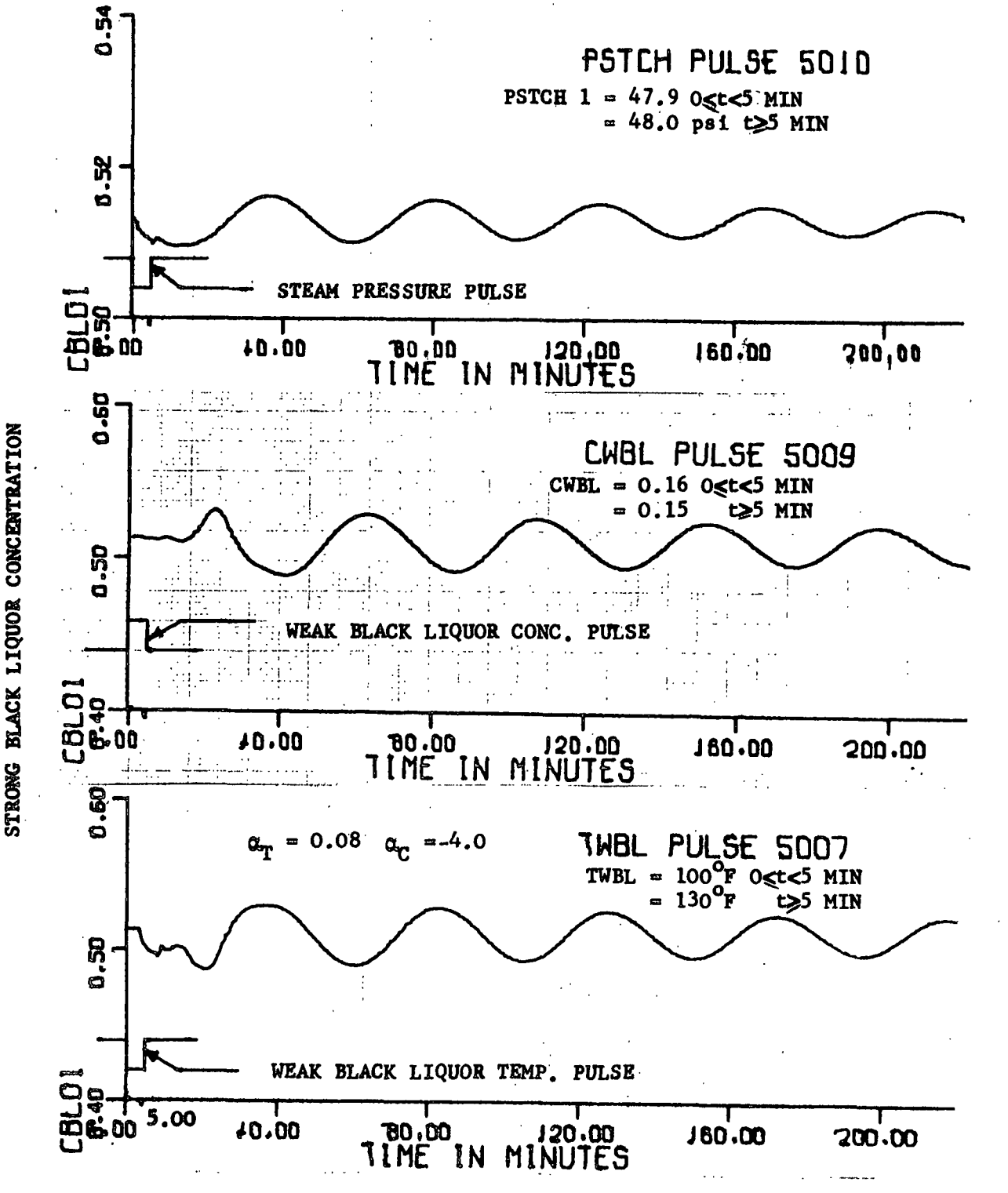

FIGURE 11

SIMULATIONS OF SYSTEM RESPONSE FOR

VARIOUS INPUT DISTURBANCES

MODIFICATIONS TO THE MODEL TO SIMULATE THE ORANGE, TEXAS, PLANT OF OWENS-ILLINOIS INCORPORATED

In this sextuple-effect evaporator system the feed is split and part of the liquor is fed forward towards high pressure effects (Effect 1) and part of the liquor is fed backwards towards low pressure effects (Effect 6), where it is concentrated and pumped forward with the remainder of the weak black liquor feed.

The non-linear model [11] for an evaporator system had already been modified by the inclusion of Equations (2-5) developed from the model of the Wisconsin Rapids Plant. The dynamic model developed for the Orange, Texas plant was further expanded by including elements representing condensate flash, liquor flash, pre-heaters and post-heaters in the system. Limits were also placed on the variations in heat transfer coefficients caused by large swings in the concentration and temperature of black liquor.

FLASH TANKS

The concentrated black liquor and steam chest condensate are flashed to a lower pressure in liquor and condensate flash tanks (or condensate flash chambers in Effects 3, 4, 5, and 6). The heat thus released evaporates some water in the flash tank into steam. This flashed steam is then lead to the steam chest of an effect operating at a lower pressure than the one from which the liquor or condensate came. This flashed steam thus improves the general steam economy of the evaporator system.

In modeling the flash tanks, the mixing of condensate (or black liquor) is neglected. The material and energy balance equations for a flash tank can then be written as

$$\dot{M}_{\text{Flash in}} H_{\text{Flash in}} = \dot{M}_{\text{Flash out}} H_{\text{Flash out}} + \dot{M}_{\text{Steam Flashed}} H_{\text{Steam Flashed}} \quad (6)$$

and

$$\dot{M}_{\text{Flash in}} = \dot{M}_{\text{Flash out}} + \dot{M}_{\text{Steam Flashed}} \quad (7)$$

where $\dot{M}_{\text{Flash in}}$, $\dot{M}_{\text{Flash out}}$, and $\dot{M}_{\text{Steam Flashed}}$ are mass flow rates of condensate (or black liquor) in, condensate (or black liquor) out, and steam flashed, respectively. $H_{\text{Flash in}}$, $H_{\text{Flash out}}$, and $H_{\text{Steam Flashed}}$ are the enthalpies of the three fluids in question.

In the model it is assumed that the flashed steam is at the pressure of the steam chest to which it is led, and that the condensate leaves at the saturation temperature of the steam. (In the case of liquor flash, the black liquor leaves at the saturation temperature of the steam plus the boiling point rise.)

PRE-HEATERS (AND POST-HEATERS)

Pre-heaters (post-heaters) consist of a few per cent total volume of the tubes in any one effect. The incoming black liquor is isolated from the evaporating liquid in that effect, and is heated under forced-circulation. Since the area of corss-section to flow is much smaller for pre-heaters (post-heaters) than for the regular evaporation region, the flow velocities and thus the heat transfer coefficients through the pre-heaters (post-heaters) are considerably higher than those in the non-boiling section. The use of pre-heaters (post-heaters) therefore reduces the non-boiling section length in that effect (in the next effect forward for post-heaters), and thereby provides a higher overall heat transfer coefficient.

The equation for heat transfer through pre-heater, $\dot{Q}_{Pre\text{-}heater}$ (and $\dot{Q}_{Post\text{-}heater}$), is analogous to the equation used for the non-boiling section, and can be expressed as

$$\dot{Q}_{Pre\text{-}heater} = U_{Pre\text{-}heater} A_{Pre\text{-}heater}(T_{STCH} - T_{BL\ Pre\text{-}heater\ in}) \quad (8)$$

where

$U_{Pre\text{-}heater}$ = The heat transfer coefficient of pre-heater which may be estimated from Sieder-Tate correlations.

$A_{Pre\text{-}heater}$ = Area of heat transfer.

T_{STCH} = Temperature of steam in the steam chest.

$T_{BL\ Pre\text{-}heater\ in}$ = The temperature of black liquor flowing to pre-heater.

The temperature of black liquor flowing out of the pre-heater can then be computed as

$$T_{BL\ Pre\text{-}heater\ out} = T_{BL\ Pre\text{-}heater\ in} + \frac{\dot{Q}_{Pre\text{-}heater}}{C_{PBL}\,\dot{M}_{BL\ Pre\text{-}heater}} \quad (9)$$

Here, $T_{BL\ Pre\text{-}heater\ out}$, C_{PBL}, and $\dot{M}_{BL\ Pre\text{-}heater}$ are the temperature of black liquor flowing into the pre-heater, $C_{PBL}(t)$, the specific heat of the black liquor, and mass flow rate of black liquor through the pre-heater.

Because of the higher velocities the transport lags in flowing through the pre-heaters (and post-heaters) are relatively small, and may be lumped with the transport lag in the non-boiling section of that effect (of the next effect forward in case of post-heater).

$$U_{\text{Pre-heater}} = \bar{U}_{\text{Pre-heater}}[1.0+\alpha_T(T_{\text{BL Pre-heater in}} - \bar{T}_{\text{BL Pre-heater in}}) + \alpha_C(C_{\text{BL Pre-heater in}} - \bar{C}_{\text{BL Pre-heater in}})] \quad (10)$$

where $C_{\text{BL Pre-heater in}}$ is the concentration of black liquor flowing into pre-heater.

The expressions for heat transfer for the temperature of the black liquor flowing out, and for the heat transfer coefficient present in the post-heaters are written in an analogous manner to Equations (8-10).

LIMITS ON VARIATIONS OF HEAT TRANSFER COEFFICIENTS

It was mentioned earlier that the computed linearized heat transfer coefficient values for large upsets as computed by Equations 2-3 may become too large to be realistic, or may even become negative. In order to avoid these possibilities, the maximum change in heat transfer coefficient due to either of the two variables (the concentration and temperature of black liquor) is limited to $\pm$ 50%, and the minimum value of heat transfer coefficient is also restricted to a value greater than or equal to one-third of its steady state value in the simulations included in this section. This was sufficient to prevent unrealistic effects in the evaporator response.

A CONTROL SCHEME TO COUNTERACT OSCILLATIONS

The Orange, Texas, evaporator system is controlled by a PI analog controller whose task is to maintain a nearly constant pressure in the steam chest of the first effect. Since this type of controller does not make use of the error in concentration of strong black liquor as its feedback signal, it can neither maintain the concentration of strong black liquor within a small range, nor attenuate any oscillations arising from the opposing effects of the temperature and concentration of the strong black liquor on evaporator heat transfer coefficients. Figure 12 gives the results of a simulation of the strong black liquor concentration from the first effect with heat transfer coefficient parameters $\alpha_T = 0.05$ and $\alpha_C = -4.0$. The input disturbance to the system was a step change of one per cent (15.0% to 16.0%) in the concentration of weak black liquor occurring at a time of one minute. It may be seen that the concentration of strong black liquor oscillates with a period of about 28 minutes, and varies in the range 45.2% - 48.8%. Figure 13 presents results similar to Figure 7 for the Orange Texas Plant.

A PI feedback control loop from strong black liquor concentration as used in our proposed digital control scheme can be shown to be sufficient to attenuate the resulting oscillations. For this example, a PI control loop which varies the mass flow rate of weak black liquor as a function of strong black liquor concentration was used. Figure 14 gives the resulting simulation of strong black liquor concentration when such a PI feedback control loop is added to the Orange, Texas evaporator system. The input disturbance is again a step change from 15% to 16% in the concentration

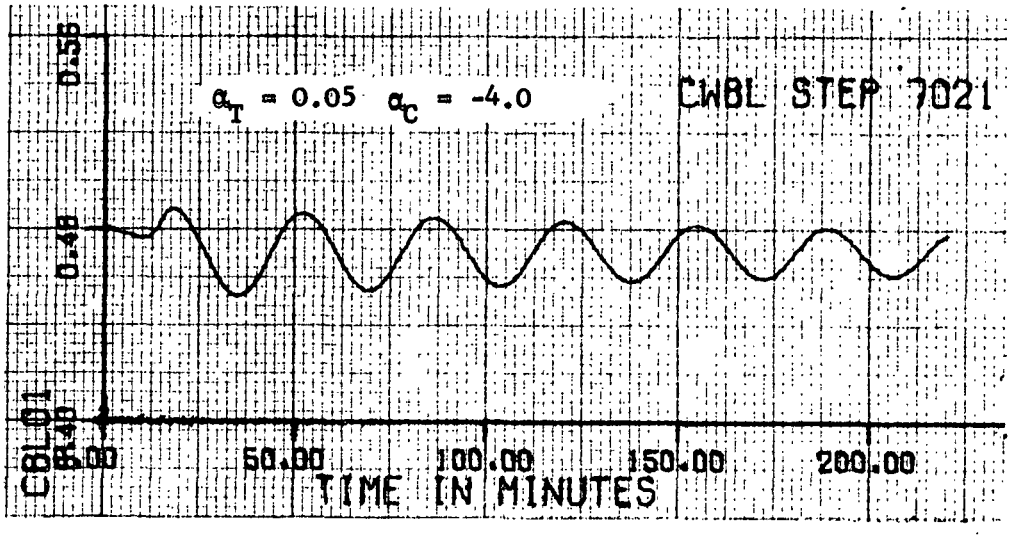

CONCENTRATION OF STRONG BLACK LIQUOR

CONCENTRATION OF WEAK BLACK LIQUOR

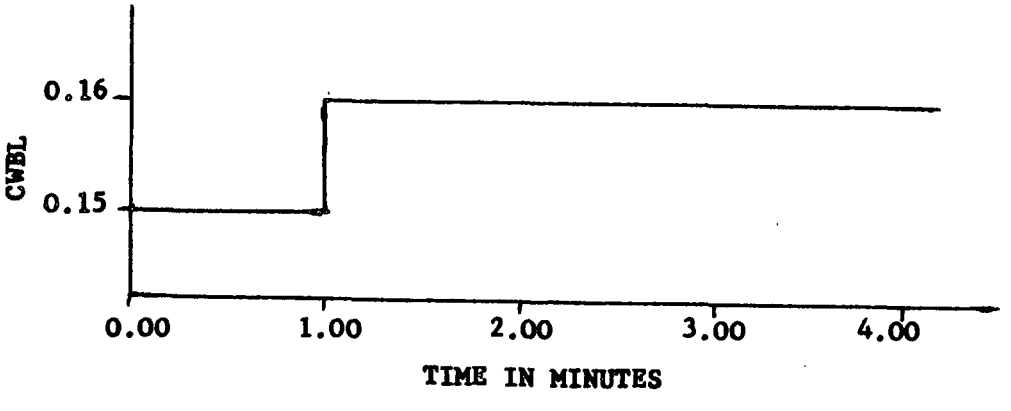

FIGURE 12

SIMULATION OF ORANGE, TEXAS, EVAPORATOR SYSTEM
WITHOUT THE PROPOSED FEEDBACK CONTROL LOOP

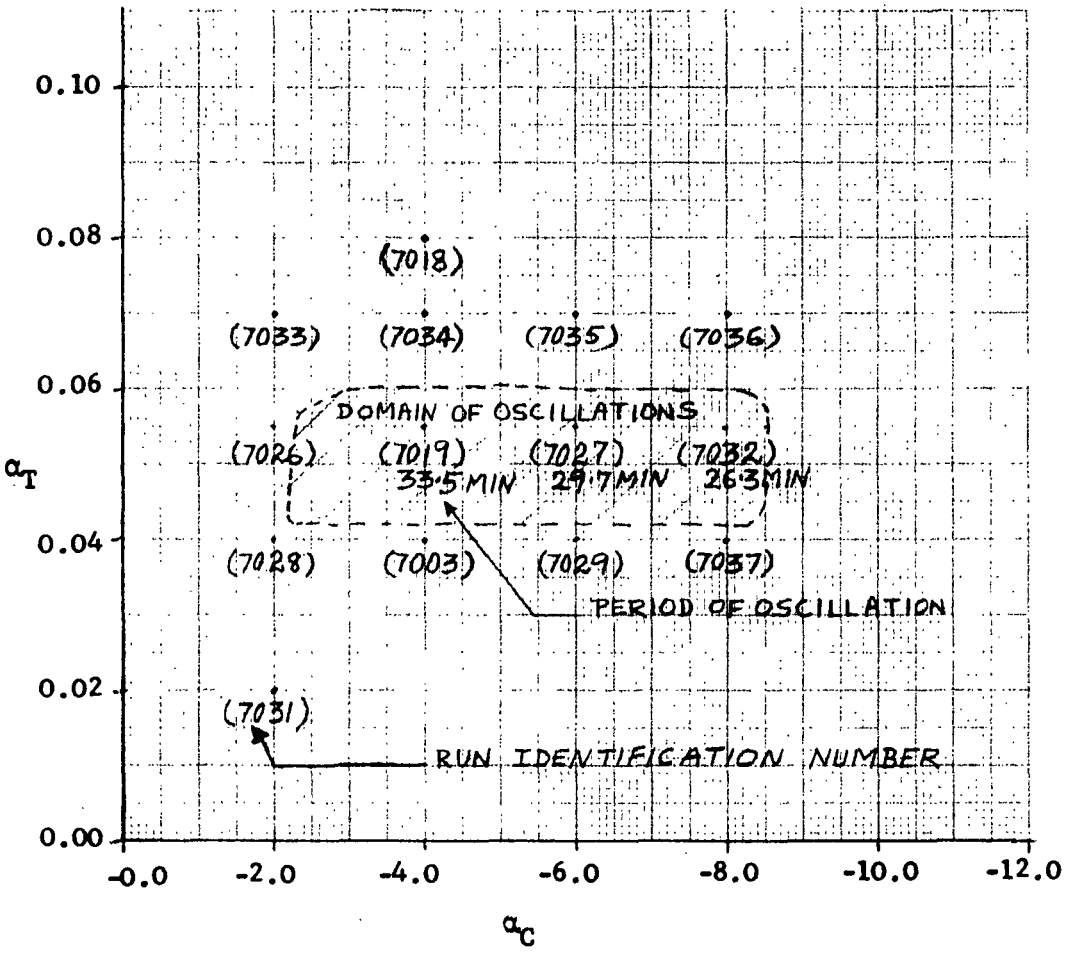

FIGURE 13

DOMAIN OF HEAT TRANSFER COEFFICIENTS

PARAMETERS α_T AND α_C FOR ORANGE, TEXAS, EVAPORATOR SYSTEM

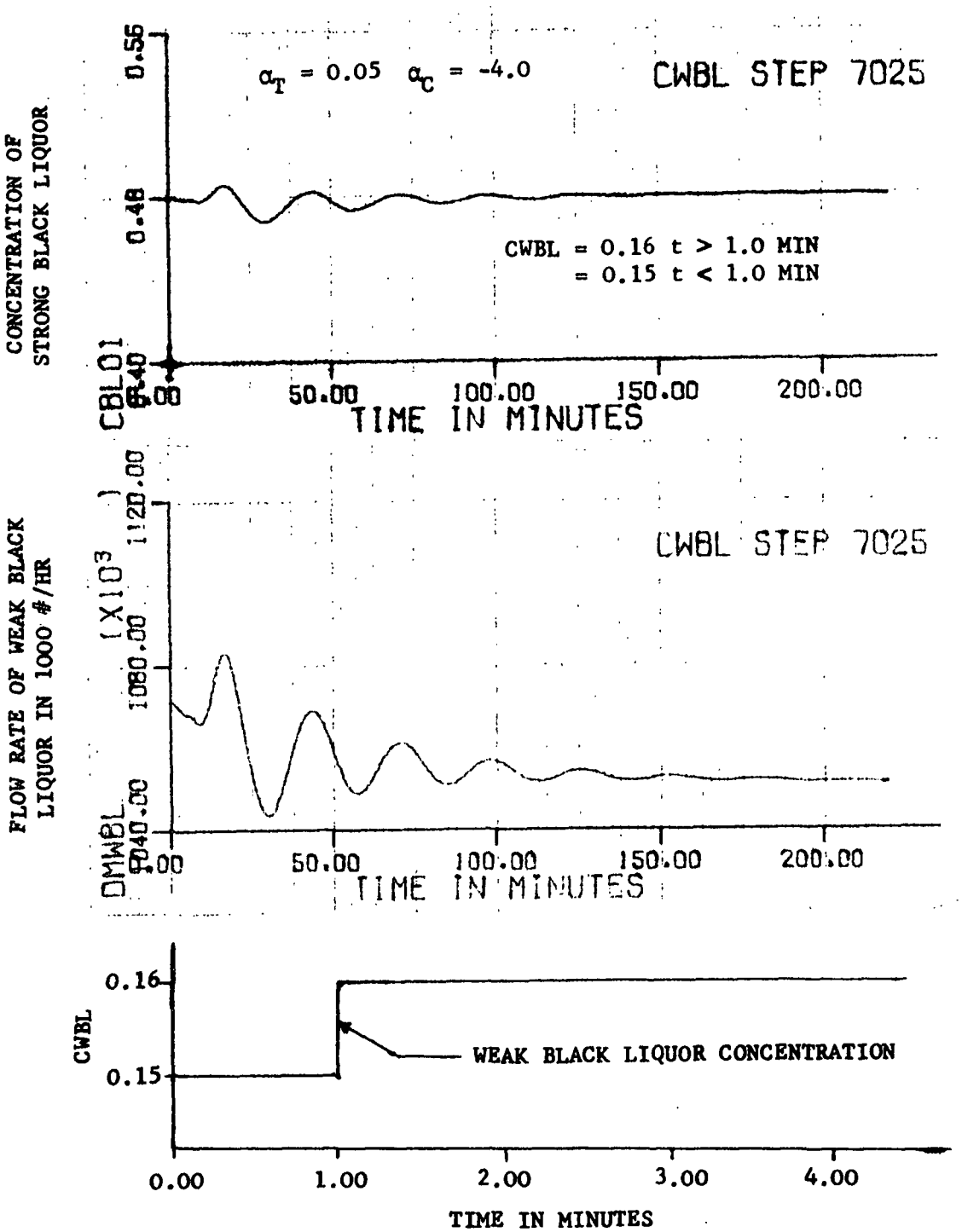

FIGURE 14

SIMULATION OF ORANGE, TEXAS, EVAPORATOR SYSTEM

WITH THE PROPOSED FEEDBACK CONTROL LOOP

of weak black liquor occurring at a time of one minute, i.e.,the same as the disturbance for the simulation of Figure 12. It is seen that strong black liquor concentration is heavily damped, and any oscillations present die out within a very few cycles. Moreover, the range of variation of strong black liquor concentration is 47.8% - 48.6%, a considerable reduction from 45.2% - 48.8% for the system without the proposed feedback control loop.

It may be recalled that the control schemes proposed in the final project report [11] do include a feedback control loop from strong black liquor concentration, and therefore the oscillations in strong black liquor concentration, if any, will be damped out by the feedback control loops.

REFERENCES CITED

1. Perry, J. H., Chemical Engineers Handbook, pp. 11-24 to 11-42, McGraw-Hill, Inc., New York, N.Y., 1963.

2. Badger, W.L., and Banchero, J.T., Introduction to Chemical Engineering, pp. 177-243, McGraw-Hill, Inc., New York, N.Y., 1955.

3. Standiford, F.C., "Evaporation," Chemical Engineering, Vol. 70, No. 25, pp. 159-176, December 9, 1963.

4. Bergstrom, R.E., and Kleinman, G., "Concentration of Black Liquor, Chemical Recovery in Alkaline Pulping Processes," TAPPI Monograph Series No. 32, Edited by Whitney, R.P., 1968.

5. Andre, H., and Ritter, R.A., "Dynamic Response of a Double Effect Evaporator," Can.J.Ch.E., Vol. 46, pp. 259-264, August 1968.

6. Galtung, F.L., and Williams, T.J., "A Survey of the Status of the Mathematical Modeling of the Chemical Recovery Section of a Kraft Paper Mill," Purdue Laboratory for Applied Industrial Control, Report Number 23, July 1969.

7. Koistinen, R., "Haihduttamon Dynaaminen Malli," Chapter IX, Publication No. 13-69, Educational Center of Finnish Engineering Societies, Helsinki, 1969.

8. Vyukov, I.E., Makarov, V.F., and Righinashvili, G.H., "Mathematical Model of an Evaporator Unit of Sulphate Cellulose Plant," Proceedings of All Union Scientific Research Institute of Paper Industry, Vol. 54, pp. 30-40, 1969. (The reference has been translated here from Russian.)

9. Wills, W.R., "Experimental and Theoretical Studies of Long Tube Vertical Evaporators," Svensk Papperstidning, årg 67, No. 11, pp. 457-466, 15 June 1964.

10. McAdams, W.H., Heat Transmission, McGraw-Hill, Inc., New York, N.Y., pp. 294-338, 1942.

11. Project Staff, "The Multi-Effect Evaporator Control System," pp. 52-77, and "A Dynamic Model of the Multi-Effect Evaporator," pp. 203-224, in Systems Analysis of Chemicals and Energy Recovery in Sulphate Pulping, IPC Report No. 3, PLAIC Report No. 45, 1971.

12. Gundmundson, C., and Olauson, L., "Harmful Pulsation Phenomenon in a Climbing Film Evaporator with Superheated Feed," Svensk Papperstidning, årg 74, No. 7, pp. 197-200, 15 April 1971.

SECTION IV

A MATHEMATICAL MODEL OF THE LIQUOR PREPARATION SYSTEM AND A PROPOSAL FOR ITS AUTOMATIC CONTROL

INTRODUCTION

The primary functions of the liquor preparation system within the kraft pulping chemical recovery process may be summarized as follows:

1. To produce a clarified white liquor at the required flow rate and concentration consistent with pulp production requirements.

2. To separate, wash, and dewater calcium carbonate ($CaCO_3$) mud to prepare it for calcination.

In a typical liquor preparation system, the first function is performed by a causticizing reaction between slaked lime ($Ca(OH)_2$) and the sodium carbonate (Na_2CO_3) recovered in the smelt from the furnace. The second function is typically performed by a series of unit operations involving mechanical separations such as gravity settling or filtration or a combination of these. The system modeled in this study involves a combination of gravity settling and filtration.

The model is used to find out which variables in the system are the most critical for a dynamic control scheme for improving the performance of the kraft recovery system.

A flow diagram for a typical kraft pulp mill liquor preparation system is shown in Figure 1. The smelt production of the recovery furnace is the primary input variable for this system. The smelt is dissolved

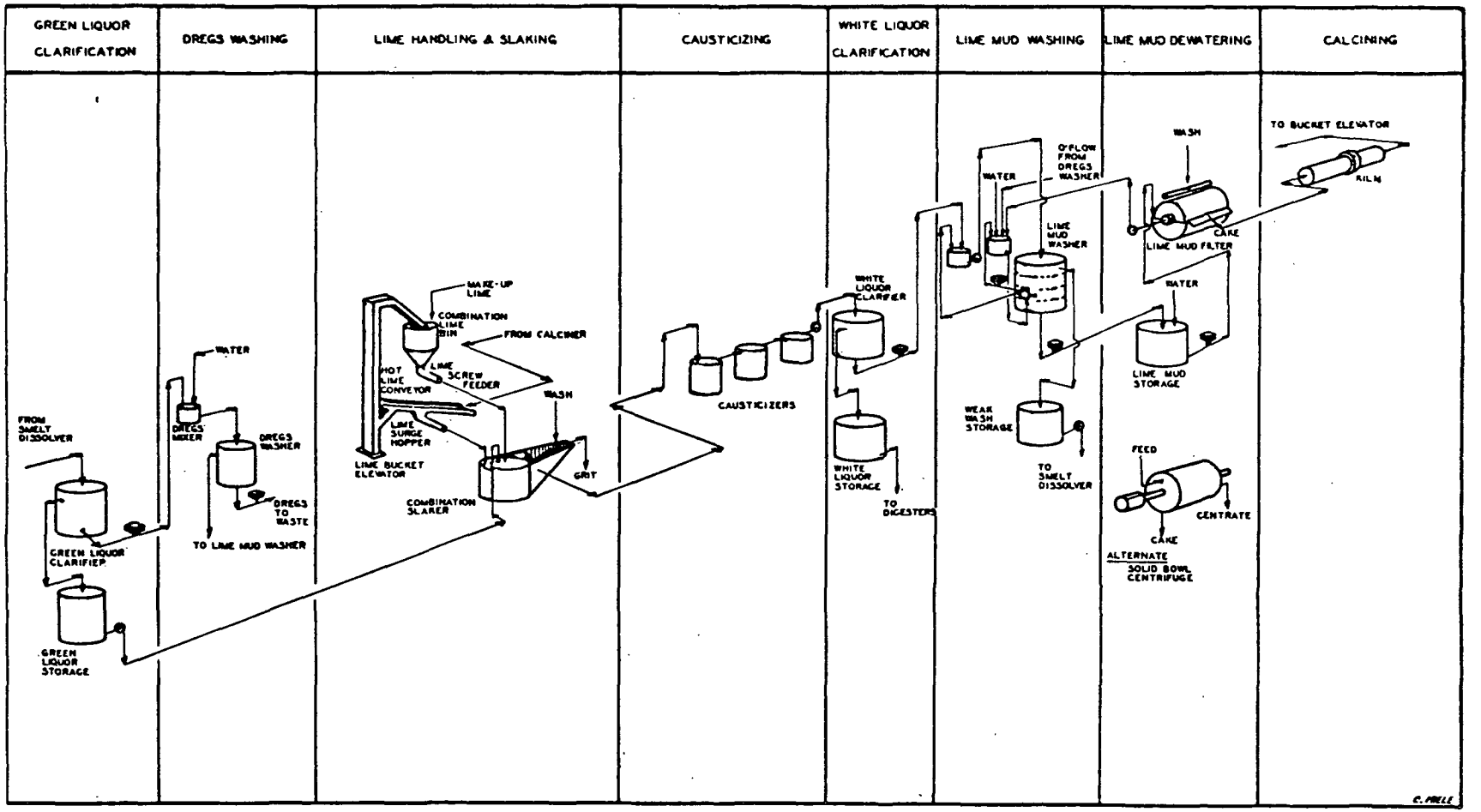

Unit operations flowsheet—conventional kraft mill recausticizing system.

FIGURE 1

to make green liquor and is transferred via density control to a clarifier. Green liquor is made up primarily of sodium carbonate (Na_2CO_3) and sodium sulfide (Na_2S) and some suspended solids such as carbon particles, iron compounds, and pieces of refractory lining, which are all picked up by the smelt in the recovery furnace. These suspended solids, which are called dregs, are removed in the green liquor clarifier. From the clarifier, the green liquor is pumped to a storage tank. From the storage tank it is transferred via flow and temperature control to slaking/causticizing.

Reburned and make-up lime (CaO) is added to the green liquor in the slaker. The subsequent causticizing reaction forms sodium hydroxide (NaOH) from the Na_2CO_3 to make white liquor for the cooking of wood chips in the digester. From causticizing, the raw white liquor is pumped to the white liquor clarifier where the $CaCO_3$ precipitate formed in the causticizing reaction settles out. The clarified white liquor is transferred to white liquor storage for use in the digester.

The underflow $CaCO_3$ from the white liquor clarifier is mixed with dilute filtrate and fresh water and transferred to the $CaCO_3$ mud washer settler. The overflow from the mud washer is called weak wash. The weak wash is recycled for the dissolving of the smelt to form green liquor. The underflow from the mud washer is stored and then dewatered and washed on a pre-coat filter. The $CaCO_3$ cake is conveyed to the calciner (usually a lime kiln) where CO_2 is driven from the $CaCO_3$ to form CaO (reburned lime) for recycling to slaking/causticizing.

SLAKING/CAUSTICIZING

The purpose of the slaking/causticizing process is to convert the Na_2CO_3 in the green liquor to sodium hydroxide (NaOH) to produce white liquor. The reaction proceeds in two stages. The first stage reaction, known as slaking, involves the addition of quicklime (CaO) to green liquor where it reacts with the water to form calcium hydroxide ($Ca(OH)_2$) and heat. The reaction equation is as follows:

$$CaO + H_2O \longrightarrow Ca(OH)_2 + 486 \text{ B.t.u. per lb. CaO} \qquad (1)$$

In the second stage, the $Ca(OH)_2$ which was formed in slaking reacts with Na_2CO_3 as written in the following chemical equation:

$$Ca(OH)_2 + Na_2CO_3 \overset{K}{\rightleftharpoons} 2\ NaOH + CaCO_3 \qquad (2)$$

Although the reactions are written in two stages, they actually overlap because part of the causticizing occurs almost coincidentally with the slaking. The causticizing reaction is reversible and thus proceeds in either direction depending upon the relative concentrations of the reactants and products. Because the $CaCO_3$ is less soluble than the $Ca(OH)_2$, the causticizing reaction proceeds to the right. However, because of the reversibility, all of the Na_2CO_3 cannot be converted to NaOH regardless of the amount of lime used. The extent of conversion is called the causticizing efficiency (C.E.) and is defined as

$$C.E. = \frac{NaOH}{NaOH + Na_2CO_3} \times 100\% \text{ (expressed as } Na_2O) \qquad (3)$$

The causticizing efficiency depends on the concentration of sodium compounds in the green liquor entering the slaker. Lower concentrations produce higher conversion, because in stronger solutions the NaOH progressively reduces the solubility of $Ca(OH)_2$. This continues until there are not enough calcium ions present to exceed the solubility limit of $CaCO_3$.

The slaking/causticizing reaction occurs in a series of four stirred tank reactors. The first is called the slaker. Quicklime is added to the green liquor in the slaker to form $Ca(OH)_2$. The slaking reaction occurs almost instantaneously compared to the causticizing reaction. The slaker has a retention time of about ten minutes. The three causticizing tanks have retention times of 30 to 40 minutes each.

In the course of development of the slaking/causticizing model, several approaches were attempted. The first approach tried was essentially like the one described in Reference(1)in which a chemical kinetic model of slaking and causticizing was used for each of the four tanks. That is, a set of five differential equations involving mass flow dynamics and chemical kinetics was solved simultaneously in each of the four tanks. Each tank also had a differential equation for temperature. This model gave satisfactory results, but the amount of computation time involved was substantial because of the small step size required for the slaking reaction and because of the complexity of the differential equations. This type of model would be satisfactory if one wanted to conduct a more detailed study of slaking/causticizing per se, but that is not the objective in the present study. Rather, the goal is to model the overall liquor preparation system.

The second approach tried was to assume that the causticizing reaction was diffusion limited (which it actually is because the reaction progresses depending on the solubilities and relative concentrations of the reactants and products). A set of differential equations describing only the chemcial kinetics of slaking and causticizing was solved until chemical equilibrium was reached, and the results were used as inputs to a flow dynamic model of the causticizing tanks.

The kinetic equations are given as follows:

$$\frac{d\left[X_{CaO}\right]}{dt} = -K_1 X_{CaO} \tag{4}$$

$$\frac{d\left[X_{Ca(OH)_2}\right]}{dt} = K_1 X_{CaO} - K_{2r} X_{Ca(OH)_2} X_{Na_2CO_3} + K_{21} X^2_{NaOH} X_{CaCO_3} \tag{5}$$

$$\frac{d\left[X_{Na_2CO_3}\right]}{dt} = -K_{2r} X_{Ca(OH)_2} X_{Na_2CO_3} + K_{21} X^2_{NaOH} X_{CaCO_3} \tag{6}$$

$$\frac{d\left[X_{NaOH}\right]}{dt} = 2K_{2r} X_{Ca(OH)_2} X_{Na_2CO_3} - 2K_{21} X^2_{NaOH} X_{CaCO_3} \tag{7}$$

$$\frac{d\left[X_{CaCO_3}\right]}{dt} = K_{2r} X_{Ca(OH)_2} X_{Na_2CO_3} - K_{21} X^2_{NaOH} X_{CaCO_3} \tag{8}$$

where:

X_{CaO} = Concentration of CaO, moles/liter

$X_{Ca(OH)_2}$ = Concentration of $Ca(OH)_2$, moles/liter

$X_{Na_2CO_3}$ = Concentration of Na_2CO_3, moles/liter

X_{NaOH} = Concentration of NaOH, moles/liter

X_{CaCO_3} = Concentration of $CaCO_3$, moles/liter

K_1 = Rate constant for slaking reaction

K_{2r} = Rate constant for right-directed causticizing reaction

K_{21} = Rate constant for left-directed causticizing reaction

This approach gave good results but was unsatisfactory because 50 to 100 iterations of the kinetic model were required for each step in the flow model.

The final approach was to assume that the slaking reaction occurred instantaneously relative to the causticizing reaction, and that the causticizing reaction was diffusion limited. This approach is similar to that of Glazunov (2). The equilibrium causticizing condition is solved for, using a simple steady state approach. The following simplifying assumptions were made for the approximate model:

1. Perfect mixing.
2. Slaking reaction occurs instantaneously relative to causticizing.
3. Causticizing reaction is diffusion limited.
4. Only slaking and causticizing reactions occur.
5. The slaking and causticizing tank temperatures do not deviate more than $\pm 10°$ F. from their nominal values. (See Figure 2.)
6. Steam flow added to heat green liquor equals water evaporation rate in slaking/causticizing.
7. Heat loss because of radiation and convection is negligible.
8. Energy input because of agitation is negligible.
9. No losses of material.

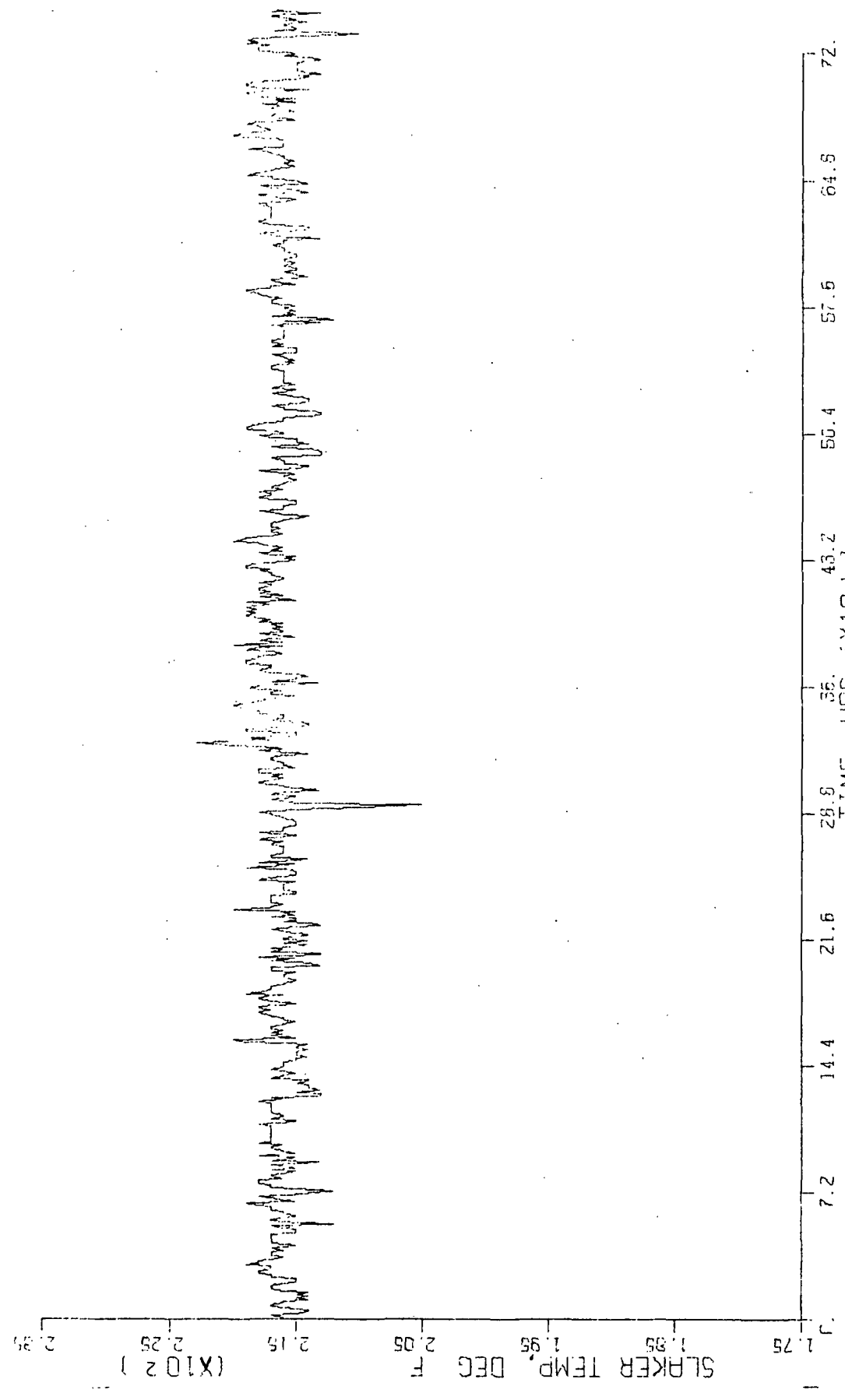

FIGURE 2. ACTUAL ONE-MONTH HISTORY FOR SLAKING/CAUSTICIZING TEMPERATURE

(OWENS-ILLINOIS, ORANGE, TEXAS; JAN. '72)

From Equation (2), one can derive the steady state equation for the equilibrium causticizing condition. Let the concentrations of $Ca(OH)_2$, Na_2CO_3, NaOH, and $CaCO_3$ be denoted by $X_{Ca(OH)_2}$, $X_{Na_2CO_3}$, X_{NaOH}, and X_{CaCO_3}, respectively. Suppose that in the green liquor entering causticizing we have

$$X_{Ca(OH)_2} = a \text{ moles/liter*}$$

$$X_{Na_2CO_3} = b \text{ moles/liter}$$

$$X_{NaOH} = c \text{ moles/liter}$$

$$X_{CaCO_3} = d \text{ moles/liter} \qquad (9)$$

Then, when equilibrium has been reached, we have

$$X_{Ca(OH)_2} = a - n \text{ moles/liter}$$

$$X_{Na_2CO_3} = b - n \text{ moles/liter}$$

$$X_{NaOH} = c + 2n \text{ moles/liter}$$

$$X_{CaCO_3} = d + n \text{ moles/liter} \qquad (10)$$

---

*Concentration is expressed in moles per liter because of the extreme simplicity of using the numbers expressed in these units when solving the chemical equations. Conversion to concentration in terms of pounds per cubic foot is simply made by multiplying the concentration in moles per liter as follows:

$$\frac{LB}{FT^3} = \left[\frac{28.32}{454.}\right] \left[\text{molecular weight}\right] \left[\frac{MOL}{LIT}\right] \qquad (11)$$

If further conversion to mass fraction in LB/LB is desired, simply multiply the concentration in pounds per cubic foot by the ratio of the total volumetric flow rate (Q, FT^3/HR) and the total mass flow rate (W, LB/HR) as follows:

$$\frac{LB_x}{LB_{tot}} = \left[\frac{Q}{W}\right] \left[\frac{LB}{FT^3}\right] . \qquad (12)$$

where n is the number of moles of each constituent that has been used up or generated in the causticizing reaction for each liter of solution. Further more, we know that at equilibrium:

$$K_e = \frac{(X_{NaOH})^2(X_{CaCO_3})}{(X_{Na_2CO_3})(X_{Ca(OH)_2})} \tag{13}$$

where K_e is the equilibrium constant for the causticizing reaction. Data on the equilibrium constant has been gathered by several investigators. The most comprehensive work has been done by Kobe and Wilkinson (3). They show that K_e is strongly dependent on the dissolved chemical concentration (particularly Na_2CO_3) of the green liquor. Their data, modified somewhat by actual operating data (See Figure 3 and Reference (2)), indicate that a linear regression can be made of K_e on the total titratable alkali (TTA)* over the practical operating region. The relationship which yields good results when compared to operating data is

$$K_e = 400 - 40(TTA) \tag{14}$$

The effect of temperature on K_e follows the Van't Hoff Equation:

$$\frac{d(\ln K_e)}{dt} = \frac{\Delta H}{RT^2} \tag{15}$$

where ΔH is the heat of the causticizing reaction at the absolute temperature T, and R is the universal gas constant. In the causticizing reaction, the heat of reaction is very small. Therefore, the temperature

*TTA = Na_2CO_3 + NaOH + Na_2S expressed as LB Na_2O/FT^3.

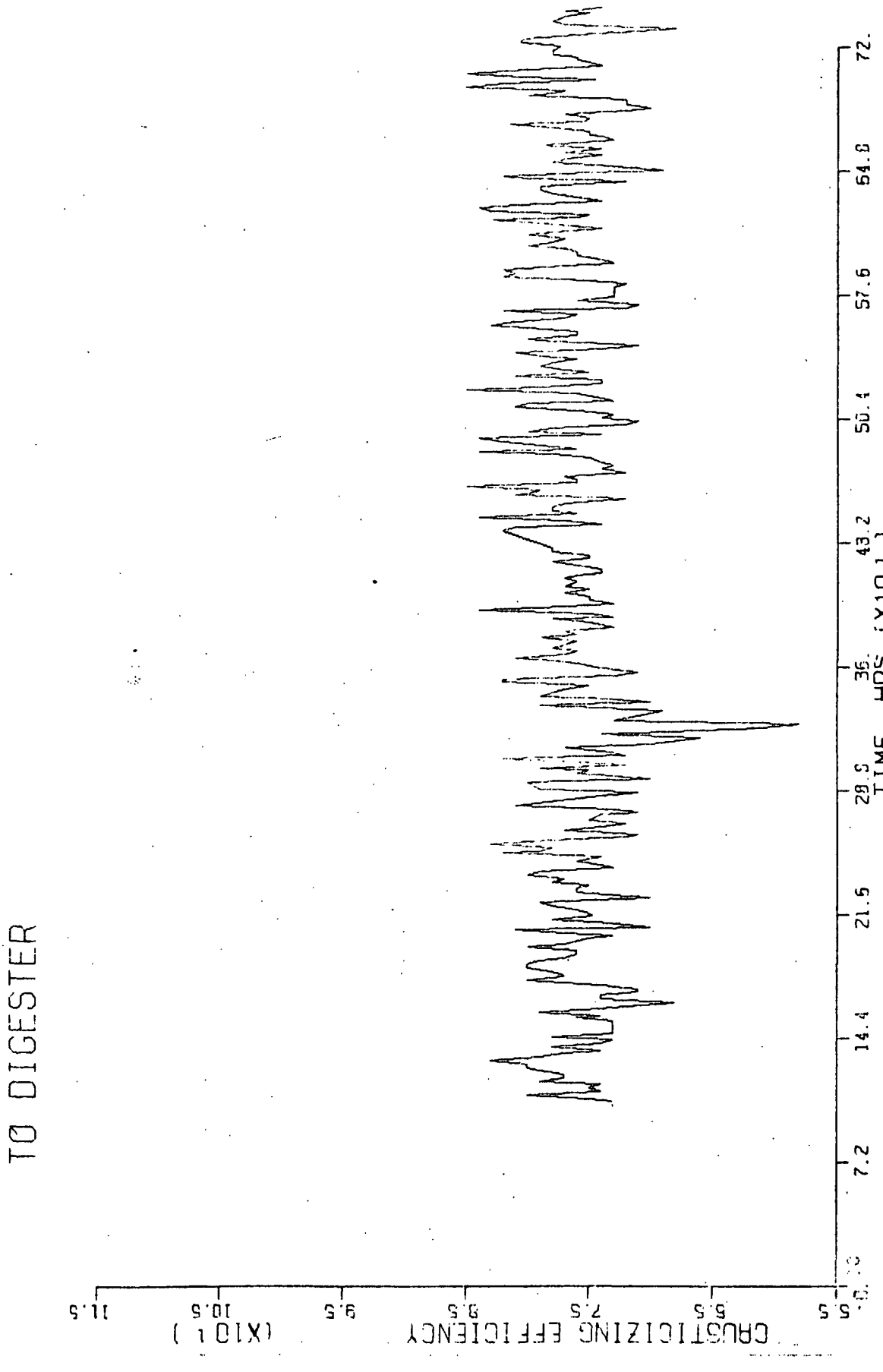

FIGURE 3. ACTUAL ONE-MONTH HISTORY FOR CAUSTICIZING EFFICIENCY

(OWENS-ILLINOIS, ORANGE, TEXAS; JAN. '72)

has only a slight influence on K_e. In addition, as Figure 2 shows, under normal operating conditions, the 2σ limits for the slaking/causticizing temperature is about $\pm 3°$ F. Thus, the effect of temperature on K_e has not been included in this model.

Substituting Equations (10) into Equation (13) yields the following polynomial expression for n:

$$4n^3 + (4c + 4d - K)n^2 + (c^2 + 4cd + K_e\{a + b\})n + (c^2d - K_e ab) = 0 \qquad (16)$$

Because a, b, c, d, and K_e are all known, Equation (16) is solved for n, using the Newton-Raphson Method. The method requires only three to five iterations for each step of the flow dynamic model.

The flow dynamic model is a simple set of linear differential equations. The causticizing tanks are regarded as three serially connected flow-through vessels with ideal mixing. The results of the solution of Equations (10) and (16) are used as inputs to the flow model. Also tracked in the flow model are the concentrations of Na_2S and Na_2SO_4 which do not enter into the slaking/causticizing reaction. The equations for the first tank are

$$\frac{d\left[X^{(out)}_{Ca(OH)_2}\right]}{dt} = \frac{1}{\tau}\left[X^{(in)}_{Ca(OH)_2} - X^{(out)}_{Ca(OH)_2}\right] \qquad (17)$$

where: $\tau = V/Q$, hours

V = Volume of tank, ft^3

Q = Liquor outlet flow rate, ft^3/hr

Equations identical to (10) are written for $X_{Na_2CO_3}$, X_{NaOH}, X_{CaCO_3}, X_{Na_2S}, and $X_{Na_2SO_4}$*. The outputs of the first tank are used as inputs to the second tank, and so on. The flow dynamic equations are repeated three times, one set for each causticizing tank. This gives a total of 18 differential equations for the three tanks, but they are very simple.

An energy balance is done around the entire slaking/causticizing process to keep track of the temperature. The basic equation is given as:

$$mc_p\frac{dT}{dt} = H_{in} - H_{out} \tag{18}$$

where: $H_{in} = W_{CaO_{I_A}} H_1 + W_{T_I} c_p T_I + W_{CaO_I} c_{pCaO} T_{CaO}$, Btu/hr.

$H_{out} = K_2 H_2 \rho_{wl}^2 V X_{Na_2CO_3} X_{Ca(OH)_2} + W_{T_o} c_p T$, Btu/hr.

$W_{CaO_{I_A}}$ = Active or available lime, lb/hr.

W_{CaO_I} = Total lime input flow, lb/hr.

H_1 = Heat of reaction of lime in slaking, Btu/hr.

W_{T_I} = Green liquor input flow, lb/hr.

c_p = Specific heat of green liquor, Btu/lb-°R.

T_I = Temperature of input green liquor, °R.

c_{pCaO} = Specific heat of lime, Btu/lb-°R.

T_{CaO} = Temperature of input lime, °R.

K_2 = Rate constant for right-directed causticizing reaction.

*The complete set of equations is given under "Overall Model."

H_2 = Heat of causticizing reaction, Btu/lb.

ϱ_{wl} = Liquor density, lb/ft^3.

W_{T_o} = White liquor output flow, lb/hr.

T = Slaking/causticizing temperature, °R.

m = Mass of material in slaking/causticizing, lb.

The "activity" or "availability" of the lime being used in slaking/causticizing is a very important consideration. When $CaCO_3$ is calcined, the particles are somewhat porous because of the emission of CO_2. Hence, water can penetrate the particles more readily in slaking. If the CaO is not completely burned, the porosity may not develop as well, which would tend to slow down the slaking reaction. If the CaO is burned at too high a temperature, its porosity is greatly diminished; and slaking will be slow, or it may effectively stop. Therefore, when the lime is being metered into the slaker, the availability or activity of the lime must be taken into consideration. This aspect of slaking/causticizing will be discussed further in the section on controllers.

SOLIDS SETTLING MODEL

Another aspect of the slaking/causticizing process which is just as important as the causticizing conversion, from a practical point of view, is the settleability of the $CaCO_3$ precipitate (lime mud) produced (References 4, 5, 6, 7, 10). To begin with, the settling rate of the lime mud has a direct effect on the white liquor clarity. Secondly, because lime recovery (calcining) is an integral part of the liquor preparation system, particularly the slaking/causticizing process, the degree of preparation of lime mud for calcining is ultimately reflected back to the slaking/causticizing process. The degree of preparation is mainly dependent upon the lime mud particle size.

Fine particle lime mud is difficult to wash and dewater. This is a critical problem because proper preparation of lime mud in terms of caustic soda removal and moisture removal is required prior to calcining. The caustic soda content of the mud must be reduced to a low level (usually less than 1% soda as Na_2O), or severe ring and ball formation will occur in the mud reburning process. Typically, the lime mud is washed in sedimentation unit similar to the white liquor clarifier. Finally, the poor-settling mud is transferred to a vacuum pre-coat filter. This filter does the final washing and dewatering of the lime mud. As mentioned previously, there is a strong relationship between settleability and lime mud particle size, the smaller particles being harder to settle. These small particles have a larger specific surface area which increases the filtration resistance. Therefore, the vacuum dewatering process is retarded, and the shower water spplied cannot penetrate the cake properly. Hence the kiln receives a mud that has a higher moisture content and a higher soda content.

The lime mud free settling rate can be approximated by using Stoke's Law. It assumes slow settling speeds, viscous friction between the mud particles and the liquid, and independent settling of spherical particles of up to 0.1 mm. in diameter. These stipulations generally agree with the conditions occurring in areas of free settling in lime mud settlers. Stoke's Law is stated as

$$u = Kg \frac{D^2(\rho_s - \rho_l)}{\mu} \tag{19}$$

where

D = Particle diameter (ft)

g = Acceleration of gravity (ft/sec^2)

u = Settling rate (ft/sec)

μ = Viscosity of the liquid (lb/ft-sec)

ρ_s = Density of dry suspended solids (lb/ft^3)

ρ_l = Density of the clear liquid (lb/ft^3)

As Equation (19) shows, the particle size has a strong influence on the settling rate.

In the dynamic modeling of the settler unit operation, two methods of defining the mud particle size, based on the conditions in causticizing and in calcining, were investigated. The first method was to consider causticizing as a crystallization process where the $CaCO_3$ particles grow at a rate dependent on the concentration and temperature of the causticizing solution. However, very little data are available in the literature as to the applicability of a crystallization model in causticizing, while a considerable wealth of empirical and laboratory data is available regarding the dependence of free settling velocity on several parameters

in causticizing and calcining. A particle size is easily inferred from free settling velocity by using Stoke's Law.

Several authors have dealt with the problem of determining the effects of different variables in slaking, causticizing, and calcining on the mud free settling velocity (6, 8, 9 and 10). Figures 4 through 8 show the results of experiments conducted by K. Kinzner (6). By comparison with the data obtained by other investigators, it can be safely assumed that the general relationships established by Kinzner in these curves are correct. However, the liquor samples he used were taken from a Kraft pulp mill recovery system for straw pulping. Straw has about the same lignin content as hardwood, but has a higher silica content than wood. Silica will generally result in smaller mud particles and thus poorer mud settleability. Thus, it is likely that Kinzner's curves show less sensitivity to some of the causticizing and calcining variables than curves derived from non-straw pulping recovery systems. In any event, it is recommended that separate experimentation be conducted at each individual pulp mill site where a solids settling model of this type is intended to be used. According to Kinzner's technique, the experimental effort required is small. Figure 4 shows the effect of causticizing time and temperature on the lime mud free settling velocity. It is evident from Figure 4 that the longer causticizing times result in a slower settling mud, probably because the added agitation decreases the flocculated particle size. That increased amounts of agitation in causticizing are detrimental to mud settling

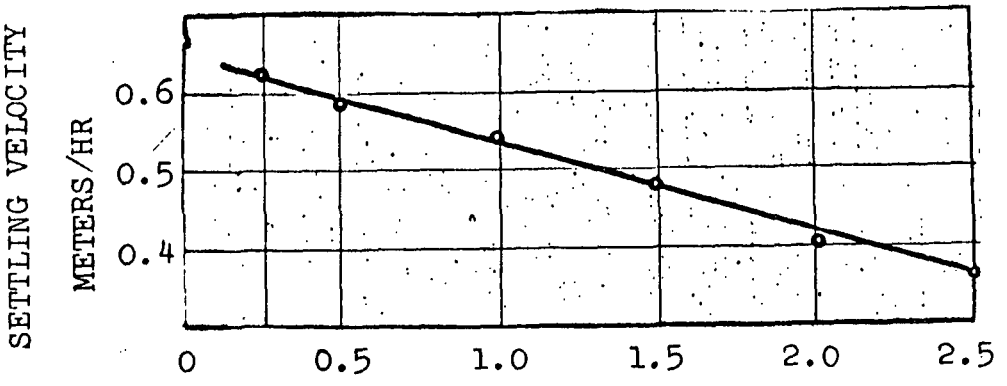

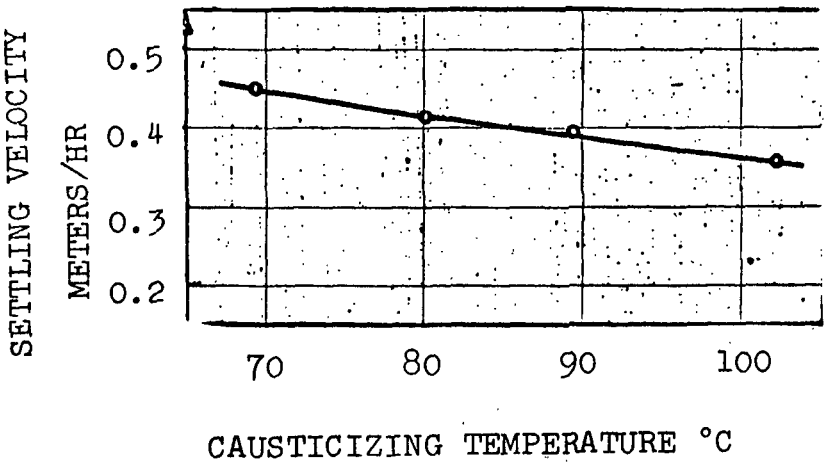

FIGURE 4

EFFECT OF CAUSTICIZING TIME AND TEMPERATURE ON LIME MUD SETTLING VELOCITY

has been established by Dorr and Bull (9) and Knowles (10). The top graph of Figure 5 shows the effect of overliming. Too much lime is detrimental to the settling rate. Evidently, overliming produces fine particles of CaO and $Ca(OH)_2$ in the causticized liquor which do not settle out readily. The bottom graph of Figure 5 shows the effect of changing the proportion of the green liquor flow being added to the slaker (the remainder being added directly to the classifier). The proportion added to the slaker is rarely below 40% in practice. Figure 6 shows the effect of the green liquor concentration (entering the slaking/causticizing reaction) on the mud settling velocity.

Calcining has a substantial effect on the size and structure of the lime mud particle. The effect of the CaO particle size on the settling rate of $CaCO_3$ has been established by Olsen and Direnga (8). In general, the larger the CaO particle entering slaking/causticizing, the faster the settling of the $CaCO_3$. The results shown in Figures 7 and 8 indicate agreement with the results of Olsen and Direnga. That is, that calcining time and temperature affect the CaO particle size which in turn affects the $CaCO_3$ particle size and its settling characteristics. The very large calcining temperature and calcining time results in a larger, more dense, CaO particle, as indicated by Figures 7 and 8. It should be noted that in practice a calcining temperature much above 2000°F. ($\cong$ 1100° C.) will result in a lime particle that is too dense and too large to slake properly. The classifier rejects (grits) increase when calcining at a higher temperature. Thus, the lime losses

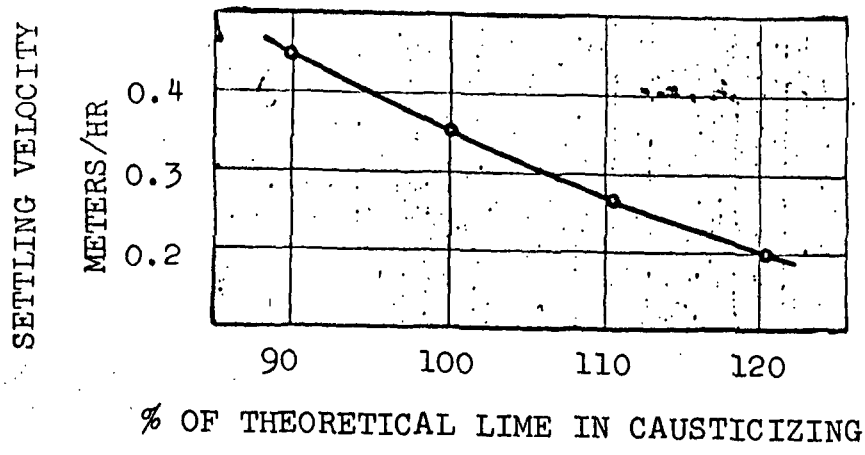

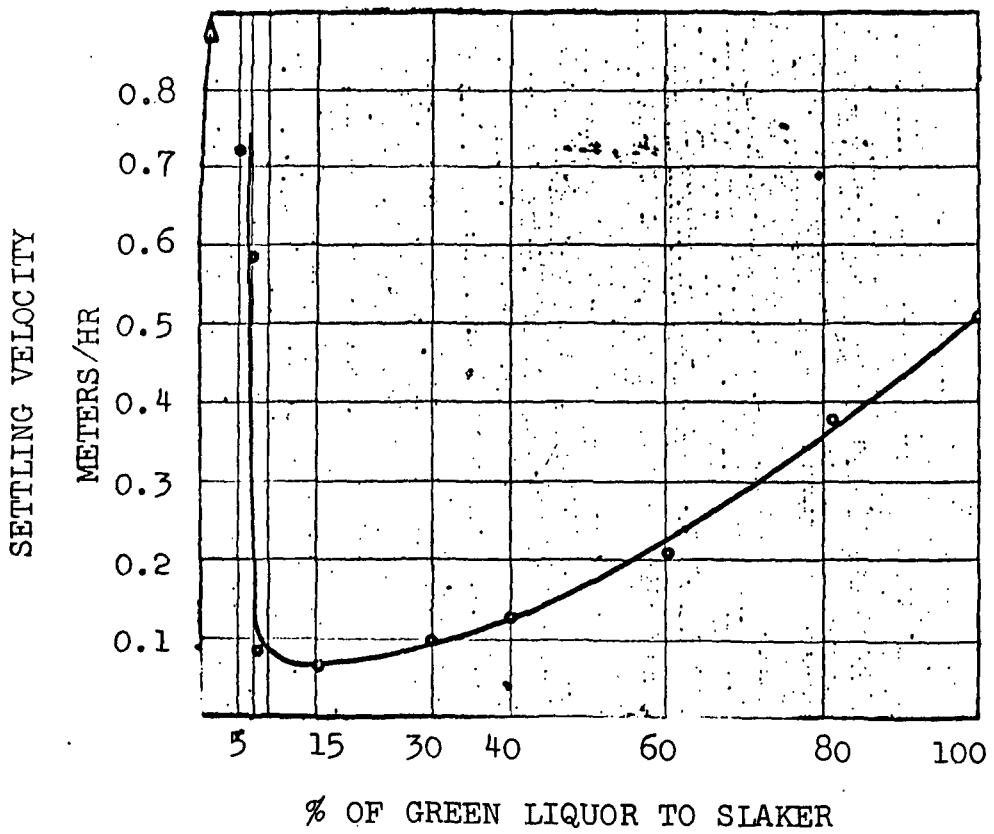

FIGURE 5

EFFECT OF LIME QUANTITY AND GREEN LIQUOR QUANTITY ON LIME MUD SETTLING VELOCITY

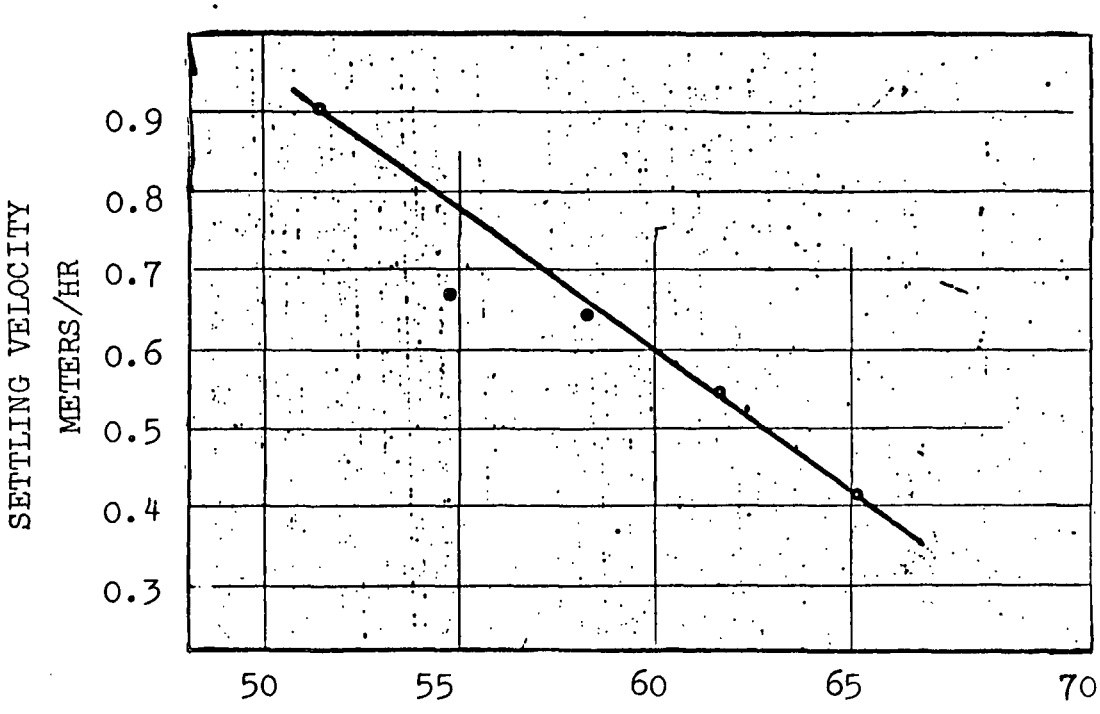

FIGURE 6

EFFECT OF GREEN LIQUOR CONCENTRATION

ON LIME MUD SETTLING VELOCITY

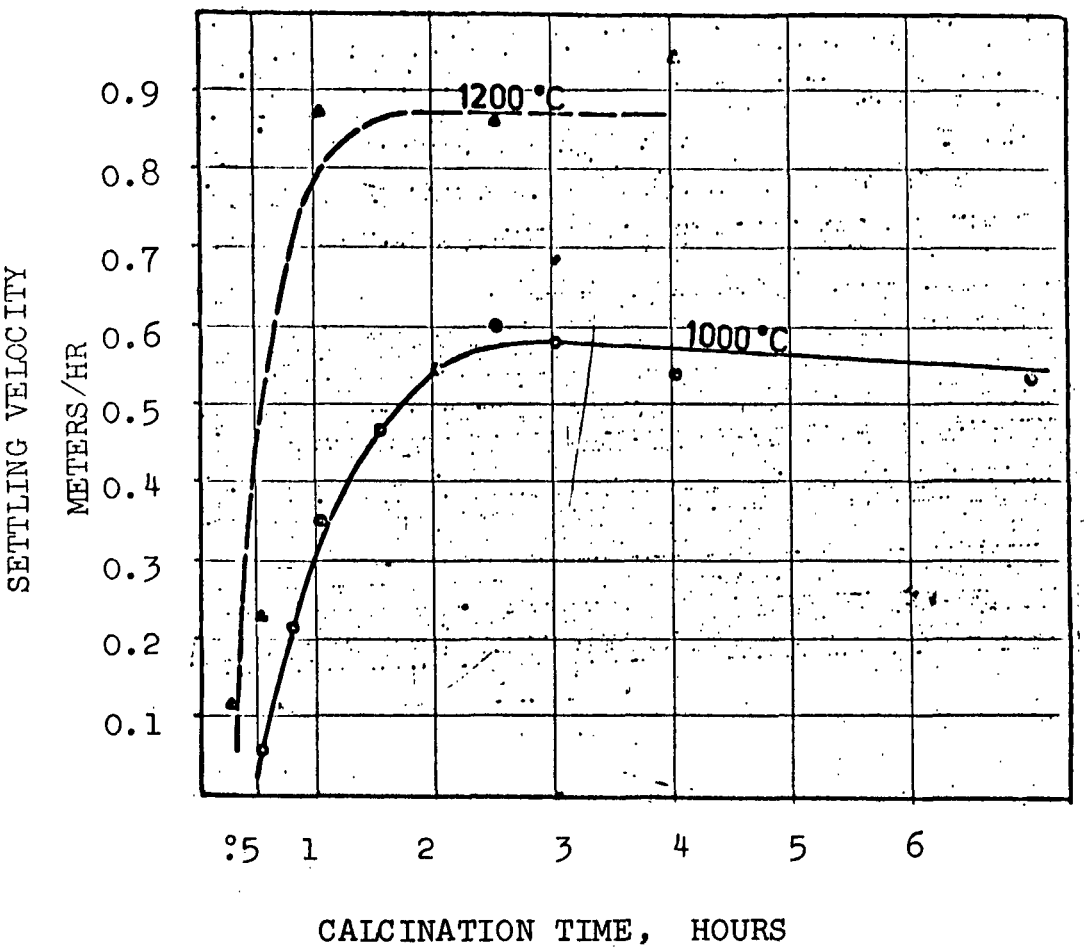

FIGURE 7

EFFECT OF CALCINATION TIME ON

LIME MUD SETTLING VELOCITY

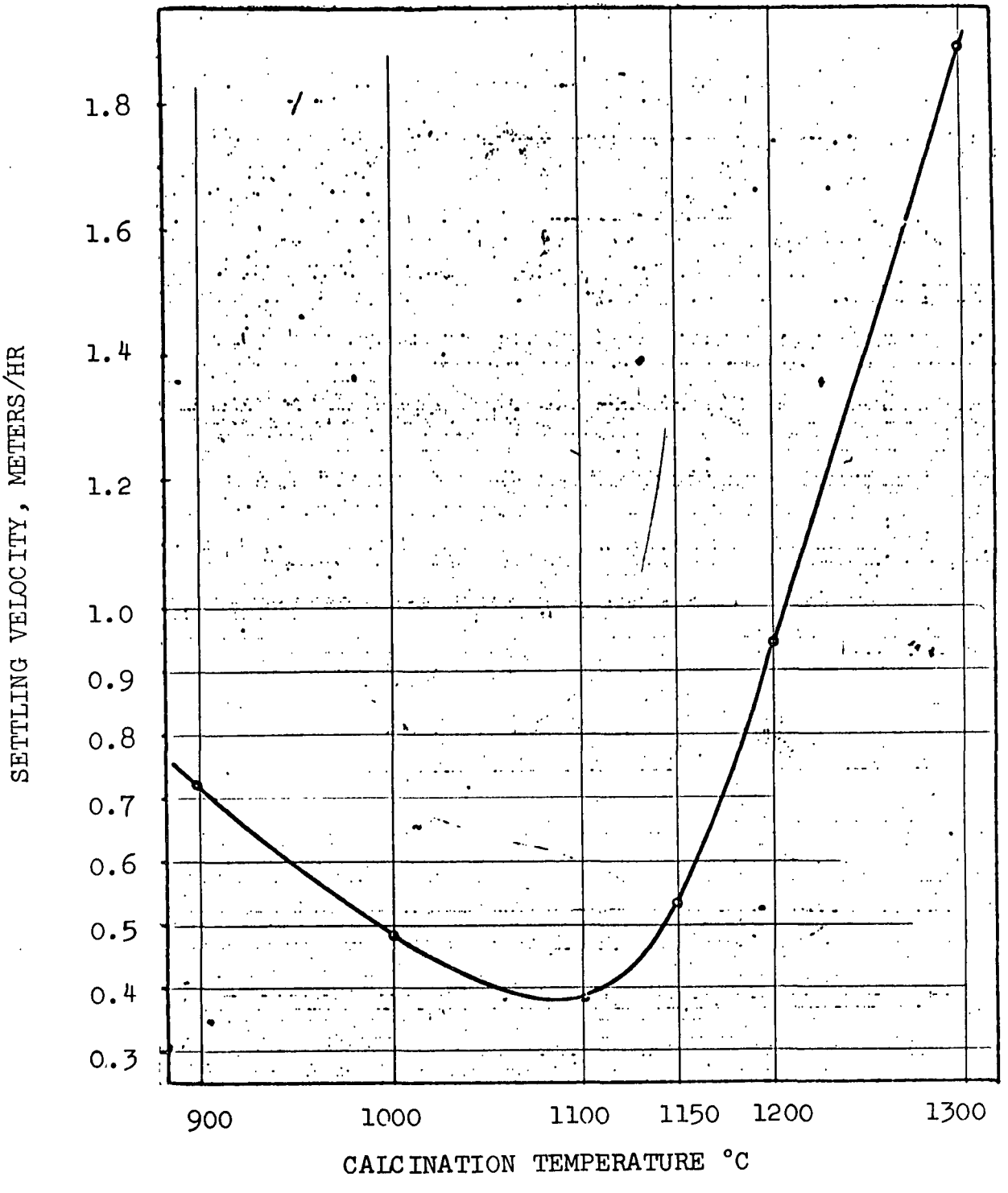

FIGURE 8

EFFECT OF CALCINATION TEMPERATURE

ON LIME MUD SETTLING VELOCITY

are also higher. Therefore, it is recommended to calcine at temperatures between 1800° and 2000°F. (1000° - 1100°C.). (See Figure 8 and Reference (7).)

Therefore, by using the data as given in Figures 4 through 8, one can establish a regression equation for the free settling velocity u_{si}:

$$u_{sim} = f(t_c, T_c, L, G, G_c, t_K, T_K) \tag{20}$$

where

G = Green liquor to Slaker (%)

G_c = Green liquor concentration (gr/liter)

L = Lime quantity (%)

T_c = Causticizing temperature (°C.)

t_c = Causticizing time (hrs)

T_K = Calcining temperature (°C.)

t_K = Calcining time (hrs)

Under normal circumstances, the free settling velocity of the mud as determined from operating data is in the range of 1.25 to 2.00 ft/hr (see Reference (10)). This agrees with the laboratory data obtained by Kinzner (6).

A linear regression model was developed using the data of Figures 4 through 8. Where the relationships are noteably nonlinear, a linear

approximation was made over the normal operating range. In Figure 5, for per cent of green liquor to slaker, the range 40% to 100% was used. In Figure 7, a nominal calcining temperature of 1800° F. (1000° C.) was assumed, and a linear approximation over the 0-2 hour range was made. In Figure 8, linear approximation over the 1650° to 2000° F. (900° to 1100° C.) range was made for the effect of calcination temperature on u_{si}. The resulting linear multiple regression is

$$u_{sim} = 4.73213 - .1155t_c - .00272T_c - .00833L + .00633G - .03629G_c - .00195T_K + .3571t_K \quad (21)$$

where

u_{sim} = free settling velocity, m/hr

$u_{si} = u_{sim}/.3048$, ft/hr

This model produced very good results over a wide range of operating conditions in the overall system simulation which will be discussed later under simulation results.

In the modeling of the settler dynamics, two approaches were attempted. The first was to solve for the solids concentration profile as a two point boundary value problem. However, because of the moving discontinuities in the solids concentration profile (See Reference 11.), the model became too complex and the computation time prohibitive.

The second approach was to use empirical data obtained from settling tests as recommended by Galtung and Williams (1). A very comprehensive study of settling and thickening in kraft recovery systems was conducted by Jernqvist (12, 13, 14, and 15). Jernqvist developed the theory and the necessary experimental data for the settling

of $CaCO_3$ mud using the concept of solids flux. The basic approach is to use actual mud-containing liquor samples in batch settling tests. The data from these tests are used to derive a solids flux curve for the mud. To obtain the procedure for the graphical construction of a solids flux curve and the theory necessary to relate the flux curve to what actually happens in settling dynamics, see References (12, 13, 14, and 15).

A typical solids flux curve for $CaCO_3$ mud is shown in Figure 9. The independent variable is the concentration. Note that between 0. and 1.0 moles/liter concentration the curve is almost linear. This represents the region in which free settling occurs. Above 1.0 moles/liter there is a nonlinear region for the dependence of solids flux on concentration. This region depicts the phenomenon of hindered settling.

Figure 10 shows a typical settling velocity vs. concentration curve for $CaCO_3$ mud. This curve can be obtained from the superimposed solids flux curve by dividing each ordinate value of the solids flux by the corresponding concentration. Between 0. and 1.0 moles/liter, the settling velocity is essentially independent of the concentration (free settling). Between 1.0 and 3.0 moles/liter, the settling velocity decreases with an increase in concentration in an essentially linear fashion.

Figure 11 illustrates what happens to the settling velocity and solids flux curves when changes in mud particle size occur at the settler inlet. A family of curves results, one for each average particle size. Note that as the concentration increases, there is less of an effect of the particle size on the settling velocity. That is, under conditions of hindered settling where the particles are interfering with each other more and more, the effect of the particle size diminishes.

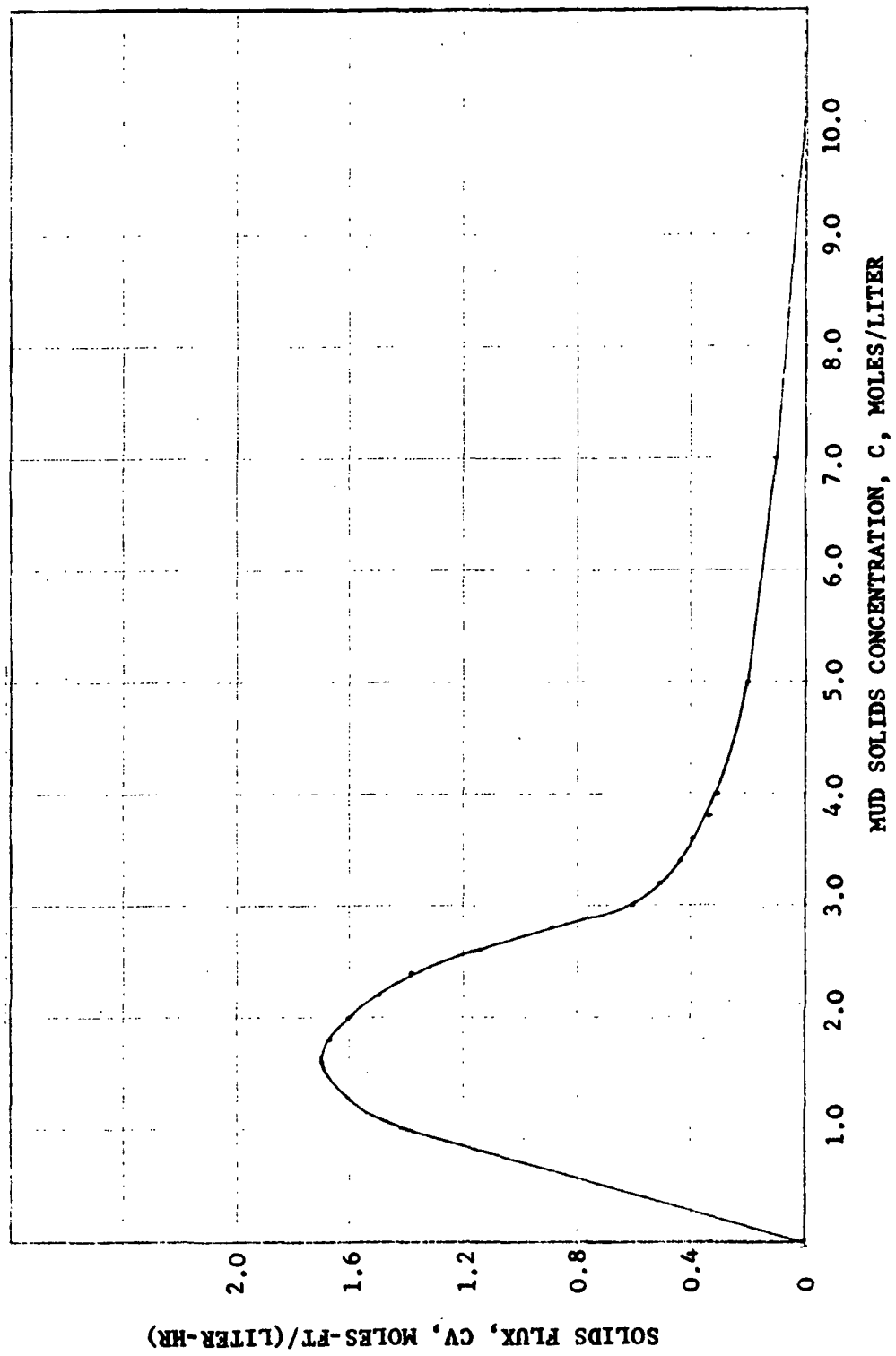

FIGURE 9

SOLIDS FLUX CURVE FOR $CaCO_3$ MUD

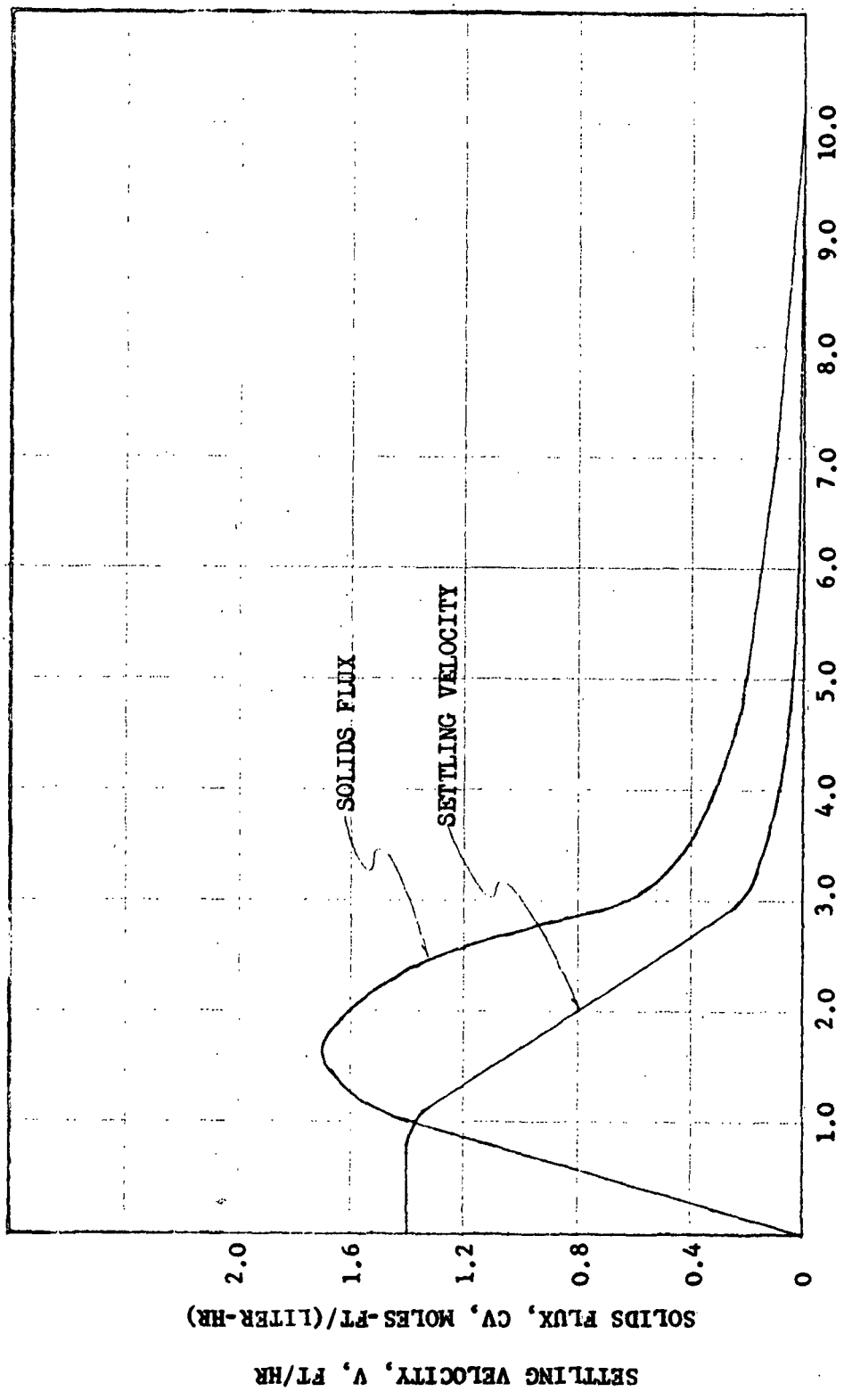

FIGURE 10

SETTLING VELOCITY AND SOLIDS FLUX CURVES FOR $CaCO_3$ MUD

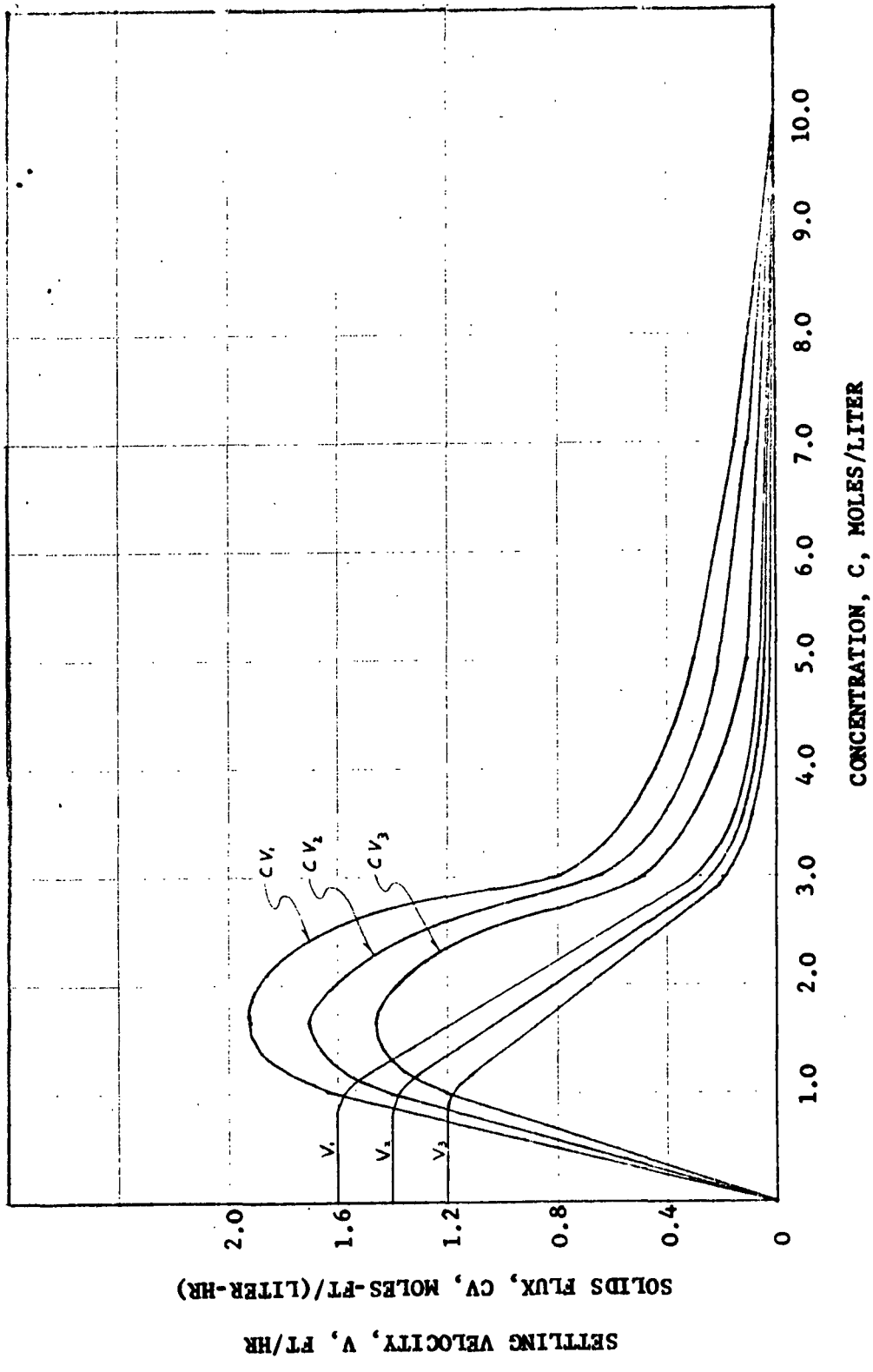

FIGURE 11

FAMILY OF FLUX CURVES FOR VARIOUS PARTICLE SIZES

Figure 12 shows a concentration profile for an 11-foot-high settler which is overloaded. C_t is the concentration of solids in the overflow, C_2 is the concentration of solids from the inlet level to the overflow level, C_{crit} is the critical concentration which has been exceeded leading to overload condition, and C_u is the underflow concentration.

Figure 13 shows a concentration profile for the same settler, but this time it is in an underload condition. C_t is now practically zero. Note that in the underload condition the concentrations C_2 and C_{crit} disappear from the profile, and C_1 appears between the inlet level and the underflow level (or the compression level).

Figure 14 illustrates graphically how each of the levels of concentration shown in Figures 12 and 13 are obtained. Points f_1 and f_2 on the ordinate axis represent the inlet flux and the underflow flux, respectively. The positions of these two points illustrate the overload condition which can be represented as a simple steady state balance:

$$\frac{Q_o}{A} C_t = \frac{Q_i}{A} C_o - \frac{Q_u}{A} C_u \qquad (22)$$

where

Q_o = Overflow, ft^3/hr

Q_u = Underflow, ft^3/hr

Q_i = Inflow, ft^3/hr

A = Area of settling tank, ft^2

C_t = Concentration of solids in overflow, mol/lit

C_u = Concentration of solids in underflow, mol/lit

C_o = Concentration of solids in inflow, mol/lit

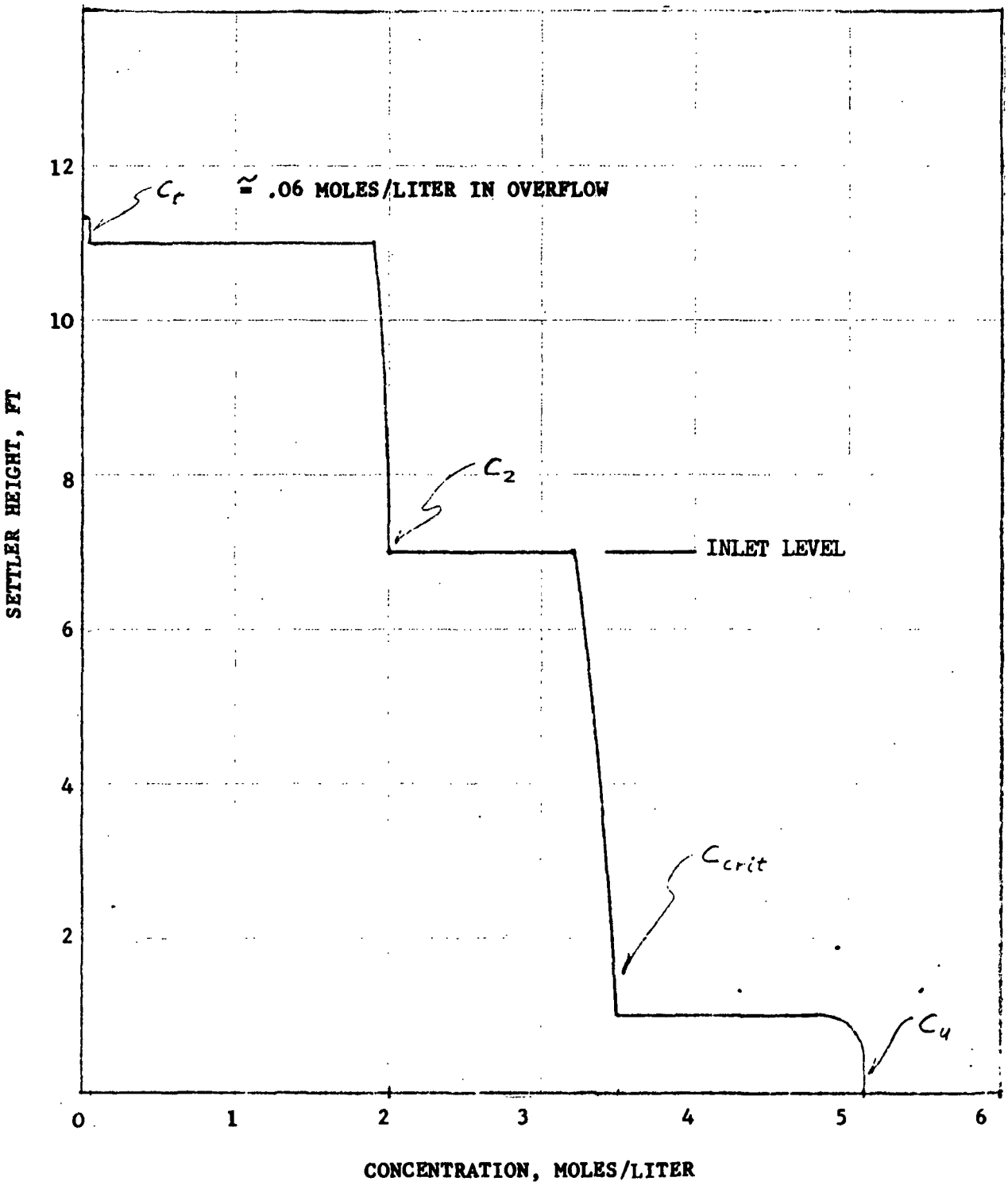

FIGURE 12

OVERLOADED SETTLER

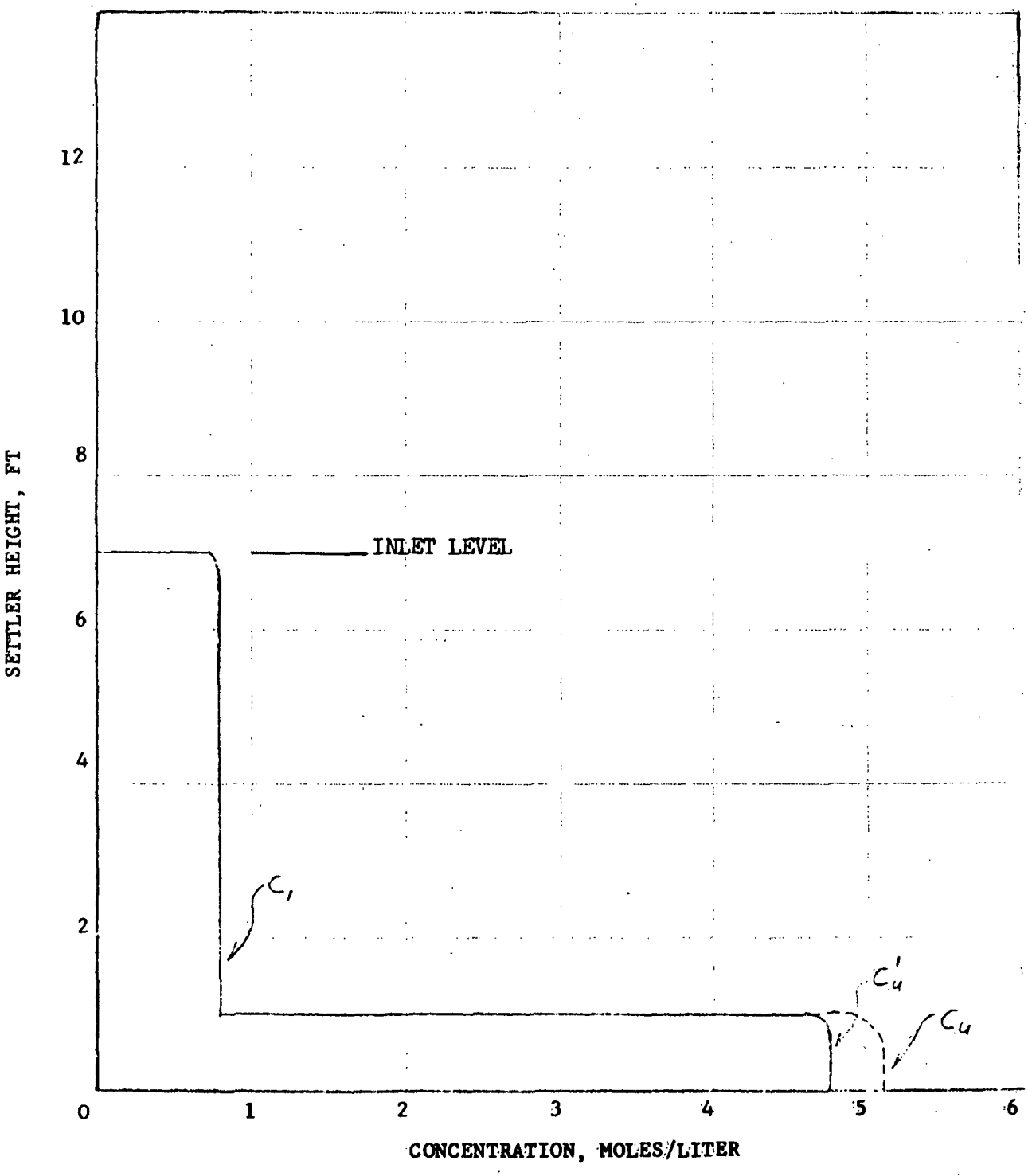

FIGURE 13

UNDERLOADED SETTLER

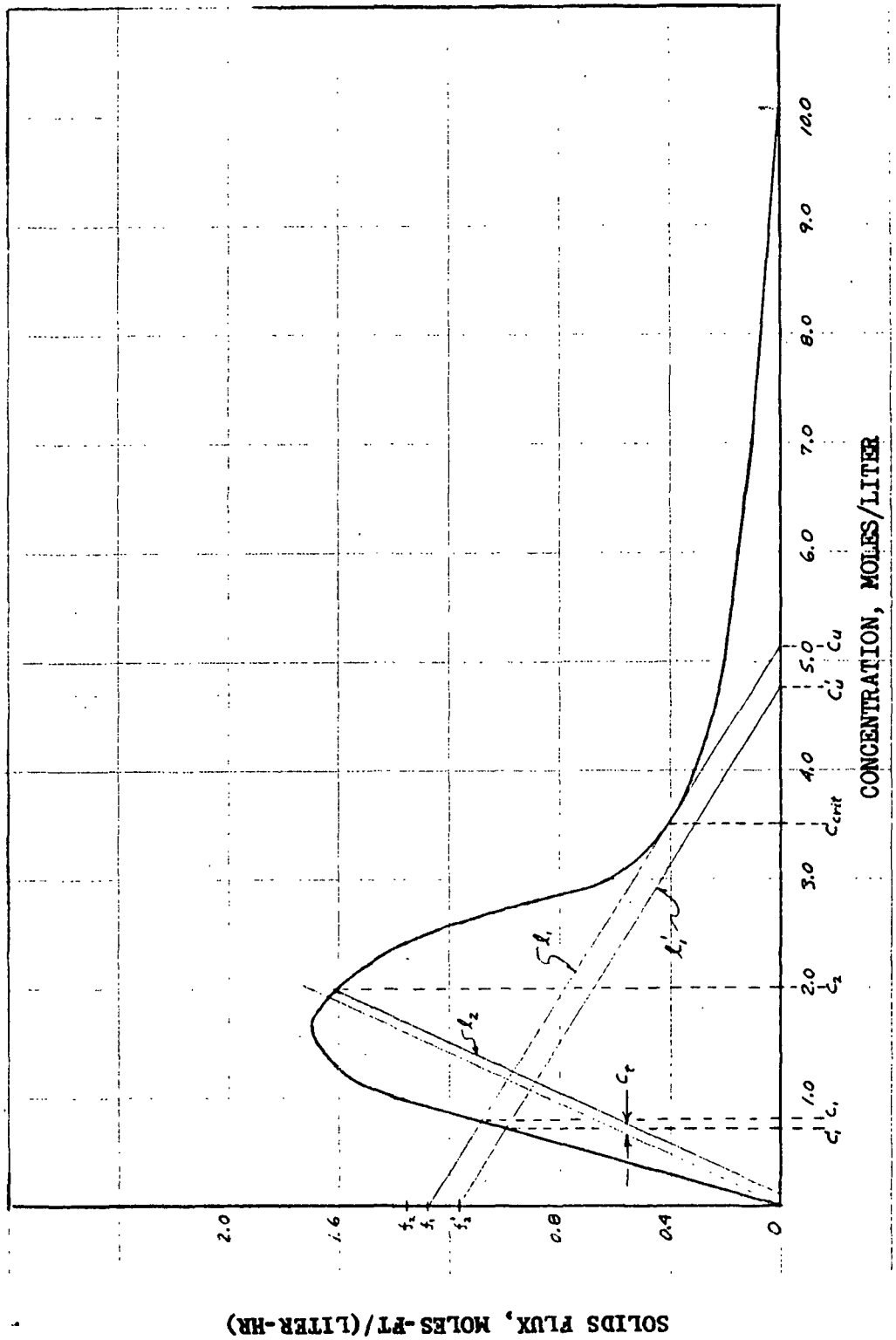

FIGURE 14. GRAPHICAL METHOD FOR FINDING MUD SETTLER SOLIDS CONCENTRATIONS

The location of Point f_1 is defined by the underflow flux $Q_u C_u/A$. The location of Point f_2 is defined by the inlet flux $Q_i C_o/A$. Figure 14 shows that f_2 is higher than f_1, and therefore we have a condition where the settler cannot handle all of the solids properly; and some must go out with the overflow.

The slope of Line l_1 is given by the underflow bulk velocity (occurring between the inlet level and the underflow outlet), $-Q_u/A$. Once the slope of l_1 is established, l_1 is moved upward until it is just tangent to the solids flux curve. This tangent point establishes the critical concentration C_{crit} (and the critical velocity v_{crit}). The points on the two axes at which the l_1 intercepts occur when the tangent point has been reached represent the underflow flux (ordinate) and the underflow concentration (abscissa). These are Points f_1 and C_u, respectively. The three Points f_1, C_{crit}, and C_u together establish the maximum load condition for the settler. If the influx is greater than f_1, as is shown by f_2 in Figure 14, the settler is overloaded, and it is easy to solve for the overflow solids concentration by using Equation(22). The point where Line l_1 intersects the solids flux curve to the left of the "hump" defines the concentration C_1.

The slope of the Line l_2 is given by the overflow bulk velocity (occurring between the inlet level and the overflow level), Q_o/A. The horizontal axis intercept for l_2 is a distance C_t to the right of the origin. The point at which l_2 intersects the solids flux curve establishes the concentration C_2.

Line l_1' in Figure 14 represents an underload condition for the settler. The influx, $Q_i C_o/A$, has dropped to Point f_2', and l_1 has dropped to the position l_1'.

Note that C_u decreases somewhat (to C_u') because the slope of l_1 remains the same. The concentration C_1' is that which corresponds to C_1 of the solids profile in Figure 13. Concentration C_u' can be found by observation of Figure 14. We can write

$$\frac{Q_u}{A} = \frac{C_1' v_1'}{C_u' - C_1'} \tag{23}$$

where $C_1' v_1'$ = solids flux corresponding to C_1'. Solving Equation 23 for C_v' we have

$$C_u' = C_1(v_1' A/Q_u + 1) \tag{24}$$

The dynamic model of solids settling involves the use of a combination of approximations to the solids flux curve, the corresponding approximate settling velocity curve, and a set of simple differential equations.

In the development of the dynamic model, several assumptions were made:

1. No horizontal gradients of the variables.
2. No chemical reactions.
3. Uniform temperature (i.e., adiabatic process).
4. The density of the clear liquid and of the dry solids does not change.

The key step in the model solution is establishing the critical flux and the corresponding C_{crit}. A polynomial approximation of the solids flux curve between the concentrations 3.0 and 5.0 moles/liter was made for this purpose:

$$X_f = K_o + K_1 C + K_2 C^2 + K_3 C^3 \tag{25}$$

where

X_f = Solids flux, mole-ft/liter-hr

$K_o = 4.50689 + U_{si}/17.$*

$K_1 = -2.44376$

$K_2 = 0.46562$

$K_3 = -0.03023$

C = Solids concentration, mol/lit.

Recall that the slope of l_1 in Figure 14 was crucial in finding the tangent point with the solids flux curve. Thus a procedure is used in which the derivative of the solids flux curve is compared to the slope of l_1 (given by $-Q_u/A$):

$$\frac{dX_f}{dC} = K_1 + 2K_2C + 3K_3C^2 \tag{26}$$

Where the absolute value of the difference between dX_f/dC and $-Q_u/A$ is minimum gives the location and value of C_{crit}. The critical flux is then obtained using Equation (25). The underflow concentration, then, is given by:

$$C_u = (X_{f_{crit}}A)/Q_u + C_{crit} \tag{27}$$

The influx, Q_iC_o/A, is used to find C_1 by solution of the differential equation for solids flux:

$$\frac{dC_1}{dt} = \left[Q_iC_o/A - (U_s + v_b)C_1\right] \tag{28}$$

*Note the dependence of K_o on the mud particle size.

where

$$U_s = \begin{cases} U_{si} & \text{if } C_1 < 1 \\ (U_{si}/2)(3 - C_1) + 0.1(C_1 - 1) & \text{if } C_1 \geq 1 \end{cases} \quad (29)^*$$

$$v_b = Q_u/A, \text{ ft/hr}$$

A test is made using Equation (22) to see if the overload condition exists. Suppose the settler has been in an underload condition for some time, as shown in Figure 13. Then there is a sudden increase in solids influx (or the mud particle size decreases, changing the flux curve). Suppose the change causes an overload condition. C_u will remain the same, but the interface at the one foot level in Figure 13 will begin to move upward at critical concentration with a velocity v_c ft/hr:

$$v_c = \frac{(Q_u/A)C_u - (Q_i/A)C_o}{C_u} \quad (30)$$

When the interface reaches the inlet level, a new interface at a concentration of C_2 will appear above the inlet level and move up to the overflow level at a velocity v_d ft/hr:

$$v_d = v_2 - (Q_o/A) \quad (31)$$

where v_2 is the hindered settling velocity corresponding to C_2 on the solids flux curve. (See Figure 14.) v_2 is obtained by solving two independent nonlinear equations in the two unknowns C_2 and v_2 simultaneously. First of all, by observing the intersection of l_2 with the solids flux

*Equation (29) represents a piecewise linear approximation of the settling velocity curve. (See Figure 10.)

curve in Figure 14, we can write

$$C_2 v_2 = (Q_o/A)(C_2 - C_t) \tag{32}$$

Secondly, C_2 and v_2 must obey the settling velocity relationship given by

$$v_2 = (U_{si}/2)(3 - C_2) + 0.1(C_2 - 1) \tag{33}$$

Equations (32) and (33) are combined leading to a quadratic equation for C_2:

$$(.5U_{si} - .1)C_2^2 + (Q_o/A - 1.5U_{si} + .1)C_2 - Q_o C_t/A = 0. \tag{34}$$

When the interface at concentration C_2 reaches the overflow, solids at a concentration C_t begin to appear in the overflow. The profile corresponding to this condition appears in Figure 12.

Now suppose a change occurs such that the settler is underloaded. This could be brought about by a decrease in the influx, an increase in particle size, or an increase in Q_u. The interface of concentration C_2 at the overflow begins to move downward toward the inlet level, and C_t decreases toward zero. The downward velocity v_e is given by:

$$v_e = \frac{(Q_u/A)C_u - (Q_i/A)C_o}{C_2} \tag{35}$$

After the C_2 interface has reached the inlet level, the interface of concentration C_{crit} will begin to move downward toward the compression zone level at a velocity given by:

$$v_f = \frac{(Q_u/A)C_u - (Q_i/A)C_o}{C_{crit} - C_l} \tag{36}$$

The interface velocities v_c, v_d, v_e, v_f are used to obtain time constants for an approximate delay model for the settling tank. The settler is divided up into a series of 17 one-half-foot-high tanks, 6 for above the inlet and 11 for below the inlet. The concentration of solids in each tank is solved for as in a series of ideally mixed tanks. This method provides a satisfactory approximation to the delay dynamics (movement of the solids-liquid interface). The set of differential equations for the overload condition is given below:

$$\frac{dx_i}{dt} = \frac{1}{\tau_d}(x_{i+1} - x_i) \qquad i = 1,5 \tag{37}$$

where

$$\tau_d = 0.5/v_d, \text{ hrs.}$$

$$x_6 = \begin{cases} C_2 \text{ if } x_7 \cong C_{crit} \\ 0 \text{ if } x_7 \cong 0. \end{cases}$$

$$\frac{dx_i}{dt} = \frac{1}{\tau_c}(x_{i+1} - x_i) \qquad i = 7,16 \tag{38}$$

where

$$\tau_a = 0.5/v_c, \text{ hrs.}$$

$$x_{17} = C_{crit}$$

A block diagram depicting the dynamic information flow in the simulation for the overload condition is shown in Figure 15.

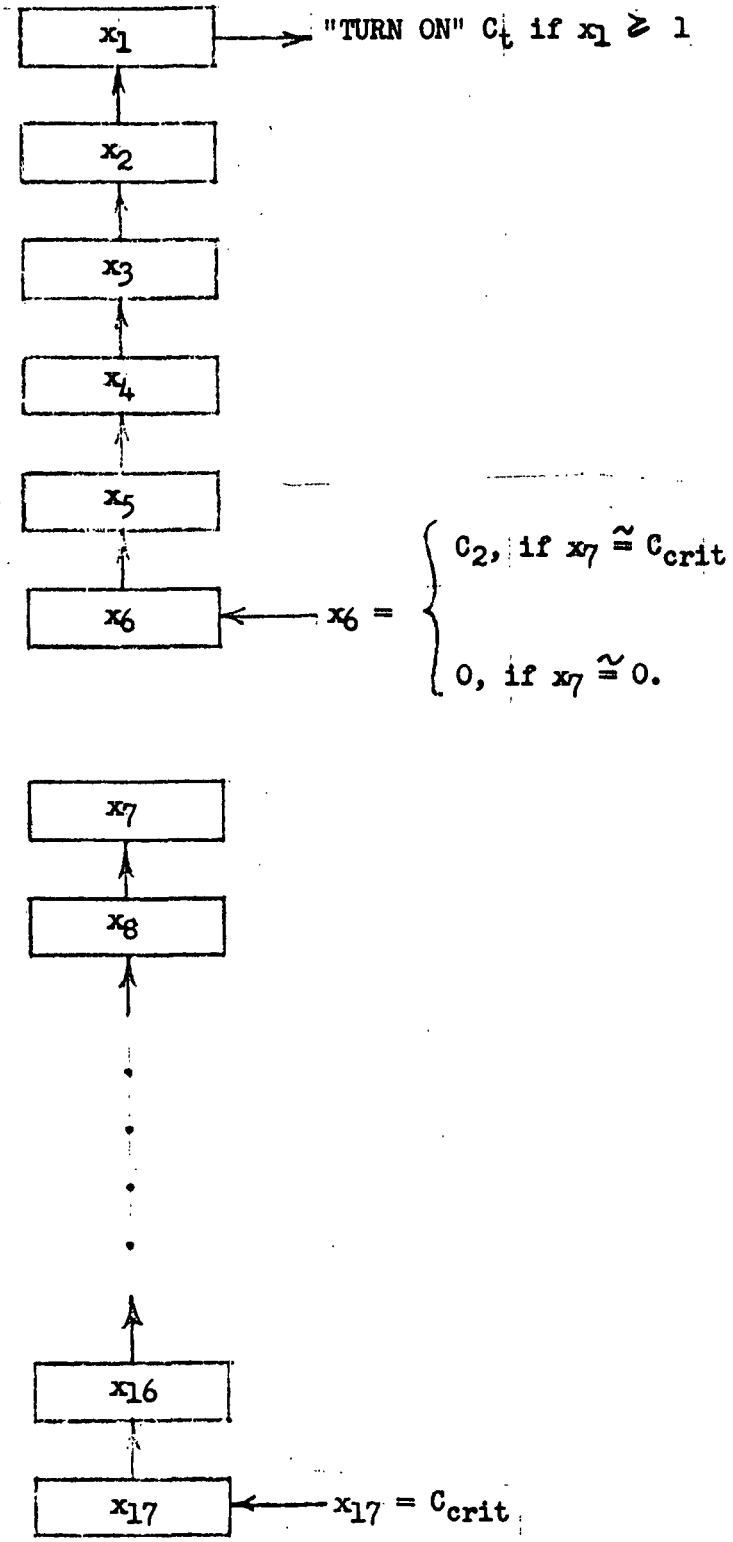

FIGURE 15. INFORMATION FLOW FOR OVERLOAD DYNAMICS

The set of differential equations for the underload conditions is given as:

$$\frac{dx_i}{dt} = \frac{1}{\tau_e}(x_{i-1} - x_i) \qquad i = 2,6 \tag{39}$$

where

$$\tau_e = 0.5/v_e, \text{ hrs.}$$

$$x_1 = 0. \quad (\text{if } C_t = 0.)$$

$$\frac{dx_i}{dt} = \frac{1}{\tau_f}(x_{i-1} - x_i) \qquad i = 8,17 \tag{40}$$

where

$$_f = 0.5/v_f, \text{ hrs.}$$

$$x_7 = \begin{cases} x_7, \text{ if } x_6 \cong C_2 \\ C_1, \text{ if } x_6 \cong 0. \end{cases}$$

A block diagram for the underload simulation is given in Figure 16.

For each dynamic iteration, at the beginning of the settler subroutine, a test is made to see if the condition is overload or underload by seeing if C_t is greater than zero using Equation (22):

1. Overload, if $C_t > 0$.

2. Underload, if $C_t \leq 0$.

It should be noted that a special case exists when an underload condition is created by an increase in the underflow from Q_u to Q_u', and when the settler initially is at maximum load or overload. Until the C_{crit} interface drops to the one foot level, C_u drops to C_u' according to the equation:

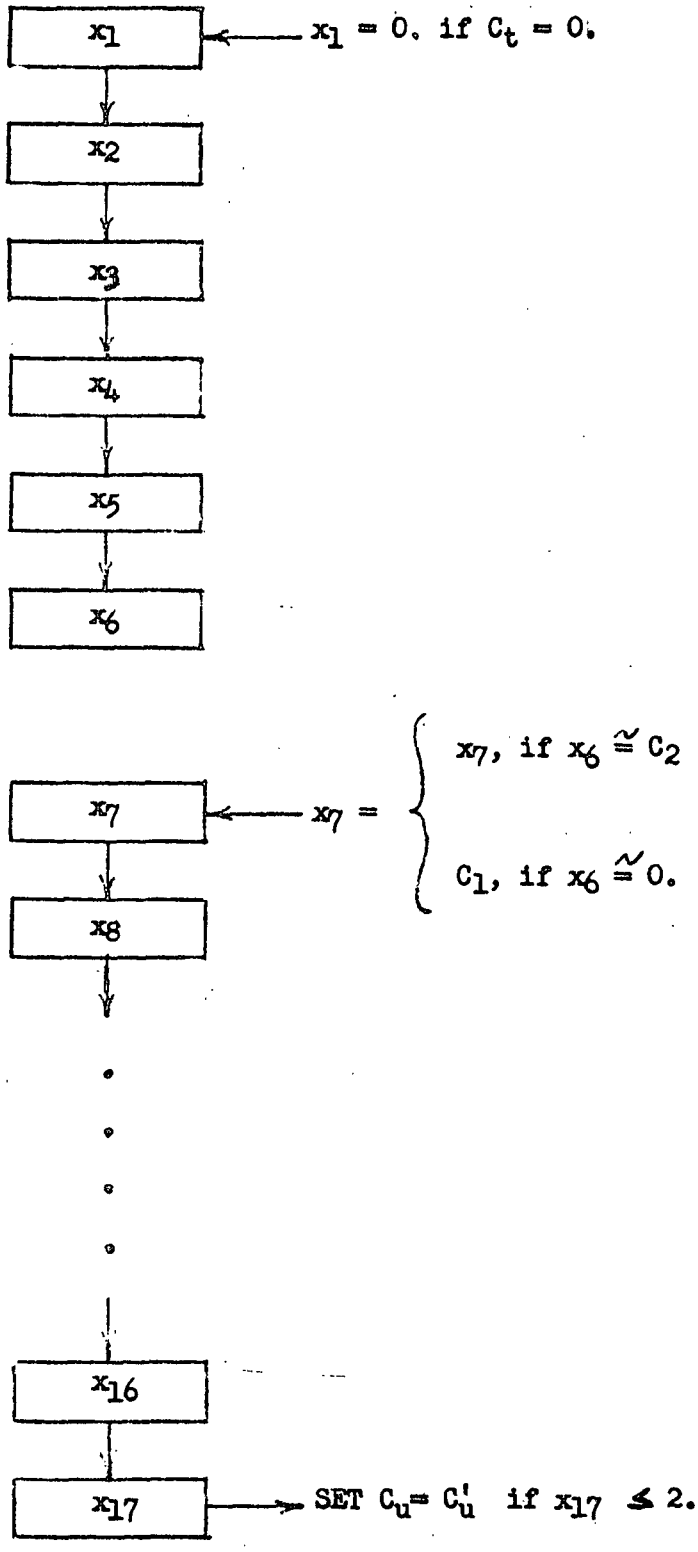

FIGURE 16. INFORMATION FLOW FOR UNDERLOAD DYNAMICS

$$\frac{X_{f_{crit}}}{C_u' - C_{crit}} = \frac{Q_u'}{A} \tag{41}$$

where $x_{f_{crit}} = C_{crit}v_{crit}$. Once the C_{crit} interface reaches the compression zone, C_u drops even further to C_u'' according to the equation:

$$\frac{C_1'' v_1''}{C_u'' - C_1''} = \frac{Q_u'}{A} \tag{42}$$

LIME MUD PRE-COAT FILTER MODEL

As mentioned previously in the discussion of the solids settling model, caustic soda removal and water removal from the lime mud is very critical prior to calcining. The unit process which is normally used to perform dewatering and to contribute to washing the mud is the pre-coat filter.

Several authors have dealt with the problem of vacuum pre-coat filtration. Textbooks which deal extensively with this problem are given by References (23, 16, and 17). A recent paper by Tiller (18), supplies a survey of work that has been done in filtration theory and practice.

There are two general approaches to modeling vacuum filtration. The first is a rather detailed procedure involving the use of a two point boundary value problem solution for the porosity and filtration resistance. The second approach is a simpler approximate method which relies on empirical data. Because there is a significant amount of empirical data available for cake filtration for $CaCO_3$, and because of the complexity of the first approach, the second method is used for this model. The second method was also used by Adler (24) in his overall steady state model of the recovery system. The model equations used in this study are similar to Adler's, except that the model for filtration resistance has been extended to include the effects of changes in the lime mud particle size.

The following assumptions were made in deriving the approximate model:

1. Flow of filtrate through pores in cake is laminar (large filter drum area).

2. The temperature of the entering lime mud and the shower wash water is essentially constant.

3. Constant pressure filtration.

4. The amount of solids passing completely through the cake with the filtrate is negligible.

5. Washing with shower water is effected through mixing rather than by displacement. This approach to modeling a shower wash is recommended by Perry in his derivation of the pulp washer model. (See Reference (19))

6. The resistance of the filter medium is negligible compared to the resistance of the cake.

A block diagram for the lumped approximation of the pre-coat filter model is shown in Figure 16A.

The basic equation for constant pressure filtration is developed in References (23,16, and 17). It involves the use of the Kozeny-Carman Equation which is a Reynolds number-friction factor relation. The resulting equation gives a relationship for the rate of generation of filtrate:

$$Q_f = \frac{dV}{dt} = A \left[\frac{K_t 2 g_c (\Delta P) f}{K_c \alpha \mu t_c} \right]^{\frac{1}{2}} \qquad (43)$$

where

$\frac{dV}{dt}$ = Filtrate generation rate, ft^3/min

A = Area of filter drum, ft^2

K_t = 60, sec/min

g_c = Gravity constant, $ft\text{-}lb_m/lb_f\text{-}sec^2$

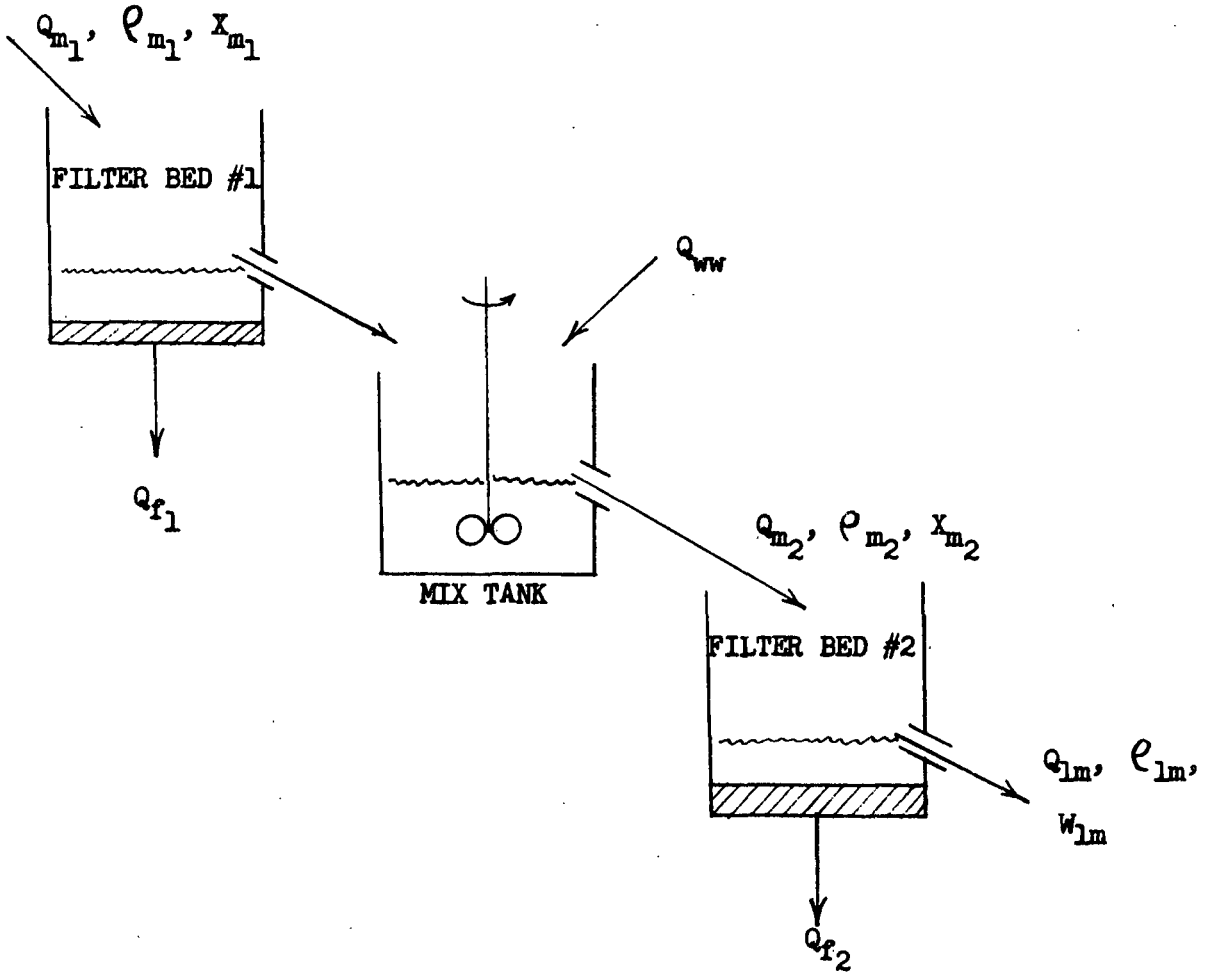

FIGURE 16A. SCHEMATIC MODEL OF THE LIME MUD PRE-COAT FILTER

ΔP = Pressure drop across filter cake, lb/ft^2

f = Fractional area of drum submerged in slurry, ft^2/ft^2

X_c = Pounds of solids deposited in the cake per cubic foot of filtrate generated, lb/ft^3

α = Filtration resistance, ft/lb_m

μ = Viscosity of filtrate, $lb_m/ft\text{-}sec$

t_c = Reciprocal of drum turning rate, min/rev.

The parameter X_c is obtained via a mass balance. If X_c is the mass of the particles deposited in the filter per unit volume of filtrate, in pounds per cubic feet, the mass of solids being filtered per unit of time is $Q_f X_c$, and then,

$$W_c = Q_f X_c = Q_m X_m \tag{44}$$

where,

W_c = Mass flow of dry solids, lbs/min

X_m = Concentration of solids in slurry fed to the filter, lbs/ft^3

Furthermore,

$$W_{lm} = \rho_m Q_m - \rho_f Q_f \tag{45}$$

where

Q_m = Flow of mud slurry to the filter, ft^3/min

ρ_m = Mud slurry density, lb/ft^3

ρ_f = Filtrate density, lb/ft^3

Q_f = Flow of filtrate, ft^3/min

The filtration resistance, α, is the most critical item in Equation (43). The resistance depends on the cake porosity and on the surface-volume ratio (specific surface) of the particles in the mud cake. Furthermore, because

the cake is compressible, α will also depend on the pressure drop across the cake. The empirical relation based on experimental results for $CaCO_3$ filtration (See Reference (23)) is

$$\alpha = \alpha_o(\Delta P)^s \tag{46}$$

where

s = compressibility factor, $\cong$ 0.3 for $CaCO_3$.

Also,

$$\alpha_o = K_1 \left[\frac{1-\epsilon}{\epsilon^3}\right] \frac{(hS)^2}{\rho_s} \tag{47}$$

where

K_1 = Constant of proportionality, $\cong$ 5.0

ϵ = Porosity of cake

S = Specific surface of cake particle, ft^2/ft^3

ρ_s = Density of $CaCO_3$ particles, lb/ft^3

h = Reciprocal of sphericity of particles

Experimental data have shown that $\epsilon \cong 0.77$ for $CaCO_3$. (See Reference (18).) Furthermore, it has been shown that porosity is closely related to sphericity. (See Reference (17).) Sphericity is defined as the area of the sphere having the same volume as the particle divided by the area of the particle. Experimental data in Reference (17) shows that for $\epsilon \cong 0.8$, $h \cong 5.0$. A value of h = 5.13 yielded results which compared well to operating data in this model.

The specific surface of the cake particles can be written

$$S = S_p/v_p = \pi D_p^2 / \left[\frac{\pi D_p^3}{6}\right] = 6/D_p \tag{48}$$

where D_p = mean diameter of the mud particles, ft.

The parosity, ϵ, is also dependent of ΔP because $CaCO_3$ mud is moderately compressible. Empirical results (See Reference (18)) show that:

$$\epsilon = \epsilon_o (\Delta P)^{\lambda} \tag{49}$$

where $\lambda \cong 0.034$ for $CaCO_3$

Also,

$$\epsilon_o = 1 - K_p D_p^3 \tag{50}$$

where K_p is a constant proportional to the number of particles contained within a volume whose sides have characteristic dimension 1. The particles have mean diameter D_p. (See Reference (16))

From Equations (47), (48), and (50) above, it is seen that α is strongly related to the mud particle size.

A typical lime mud slurry particle size distribution is given in Reference (20, Page 105) The mean diameter for the typical mud particles is about 10 μ. A typical free settling velocity for lime mud is 1.5 ft/hr. (See References (6 and 10)) Therefore, through the use of a constant multiplying factor in Stokes' Law, we can infer a mean particle diameter, D_p, from the free settling velocity U_{si}:

$$U_{si} = K_s \left[\frac{\rho_p - \rho_f}{18\, g_c \mu} \right] D_p^2 \tag{51}$$

Using typical values for u_{si}, D_p, ρ_p, ρ_f, and μ we get that $K_s \cong 2.18 \times 10^6$. Therefore,

$$D_p = \left\{ U_{si} \Big/ \left[\frac{K_s(\rho_p - \rho_f)}{18\, g_c \mu} \right] \right\}^{\frac{1}{2}} \tag{52}$$

Because ρ_p, ρ_f, and μ do not vary appreciably, we can write

$$D_p = \sqrt{U_{si}/K_q} \quad , \quad \text{ft.} \tag{53}$$

where

$$K_q = \frac{K_s(\rho_p - \rho_f)}{18\, g_c/\mu} .$$

The mud filter model used in this study has no dynamics. The time constants involved are very small compared to those of slaking/causticizing and solids settling. Therefore, the use of steady state equations is justified. At each time iteration of the overall model, a new value for the filtration resistance, α, is generated using Equations (46) through (50), and (53). Then follows solution of the three Equations (43) through (45) for the three unknowns Q_f, X_c, and W_{lm}. Substituting Equation (44) into (43) yields

$$Q_f = \frac{Q_m X_m}{X_c} = A \left[\frac{K_t 2 g_c (\Delta P) f}{X_c \alpha \mu t_c} \right]^{\frac{1}{2}} \tag{54}$$

Furthermore, if we write

$$Y = A \left[\frac{K_t 2 g_c (\Delta P) f}{\alpha \mu t_c} \right]^{\frac{1}{2}} \tag{55}$$

Equation (54) becomes

$$Q_f = \frac{Q_m X_m}{X_c} = \frac{Y}{\sqrt{X_c}} \tag{56}$$

or

$$\frac{X_c^2}{Q_m^2 X_m^2} = \frac{X_c}{Y^2}$$

Finally, we can write,

$$X_c = \left[\frac{Q_m X_m}{Y}\right]^2 \qquad (57)$$

Recall that X_c is the mass of solids deposited per cubic foot of filtrate generated in the filter. Q_f is now easily obtained using Equation 44. The ratio, W_c/W_{lm} gives the per cent solids by weight going to the kiln.

OVERALL MODEL

A block diagram of the overall liquor preparation system modeled in this study is given in Figure 17. The basic flows within the system are as discussed in the introduction to this section of the report. Note that the primary inputs to the system are

1. Smelt and steam at smelt dissolving.
2. Lime at slaking/causticizing.
3. Fresh water
   a. at mud mix tank for makeup.
   b. at precoat filter for washing mud cake.
   c. at inlet to precoat filter for mud density control.

The primary system outputs are

1. White liquor to digester holding tank.
2. Dewatered mud to calcining (kiln).

Four standard automatic controls* are included in the present model:

1. Density control of green liquor leaving smelt dissolving.
2. Temperature control of green liquor entering slaking/causticizing (190° F.).
3. Density control of the lime mud mix entering the precoat filter.
4. Flow control of lime mud mix entering the precoat filter.

One non-standard automatic control loop was used in this simulation. It meters active lime into the slaker based on a measurement of the lime causticizing power and based on the measurement of Na_2CO_3 concentration in the green liquor. Further discussion on the design and operation of this simple feedforward controller is given in the section on control

*These automatic controls are standard in that they are typically used as standard equipment in liquor preparation systems.

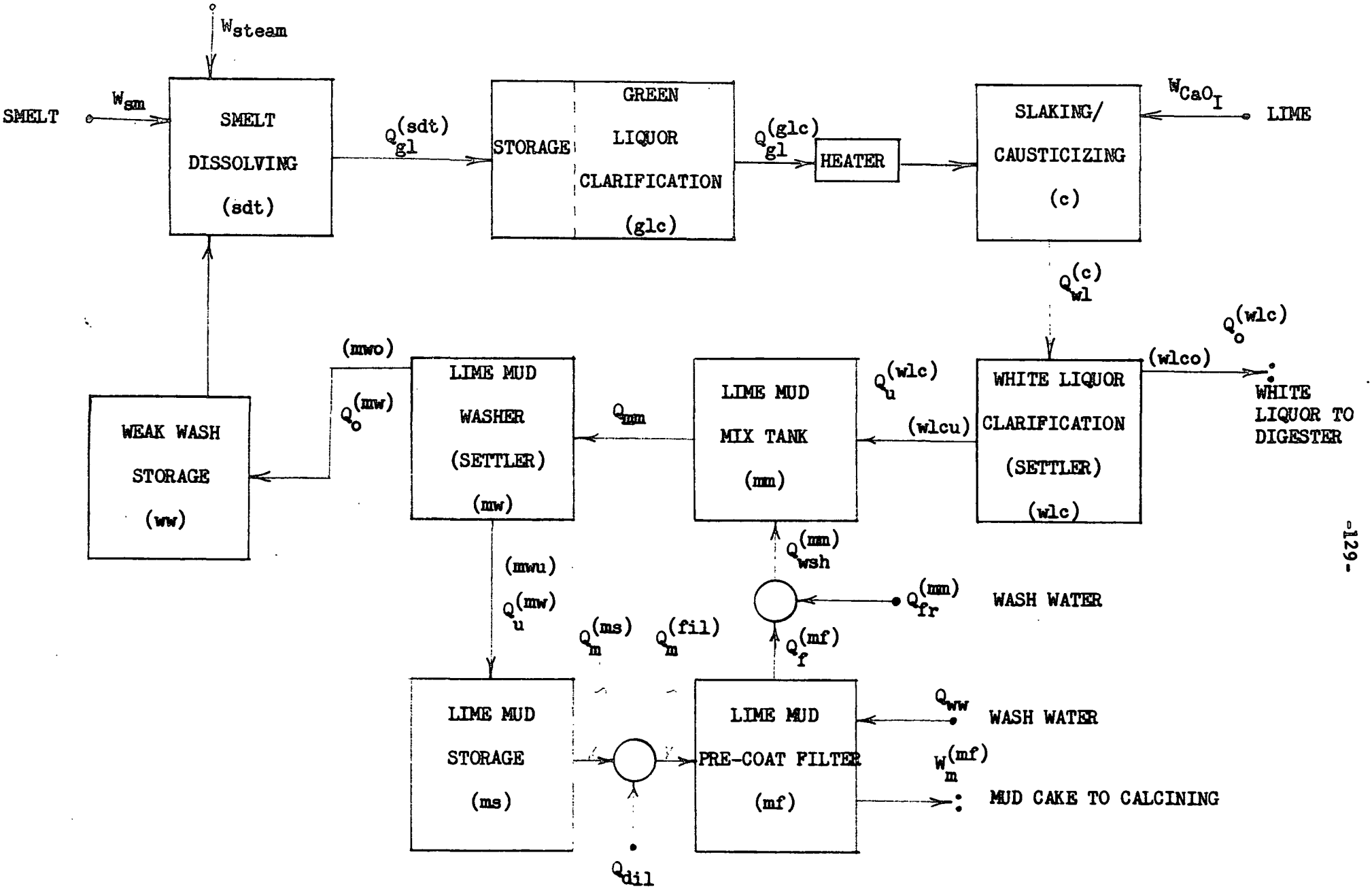

FIGURE 17. OVERALL LIQUOR PREPARATION SYSTEM

The general method used in modeling the overall system is one of solids balance and volume balance. The volume balance method was used primarily because of the large amount of storage capacity in the liquor preparation system. The storage tanks and storage capacities of the settling tanks dominate the dynamics of the system. Furthermore, the slaking/causticizing reaction computations are done much more simply when the concentrations are expressed in moles per unit volume. Therefore, it is most convenient to express flow rates in volume per unit time, and concentrations in mass per unit volume. Because of this, the units of the concentrations will be different from those used in the overall steady state model (24). However, the conversion from concentrations in terms of mass per unit volume to mass fractions is simple and is given in the introduction to this section of the report.

For the sake of simplicity, the temperatures of the liquors at the various unit processes throughout the liquor preparation system (with the exception of slaking/causticizing and calcining) are assumed to be at an average of 180° F. The corresponding density of water is 60.5 lb/ft^3. It is also assumed that solids which dissolve completely in the liquor cause only a negligible increase in the volume of the liquor after dissolution.

1. Smelt Dissolving

In smelt dissolving, medium pressure steam is applied to the smelt coming out of the furnace to help break it up so that it will dissolve more readily. The smelt is made up primarily of Na_2CO_3, Na_2S, and Na_2SO_4. A small amount of inert matter is carried with the smelt, but that is ignored in the present model. This should not affect the results of the overall system simulation significantly. Weak wash liquor from storage is fed to the dissolving tank to dissolve the smelt. The weak wash contains small concentrations of NaOH, Na_2S, Na_2CO_3, and Na_2SO_4. In terms of state variables coming out of the weak liquor tank:

$$X_{soda}^{(wwl)} = X_{Na_2CO_3}^{(wwl)} + X_{NaOH}^{(wwl)} + X_{Na_2S}^{(wwl)} + X_{Na_2SO_4}^{(wwl)} \tag{58}$$

where

$X_{soda}^{(wwl)}$ = total dissolved solids in weak wash liquor, lb/ft^3

$X_{NaXX}^{(wwl)}$ = concentration of NaXX in weak wash liquor, lb/ft^3

wwl = weak wash liquor

Therefore the mass flow of soda going into smelt dissolving in the weak wash is

$$W_{soda}^{(wwl)} = X_{soda}^{(wwl)} Q_{wwl} \tag{59}$$

where Q is the flow rate of weak wash in ft^3/hr. The flow rate of green liquor out of smelt dissolving is determined by the mass flow of smelt, the mass of soda in the weak wash, and by the desired green liquor density. The density can be expressed as a concentration of total soda. Thus,

$$Q_{gl}^{(sdt)} = (W_{sm} + W_{soda}^{(wwl)})/X_{soda}^{(sdt)} \tag{60}$$

where

$Q_{gl}^{(sdt)}$ = green liquor flow rate, ft^3/hr

W_{sm} = mass flow of smelt, lb/hr

$X_{soda}^{(sdt)}$ = desired soda concentration in green liquor, lb/ft^3

sdt = smelt dissolving tank

The flow of weak wash liquor is, therefore:

$$Q_{wwl} = Q_{gl}^{(sdt)} - W_{st}/60.5 \tag{61}$$

where W_{st} is the mass flow rate of steam in lb/hr.

An alternate method of modeling the green liquor density control would be to specify the flow, $Q_{gl}^{(sdt)}$, in addition to $X_{soda}^{(sdt)}$. Q_{wwl} would then be determined by an iterative procedure in which the error between the actual soda (density) and the desired soda (density) would be minimized. This alternate method is more complicated than the method used above. In practice, the process operator tries to fix $Q_{gl}^{(sdt)}$. However, if a change in the smelt generation rate occurs, he eventually must change the green liquor flow rate or else overfill (or empty) the green liquor storage tank. A computer logic diagram (in FORTRAN) for the iterative procedure is given in Figure 18.

The dynamics of the density control are not included in this model because the time constants involved are less than one-tenth of those of the storage tanks in the rest of the system. Thus, control is effectively instantaneous.

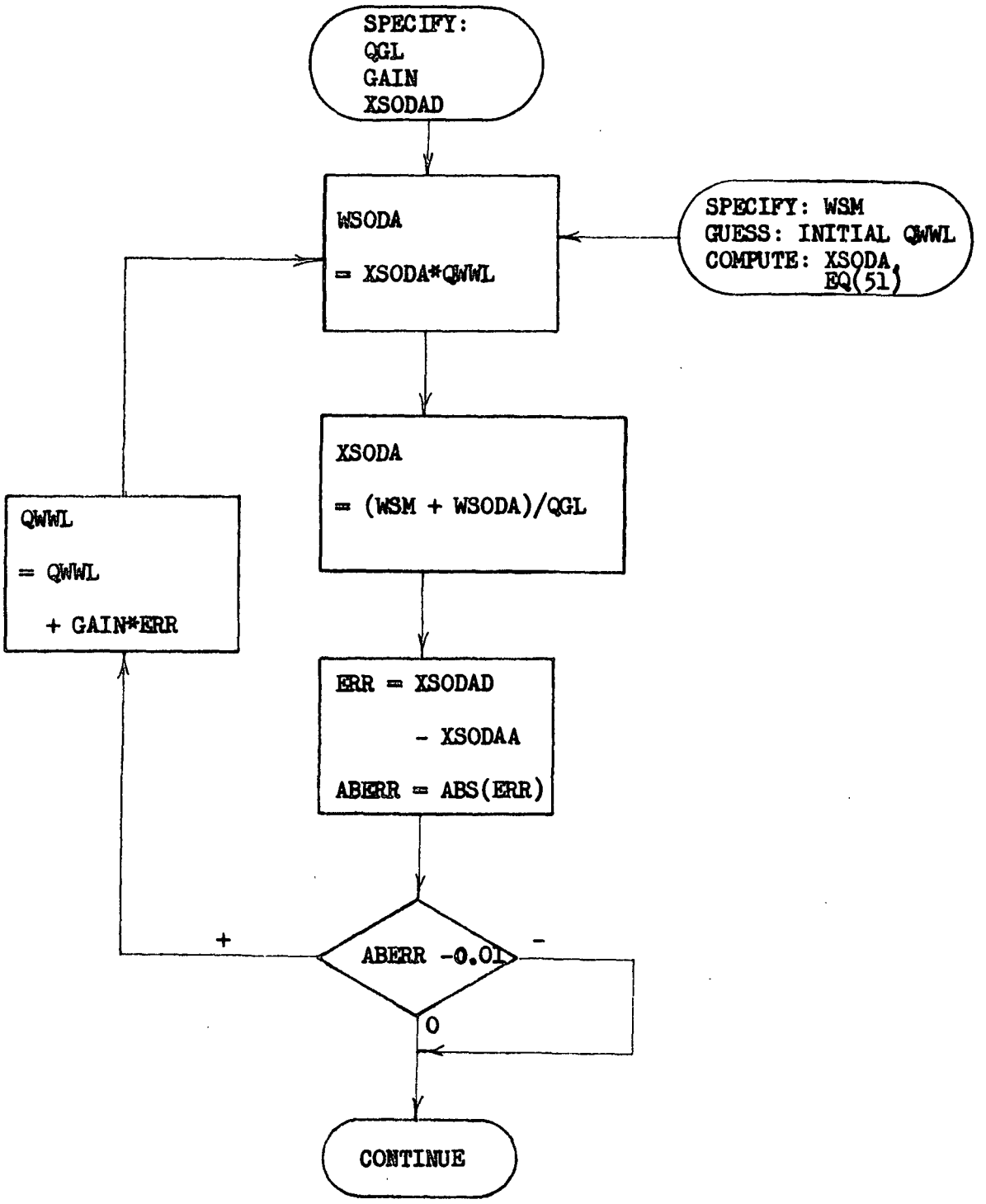

FIGURE 18. ITERATIVE PROCEDURE FOR GREEN LIQUOR DENSITY CONTROL

The concentrations of dissolved soda flowing out of smelt dissolving is given by:

$$X^{(sdt)}_{Na_2CO_3} = (W_{Na_2CO_3} + X^{(wwl)}_{Na_2CO_3} Q_{wwl})/Q^{(sdt)}_{gl}$$

$$X^{(sdt)}_{NaOH} = X^{(wwl)}_{NaOH} Q_{wwl}/Q^{(sdt)}_{gl}$$

$$X^{(sdt)}_{Na_2S} = (W_{Na_2S} + X^{(wwl)}_{Na_2S} Q_{wwl})/Q^{(sdt)}_{gl}$$

$$X^{(sdt)}_{Na_2SO_4} = (W_{Na_2SO_4} + X^{(wwl)}_{Na_2SO_4} Q_{wwl})/Q^{(sdt)}_{gl} \qquad (62)$$

where

W_{NaXX} = mass flow of NaXX in smelt, lb/hr

X_{NaXX} = concentration of NaXX in, lb/ft^3

The mass flow of green liquor is

$$W^{(sdt)}_{gl} = W_{sm} + W_{st} + (60.5 + X^{(wwl)}_{soda}) Q_{wwl} \qquad (63)$$

No dynamics are included in smelt dissolving because of the small tank retention time compared to that of the tanks in the rest of the system.

2. Green Liquor Storage

The green liquor storage tank and the green liquor clarifier dynamics were modeled as a unit with some delay and some mixing. Because the underflow in the green liquor clarifier is so small (about 1% of the inflow), dregs production and underflow soda losses were considered to be constant. Thus, the model for green liquor storage and clarification considers only the flow-through dynamics for soda.

The storage equation is

$$\dot{x}_1 = \frac{dV^{(glc)}}{dt} = Q_{gl}^{(sdt)} - Q_{gl}^{(glc)} \tag{64}$$

where

V = volume of green liquor in storage, ft^3

glc = green liquor clarifier

The total retention time is

$$\tau^{(glc)} = V^{(glc)}/Q_{gl}^{(glc)} \tag{65}$$

For the delay, divide $\tau^{(glc)}$ by 3:

$$\tau_1^{(glc)} = \tau_2^{(glc)} = \tau_3^{(glc)} = \tau^{(glc)}/3. \tag{66}$$

The dynamic equations in state variable form for the dissolved solids concentrations are

$$\dot{x}_2 = (X_{Na_2CO_3}^{(sdt)} - x_2)/\tau_1^{(glc)}$$

$$\dot{x}_3 = (X_{NaOH}^{(sdt)} - x_3)/\tau_1^{(glc)}$$

$$\dot{x}_4 = (X_{Na\ S}^{(sdt)} - x_4)/\tau_1^{(glc)}$$

$$\dot{x}_5 = (X_{Na_2SO_4}^{(sdt)} - x_5)/\tau_1^{(glc)}$$

$$\dot{x}_6 = (x_2 - x_6)/\tau_2^{(glc)}$$

$$\dot{x}_7 = (x_3 - x_7)/\tau_2^{(glc)}$$

$$\dot{x}_8 = (x_4 - x_8)/\tau_2^{(glc)}$$

$$\dot{x}_9 = (x_5 - x_9)/\tau_2^{(glc)}$$

$$\dot{x}_{10} = (x_6 - x_{10})/\tau_3^{(glc)}$$

$$\dot{x}_{11} = (x_7 - x_{11})/\tau_3^{(glc)}$$

$$\dot{x}_{12} = (x_8 - x_{12})/\tau_3^{(glc)}$$

$$\dot{x}_{13} = (x_9 - x_{13})/\tau_3^{(glc} \qquad (67)$$

where

$\dot{x}_i = dx_i/dt$

$x_{10} = X_{Na_2CO_3}^{(glc)}$, the output concentration of Na_2CO_3 from green liquor clarification, lb/ft^3

$x_{11} = X_{NaOH}^{(glc)}$, lb/ft^3

$x_{12} = X_{Na_2S}^{(glc)}$, lb/ft^3

$x_{13} = X_{Na_2SO_4}^{(glc)}$, lb/ft^3

3. Slaking/Causticizing

The reaction model for slaking/causticizing is given by Equations (10),(14) and (16). The outputs of green liquor clarification, $X_{NaXX}^{(glc)}$, are converted from units of lb/ft^3 to units of moles/liter as per the footnote in the introduction to this section of the report. Lime is added at the slaker, and it is assumed that all of the active lime is converted to $Ca(OH)_2$. It is assumed that the amount of inactive lime is essentially constant and does not affect the results significantly. Therefore, the amount of inactive lime is not tracked in the system. The outputs of the reaction model serve as inputs to the flow dynamic model. Assuming that the causticizing tanks are of equal volume, and $\tau^{(c)}$ is the total retention time, we have that:

$$\tau_1^{(c)} = \tau_2^{(c)} = \tau_3^{(c)} = \tau^{(c)}/3 = V^{(c)}/3Q_{wl}^{(c)} \qquad (68)$$

In state variable form, the flow dynamics are

$$\dot{x}_{14} = (X_{Ca(OH)_2}^{(scr)} - x_{14})/\tau_1^{(c)}$$

$$\dot{x}_{15} = (X_{Na_2CO_3}^{(scr)} - x_{15})/\tau_1^{(c)}$$

$$\dot{x}_{16} = (X_{NaOH}^{(scr)} - x_{16})/\tau_1^{(c)}$$

$$\dot{x}_{17} = (X_{CaCO_3}^{(scr)} - x_{17})/\tau_1^{(c)}$$

$$\dot{x}_{18} = (X_{Na_2S}^{(glc)} - x_{18})/\tau_1^{(c)}$$

$$\dot{x}_{19} = (X_{Na_2SO_4}^{(glc)} - x_{19})/\tau_1^{(c)}$$

$$\dot{x}_{20} = (x_{14} - x_{20})/\tau_2^{(c)}$$

$$\dot{x}_{21} = (x_{15} - x_{21})/\tau_2^{(c)}$$

$$\dot{x}_{22} = (x_{16} - x_{22})/\tau_2^{(c)}$$

$$\dot{x}_{23} = (x_{17} - x_{23})/\tau_2^{(c)}$$

$$\dot{x}_{24} = (x_{18} - x_{24})/\tau_2^{(c)}$$

$$\dot{x}_{25} = (x_{19} - x_{25})/\tau_2^{(c)}$$

$$\dot{x}_{26} = (x_{20} - x_{26})/\tau_3^{(c)}$$

$$\dot{x}_{27} = (x_{21} - x_{27})/\tau_3^{(c)}$$

$$\dot{x}_{28} = (x_{22} - x_{28})/\tau_3^{(c)}$$

$$\dot{x}_{29} = (x_{23} - x_{29})/\tau_3^{(c)}$$

$$\dot{x}_{30} = (x_{24} - x_{30})/\tau_3^{(c)}$$

$$\dot{x}_{31} = (x_{25} - x_{31})/\tau_3^{(c)} \qquad (69)$$

where

scr = slaking/causticizing reaction

$x_{26} = X^{(c)}_{Ca(OH)_2}$, the output concentration of $Ca(OH)_2$ from causticizing, mol/lit.

$$x_{27} = X^{(c)}_{Na_2CO_3}, \text{ mol/lit}$$

$$x_{28} = X^{(c)}_{NaOH}, \text{ mol/lit}$$

$$x_{29} = X^{(c)}_{CaCO_3}, \text{ mol/lit}$$

$$x_{30} = X^{(c)}_{Na_2S}, \text{ mol/lit}$$

$$x_{31} = X^{(c)}_{Na_2SO_4}, \text{ mol/lit}$$

The 32nd state variable, x_{32}, is the slaking/causticizing temperature described by the differential Equation (18).

When the lime is added at slaking/causticizing, there is a slight increase in the total volume of the liquor because of the formation of $CaCO_3$ precipitate. Thus, at the outlet of causticizing we have

$$Q^{(c)}_{wl} = Q^{(glc)}_{ql} + .003W_{CaO_I} \tag{70}$$

The density of the liquid part of white liquor at the outlet of causticizing is given by:

$$\rho^{(c)}_{lo} = K_{CO}X^{(c)}_{Na_2CO_3} + K_{OH}X^{(c)}_{NaOH} + K_{2S}X^{(c)}_{Na_2S} + K_{SO}X^{(c)}_{Na_2SO_4} + 60.5 \tag{71}$$

where

$K_{CO} = K_{qq}(106)$, converts Na_2CO_3 in moles/liter to Na_2CO_3 in lb/ft^3

$$K_{qq} = (28.32/454)\ \frac{\text{liter-lb}}{ft^3 - gr}$$

$$K_{OH} = K_{qq}(40)$$

$$K_{2S} = K_{qq}(78)$$

$$K_{SO} = K_{qq}(142)$$

The concentration of suspended solids in the outlet white liquor is

$$X_{sol}^{(c)} = K_{CAOH} X_{Ca(OH)_2}^{(c)} + K_{CACO} X_{CaCO_3}^{(c)} \tag{72}$$

where

$$K_{CAOH} = K_{qq}(74)$$

$$K_{CACO} = K_{qq}(100)$$

Data on the specific gravity of precipated $CaCO_3$ slurries was obtained from the TAPPI Standards (See Reference(21)) and from Reference(22). A polynomial regression of these data gives

$$\rho_{wl}^{(c)} = \rho_{lo}^{(c)} + a_1 X_{sol}^{(c)} + a_2 \left[X_{sol}^{(c)}\right]^2 + a_3 \left[X_{sol}^{(c)}\right]^2 \tag{73}$$

where

$$a_1 = 0.7188691$$

$$a_2 = -0.0028773$$

$$a_3 = 0.0000213$$

Therefore, in Equation (18)

$$m = \rho_{wl}^{(c)} V^{(c)} \tag{74}$$

$$W_{wl}^{(c)} = \rho_{wl}^{(c)} Q_{wl}^{(c)} \tag{75}$$

The flow dynamics for U_{si} (particle size) in causticizing are

$$\dot{x}_{33} = (U_{si} - x_{33})/\tau_1^{(c)}$$

$$\dot{x}_{34} = (x_{33} - x_{34})/\tau_2^{(c)}$$

$$\dot{x}_{35} = (x_{34} - x_{35})/\tau_3^{(c)} \qquad (76)$$

where

x_{35} = the characteristic settling velocity at the outlet of causticizing, ft/hr.

4. White Liquor Clarification

The weighted average molecular weight of the suspended solids entering the white liquor clarifier (settler) from causticizing is given by:

$$M_{avg}^{(c)} = (74\ X_{Ca(OH)_2}^{(c)} + 100\ X_{CaCO_3}^{(c)})/(X_{Ca(OH)_2}^{(c)} + X_{CaCO_3}^{(c)}) \qquad (77)$$

The underflow flow rate is about 28% of the input flow rate. Thus,

$$Q_u^{(wlc)} = 0.28\ Q_{wl}^{(c)} \qquad (78)$$

The overflow flow rate is

$$Q_o^{(wlc)} = Q_{wl}^{(c)} - Q_u^{(wlc)} \qquad (79)$$

The corresponding bulk velocities inside the clarifier tank are

$$v_i^{(wlc)} = Q_{wl}^{(c)}/A^{(wlc)}$$

$$v_u^{(wlc)} = Q_u^{(wlc)}/A^{(wlc)}$$

$$v_o^{(wlc)} = Q_o^{(wlc)}/A^{(wlc)} \qquad (80)$$

where A is the area of the white liquor clarifier. Note that $Q_{wl}^{(c)}$ corresponds to Q_i in Equation (22). The details of the solids settling for white liquor clarification are given in the solids settling model discussion in this section of the report. The flow dynamics for the overflow dissolved solids are

$$\dot{x}_{36} = (X_{Na_2CO_3}^{(c)} - x_{36})/\tau_1^{(wlc)}$$

$$\dot{x}_{37} = (X^{(c)}_{NaOH} - x_{37})/\tau_1^{(wlc)}$$

$$\dot{x}_{38} = (X^{(c)}_{Na_2S} - x_{38})/\tau_1^{(wlc)}$$

$$\dot{x}_{39} = (X^{(c)}_{Na_2SO_4} - x_{39})/\tau_1^{(wlc)}$$

$$\dot{x}_{40} = (x_{36} - x_{40})/\tau_2^{(wlc)}$$

$$\dot{x}_{41} = (x_{37} - x_{41})/\tau_2^{(wlc)}$$

$$\dot{x}_{42} = (x_{38} - x_{42})/\tau_2^{(wlc)}$$

$$\dot{x}_{43} = (x_{39} - x_{42})/\tau_2^{(wlc)} \qquad (81)$$

where

$\tau_1 = \tau_2 = 1.5$ ft/v_o, hrs.

$x_{40} = X^{(wlco)}_{Na_2CO_3}$, concentration of Na_2CO_3 in white liquor in the overflow, mol/lit.

$x_{41} = X^{(wlco)}_{NaOH}$, mol/lit.

$x_{42} = X^{(wlco)}_{Na_2S}$, mol/lit.

$x_{43} = X^{(wlco)}_{Na_2SO_4}$, mol/lit.

The flow rate $Q_o^{(wlc)}$ and the concentrations $X^{(wlco)}_{NaXX}$ represent the characteristics of the white liquor going to the digester. The clarity of white liquor is given in terms of parts of solids per million.

$$PPM^{(wlco)} = \frac{C_t^{(wlco)} M_{avg} (1 \times 10^6)}{(S.G.)(1000)} \qquad (82)$$

where

C_t = concentration of solids in overflow, mol/lit. (See Equation 22.)

S.G. = specific gravity of white liquor

The flow dynamics for the underflow dissolved solids are

$$\dot{x}_{44} = (X^{(c)}_{Na_2CO_3} - x_{44})/\tau_3^{(wlc)}$$

$$\dot{x}_{45} = (X^{(c)}_{NaOH} - x_{45})/\tau_3^{(wlc)}$$

$$\dot{x}_{46} = (X^{(c)}_{Na_2S} - x_{46})/\tau_3^{(wlc)}$$

$$\dot{x}_{47} = (X^{(c)}_{Na_2SO_4} - x_{47})/\tau_3^{(wlc)}$$

$$\dot{x}_{48} = (x_{44} - x_{48})/\tau_4^{(wlc)}$$

$$\dot{x}_{49} = (x_{45} - x_{49})/\tau_4^{(wlc)}$$

$$\dot{x}_{50} = (x_{46} - x_{50})/\tau_4^{(wlc)}$$

$$\dot{x}_{51} = (x_{47} - x_{51})/\tau_4^{(wlc)}$$

$$\dot{x}_{52} = (x_{48} - x_{52})/\tau_5^{(wlc)}$$

$$\dot{x}_{53} = (x_{49} - x_{53})/\tau_5^{(wlc)}$$

$$\dot{x}_{54} = (x_{50} - x_{54})/\tau_5^{(wlc)}$$

$$\dot{x}_{55} = (x_{51} - x_{55})/\tau_5^{(wlc)} \qquad (83)$$

where

$$\tau_3 = \tau_4 = \tau_5 = 2 \text{ ft}/v_u, \text{ hrs.}$$

$x_{52} = X^{(wlcu)}_{Na_2CO_3}$, the concentration of Na_2CO_3 in the underflow (with the mud), mol/lit.

$x_{53} = X^{(wlcu)}_{NaOH}$, mol/lit.

$x_{54} = X^{(wlcu)}_{Na_2S}$, mol/lit.

$x_{55} = X^{(wlcu)}_{Na_2SO_4}$, mol/lit.

The flow dynamics for particle size in the white liquor clarifier underflow are

$$\dot{x}_{56} = (x_{35} - x_{56})/\tau_3^{(wlc)}$$

$$\dot{x}_{57} = (x_{56} - x_{57})/\tau_4^{(wlc)}$$

$$\dot{x}_{58} = (x_{57} - x_{58})/\tau_5^{(wlc)} \qquad (83a)$$

where

x_{58} = characteristic settling velocity at underflow of white liquor clarifier, ft/hr.

5. Lime Mud Mix Tank

The lime mud mix tank is very small compared to the other tanks in the system, so no dynamics were included for it. Fresh water and filtrate from the mud precoat filter are added to the underflow slurry from the white liquor clarifier. The fresh water flow rate is given by:

$$Q_{fr}^{(mm)} = Q_{wwl} + Q_u^{(mw)} - Q_f^{(mf)} - Q_u^{(wlc)} \tag{84}$$

where

$Q_{fr}^{(mm)}$ = fresh water flow rate to mud mix tank, $ft^3/hr.$

$Q_u^{(mw)}$ = mud washer underflow, $ft^3/hr.$

$Q_f^{(mf)}$ = filtrate flow from mud filter, $ft^3/hr.$

The total flow of wash water added to the mud slurry is

$$Q_{wsh}^{(mm)} = Q_{fr}^{(mm)} + Q_f^{(mf)} \tag{85}$$

where $Q_{wsh}^{(mm)}$ = wash water flow to mud mix, $ft^3/hr.$

The concentration of dissolved solids in the wash water is given by:

$$X_{Na_2CO_3}^{(wsh)} = D_1 X_{Na_2CO_3}^{(mf)}$$

$$X_{NaOH}^{(wsh)} = D_1 X_{NaOH}^{(mf)}$$

$$X_{Na_2S}^{(wsh)} = D_1 X_{Na_2S}^{(mf)}$$

$$X_{Na_2SO_4}^{(wsh)} = D_1 X_{Na_2SO_4}^{(mf)} \tag{86}$$

where

$$D_1 = Q_f^{(mf)}/Q_{wsh}^{(mm)}$$

wsh $\Longrightarrow$ concentration in wash water

mf $\Longrightarrow$ concentration from mud filter

The total flow rate from the mud mix tank to the mud washer (settler) is

$$Q_{mm} = Q_u^{(wlc)} + Q_{wsh}^{(mm)} \tag{87}$$

The concentrations of dissolved solids in the Q_{mm} flow are

$$X_{Na_2CO_3}^{(mm)} = (Q_u^{(wlc)} X_{Na_2CO_3}^{(wlcu)} + Q_{wsh}^{(mm)} X_{Na_2CO_3}^{(wsh)})/Q_{mm}$$

$$X_{NaOH}^{(mm)} = (Q_u^{(wlc)} X_{NaOH}^{(wlcu)} + Q_{wsh}^{(mm)} X_{NaOH}^{(wsh)})/Q_{mm}$$

$$X_{Na_2S}^{(mm)} = Q_u^{(wlc)} X_{Na_2S}^{(wlcu)} + Q_{wsh}^{(mm)} X_{Na_2S}^{(wsh)})/Q_{mm}$$

$$X_{Na_2SO_4}^{(mm)} = (Q_u^{(wlc)} X_{Na_2SO_4}^{(wlcu)} + Q_{wsh}^{(mm)} X_{Na_2SO_4}^{(wsh)})/Q_{mm} \tag{88}$$

The mud solids concentration in the Q_{mm} flow is

$$X_{sol}^{(mm)} = (Q_u^{(wlc)}/Q_{mm})\ C_u^{(wlc)} \tag{89}$$

where

C_u = concentration of solids in white liquor clarifier underflow, mol/lit. (See Equation 22.)

6. Mud Washing

The mud washer underflow flow rate is about 19% of the input flow rate. Thus,

$$Q_u^{(mw)} = 0.19 Q_{mm} \tag{90}$$

The overflow flow rate is

$$Q_o^{(mw)} = Q_{mm} - Q_u^{(mw)} \tag{91}$$

The corresponding bulk velocities inside the settler tank are

$$v_i^{(mw)} = Q_{mm}/A^{(mw)}$$

$$v_u^{(mw)} = Q_u^{(mw)}/A^{(mw)}$$

$$v_o^{(mw)} = Q_o^{(mw)}/A^{(mw)} \tag{92}$$

Note that Q_{mm} corresponds to Q_i in Equation 22. The flow dynamics for the overflow dissolved solids are

$$\dot{x}_{59} = (X_{Na_2CO_3}^{(mm)} - x_{59})/\tau_1^{(mw)}$$

$$\dot{x}_{60} = (X_{NaOH}^{(mm)} - x_{60})/\tau_1^{(mw)}$$

$$\dot{x}_{61} = (X_{Na_2S}^{(mm)} - x_{61})/\tau_1^{(mw)}$$

$$\dot{x}_{62} = (X_{Na_2SO_4}^{(mm)} - x_{62})/\tau_1^{(mw)}$$

$$\dot{x}_{63} = (x_{59} - x_{63})/\tau_2^{(mw)}$$

$$\dot{x}_{64} = (x_{60} - x_{64})/\tau_2^{(mw)}$$

$$\dot{x}_{65} = (x_{61} - x_{65})/\tau_2^{(mw)}$$

$$\dot{x}_{66} = (x_{62} - x_{66})/\tau_2^{(mw)} \qquad (93)$$

where

$$\tau_1 = \tau_2 = 1.5 \text{ ft}/v_o, \text{ hrs.}$$

$x_{63} = X_{Na_2CO_3}^{(mwo)}$, concentration of Na_2CO_3 in mud washer overflow, mol/lit.

$x_{64} = X_{NaOH}^{(mwo)}$, mol/lit.

$x_{65} = X_{Na_2S}^{(mwo)}$, mol/lit.

$x_{66} = X_{Na_2SO_4}^{(mwo)}$, mol/lit.

The flow rate $Q_o^{(mw)}$ and the concentrations $X_{NaXX}^{(mwo)}$ represent the characteristics of the weak wash liquor going to the weak liquor storage tank and subsequently to smelt dissolving.

The flow dynamics for the washer underflow dissolved solids are

$$\dot{x}_{67} = (X_{Na_2CO_3}^{(mm)} - x_{67})/\tau_3^{(mw)}$$

$$\dot{x}_{68} = (X_{NaOH}^{(mm)} - x_{68})/\tau_3^{(mw)}$$

$$\dot{x}_{69} = (X_{Na_2S}^{(mm)} - x_{69})/\tau_3^{(mw)}$$

$$\dot{x}_{70} = (X^{(mm)}_{Na_2SO_4} - x_{70})/\tau_3^{(mw)}$$

$$\dot{x}_{71} = (x_{67} - x_{71})/\tau_4^{(mw)}$$

$$\dot{x}_{72} = (x_{68} - x_{72})/\tau_4^{(mw)}$$

$$\dot{x}_{73} = (x_{69} - x_{73})/\tau_4^{(mw)}$$

$$\dot{x}_{74} = (x_{70} - x_{74})/\tau_4^{(mw)}$$

$$\dot{x}_{75} = (x_{71} - x_{75})/\tau_5^{(mw)}$$

$$\dot{x}_{76} = (x_{72} - x_{76})/\tau_5^{(mw)}$$

$$\dot{x}_{77} = (x_{73} - x_{77})/\tau_5^{(mw)}$$

$$\dot{x}_{78} = (x_{74} - x_{78})/\tau_5^{(mw)} \qquad (94)$$

where

$\tau_3 = \tau_4 = \tau_5 = 2$ ft/v_u, hrs.

$x_{75} = X^{(mwu)}_{Na_2CO_3}$, the concentration of Na_2CO_3 in the underflow (with the mud), mol/lit.

$x_{76} = X^{(mwu)}_{NaOH}$, mol/lit.

$x_{77} = X^{(mmu)}_{Na_2S}$, mol/lit.

$x_{78} = X^{(mwu)}_{Na_2SO_4}$, mol/lit.

7. Lime Mud Storage and Mud Density Control

The mud tank storage equation is

$$x_{79} = \frac{dV^{(ms)}}{dt} = Q_u^{(mw)} - Q_m^{(ms)} \tag{95}$$

where

V = volume of mud storage, ft^3

ms = mud storage

The total retention time is

$$\tau^{(ms)} = V^{(ms)}/Q_m^{(ms)} \tag{96}$$

The mud tank is continuously stirred. Therefore, the dynamics for concentrations of dissolved solids are

$$\dot{x}_{80} = (X_{Na_2CO_3}^{(mwu)} - x_{80})/\tau^{(ms)}$$

$$\dot{x}_{81} = (X_{NaOH}^{(mwu)} - x_{81})/\tau^{(ms)}$$

$$\dot{x}_{82} = (X_{Na_2S}^{(mwu)} - x_{82})/\tau^{(ms)}$$

$$\dot{x}_{83} = (X_{Na_2SO_4} - x_{83})/\tau^{(ms)} \tag{97}$$

where

$x_{80} = X_{Na_2CO_3}^{(ms)}$, concentration of Na_2CO_3 in outlet of mud storage, mol/lit.

$x_{81} = X_{NaOH}^{(ms)}$, mol/lit.

$x_{82} = X_{Na_2S}^{(ms)}$, mol/lit.

$x_{83} = X_{Na_2SO_4}^{(ms)}$, mol/lit.

The flow dynamics for mud solids is

$$\dot{x}_{84} = (C_u^{(mw)} - x_{84})/\tau^{(ms)} \tag{98}$$

where C_u is as defined in Equation 22, and

x_{84} = concentration of solids in the storage tank outlet, mol/lit.

The flow dynamics for the particle size in the mud washer underflow and subsequent storage tank outlet flow is

$$\dot{x}_{85} = (x_{58} - x_{85})/\tau_3^{(mw)}$$

$$\dot{x}_{86} = (x_{85} - x_{86})/\tau_4^{(mw)}$$

$$\dot{x}_{87} = (x_{86} - x_{87})/\tau_5^{(mw)}$$

$$\dot{x}_{88} = (x_{87} - x_{88})/\tau^{(mw)} \tag{99}$$

where

x_{88} = characteristic settling velocity at outlet of mud storage, ft/hr.

The concentration of mud solids converted to lb/ft^3 is

$$X_{sol}^{(ms)} = K_{qq} x_{84} M_{avg} \tag{100}$$

The soda concentration of the mud slurry at outlet of mud storage is

$$X_{soda}^{(ms)} = K_{CO} X_{Na_2CO_3}^{(ms)} + K_{OH} X_{NaOH}^{(ms)} + K_{2S} X_{Na_2S}^{(ms)} + K_{SO} X_{Na_2SO_4}^{(ms)} \tag{101}$$

The corresponding liquor density <u>without</u> suspended solids is

$$\rho_{lo}^{(ms)} = X_{soda}^{(ms)} + 60.5,\ lb/ft^3 \tag{102}$$

The corresponding total slurry density is

$$\rho_m^{(ms)} = \rho_{lo}^{(ms)} + a_1 X_{sol}^{(ms)} + a_2 \left[X_{sol}^{(ms)}\right]^2 + a_3 \left[X_{sol}^{(ms)}\right]^3 \qquad (103)$$

where a_1, a_2, and a_3 are defined in Equation 73.

The lime mud slurry flow rate and density are controlled prior to the pre-coat filter. Thus, $Q_m^{(fil)}$ and $\rho_m^{(fil)}$ are specified. Fresh water is used to dilute the slurry to the desired density $\rho_m^{(fil)}$. The

The flow rate from mud storage is then given by:

$$Q_m^{(ms)} = Q_m^{(fil)} \Big/ \left[1 + \left(\rho_m^{(ms)} - \rho_m^{(fil)}\right)/\left(\rho_m^{(fil)} - 60.5\right)\right] \qquad (104)$$

The dilution flow is given by:

$$Q_{dil} = Q_m^{(fil)} - Q_m^{(ms)} \qquad (105)$$

The concentrations of dissolved solids going to the filter is

$$X_{Na_2CO_3}^{(fil)} = D_2 X_{Na_2CO_3}^{(ms)}$$

$$X_{NaOH}^{(fil)} = D_2 X_{NaOH}^{(ms)}$$

$$X_{Na_2S}^{(fil)} = D_2 X_{Na_2S}^{(ms)}$$

$$X_{Na_2SO_4}^{(fil)} = D_2 X_{Na_2SO_4}^{(ms)} \qquad (106)$$

where

$$D_2 = Q_m^{(ms)}/Q_m^{(fil)}$$

The suspended solids concentration to the filter is

$$X_{sol}^{(fil)} = D_2 X_{sol}^{(ms)} \tag{107}$$

The soda concentration, the corresponding liquor density and total slurry density going to the filter is

$$X_{soda}^{(fil)} = D_2 X_{soda}^{(ms)}$$

$$\varrho_l^{(fil)} = X_{soda}^{(fil)} + 60.5$$

$$\varrho_m^{(fil)} = \varrho_l^{(fil)} + a_1 X_{sol}^{(fil)} + a_2 \left[X_{sol}^{(fil)}\right]^2 + a_3 \left[X_{sol}^{(fil)}\right]^3 \tag{108}$$

The per cent suspended solids going to the filter is

$$P_{sol}^{(fil)} = 100 \left(X_{sol}^{(fil)} / \varrho_m^{(fil)}\right) \tag{109}$$

8. Lime Mud Pre-coat Filter

The equations for pre-coat filtration are given under the main heading "Lime Mud Pre-coat Filter Model" in this section of the report. As shown in Figure 16, the pre-coat filter is modeled as a dewatering filter followed by an ideally mixed tank (for washing) and another dewatering filter in series. The mass flow of suspended solids going to the filter is given by:

$$W_{sol}^{(fil)} = X_{sol}^{(fil)} Q_m^{(fil)}, \text{ lb/hr} \tag{110}$$

Solution of Equation (57) gives the filtrate flow rate, Q_f. In Equation 57,

$$\rho_f = \rho_l^{(fil)}$$

$$Q_m = Q_m^{(fil)}$$

$$X_m = X_{sol}^{(fil)} \tag{111}$$

The flow rate remaining after first dewatering is

$$Q_{left} = Q_m^{(fil)} - Q_f \tag{112}$$

The flow resulting after wash water is added is

$$Q_{wshng} = Q_{left} + Q_{ww} \tag{113}$$

where Q_{ww} = wash water flow rate, ft^3/hr.

The soda concentration, suspended solids concentration, and mud slurry density going to final dewatering is given by:

$$X^{(f)}_{Na_2CO_3} = D_3 X^{(fil)}_{Na_2CO_3}$$

$$X^{(f)}_{NaOH} = D_3 X^{(fil)}_{NaOH}$$

$$X^{(f)}_{Na_2S} = D_3 X^{(fil)}_{Na_2S}$$

$$X^{(f)}_{Na_2SO_4} = D_3 X^{(fil)}_{Na_2SO_4}$$

$$X^{(f)}_{soda} = D_3 X^{(fil)}_{soda}$$

$$D_3 = Q_{left}/Q_{wshng}$$

$$\rho_1^{(f)} = X^{(fil)}_{soda} + 60.5$$

$$X^{(fil)}_{sol\ 2} = W^{(fil)}_{sol}/Q_{wshing}$$

$$\rho_{m2}^{(fil)} = \rho_1^{(f)} + a_1 X^{(fil)}_{sol\ 2} + a_2 \left[X^{(fil)}_{sol\ 2}\right]^2 + a_3 \left[X^{(fil)}_{sol\ 2}\right]^3 \qquad (114)$$

A second solution of Equation (57) gives the filtrate generated after wash, Q_{fw}. In Equation (57)

$$\rho_f = \rho_1^{(f)}$$

$$Q_m = Q_{wshng}$$

$$X_m = X^{(fil)}_{sol\ 2} \qquad (115)$$

The total flow of filtrate leaving the mud filter is given by

$$Q_f^{(mf)} = Q_f + Q_{fw} \tag{116}$$

The soda concentrations in the filtrate are

$$X_{Na_2CO_3}^{(mf)} = (Q_f X_{Na_2CO_3}^{(fil)} + Q_{fw} X_{Na_2CO_3}^{(f)})/Q_f^{(mf)}$$

$$X_{NaOH}^{(mf)} = (Q_f X_{NaOH}^{(fil)} + Q_{fw} X_{NaOH}^{(f)})/Q_f^{(mf)}$$

$$X_{Na_2S}^{(mf)} = (Q_f X_{Na_2S}^{(fil)} + Q_{fw} X_{Na_2S}^{(f)})/Q_f^{(mf)}$$

$$X_{Na_2SO_4}^{(mf)} = (Q_f X_{Na_2SO_4}^{(fil)} + Q_{fw} X_{Na_2SO_4}^{(f)})/Q_f^{(mf)} \tag{117}$$

The density of the filtrate is

$$\rho_l^{(mf)} = K_{CO} X_{Na_2CO_3}^{(mf)} + K_{OH} X_{NaOH}^{(mf)} + K_{2S} X_{Na_2S}^{(mf)} + K_{SO} X_{Na_2SO_4}^{(mf)} + 60.5 \tag{118}$$

The total mass flow of mud cake going to calcining is

$$W_m^{(mf)} = Q_m^{(fil)} \rho_m^{(fil)} - Q_f^{(mf)} \rho_l^{(mf)} + 60.5\, Q_{ww} \tag{119}$$

Per cent suspended solids in the mud cake to calcining is given by:

$$P_{sol}^{(mf)} = 100\ (W_{sol}^{(fil)}/W_m^{(mf)}) \tag{120}$$

The soda in the mud cake (expressed as Na_2O equivalents) is

$$X_{soda}^{(cake)} = 62K_{qq} X_{Na_2CO_3}^{(f)} + 31K_{qq} X_{NaOH}^{(f)} + 62K_{qq} X_{Na_2S}^{(f)} + 62K_{qq} X_{Na_2SO_4}^{(f)} \tag{121}$$

The mud solids in the cake is (as Na_2O)

$$X_{sol}^{(cake)} = (62/M_{avg}^{mf})(W_{sol}^{(fil)}/[Q_{wshng} - Q_{fw}]) \qquad (122)$$

The per cent soda in the cake as Na_2O is

$$P_{soda}^{(cake)} = 100\left[X_{soda}^{(cake)}/(X_{soda}^{(cake)} + X_{sol}^{(cake)})\right] \qquad (123)$$

9. Weak Wash Storage

The storage equation for the weak wash tank:

$$\dot{x}_{89} = \frac{dV^{(ww)}}{dt} = Q_o^{(mw)} - Q_{wwl} \tag{124}$$

The storage retention time is

$$\tau^{(ww)} = V^{(ww)}/Q_{wwl} \tag{125}$$

The soda concentration flow dynamics are given by:

$$\dot{x}_{90} = (X_{Na_2CO_3}^{(mwo)} - x_{90})/\tau_1^{(ww)}$$

$$\dot{x}_{91} = (X_{NaOH}^{(mwo)} - x_{91})/\tau_1^{(ww)}$$

$$\dot{x}_{92} = (X_{Na_2S}^{(mwo)} - x_{92})/\tau_1^{(ww)}$$

$$\dot{x}_{93} = (X_{Na_2SO_4}^{(mwo)} - x_{93})/\tau_1^{(ww)}$$

$$\dot{x}_{94} = (x_{90} - x_{94})/\tau_2^{(ww)}$$

$$\dot{x}_{95} = (x_{91} - x_{95})/\tau_2^{(ww)}$$

$$\dot{x}_{96} = (x_{92} - x_{96})/\tau_2^{(ww)}$$

$$\dot{x}_{97} = (x_{93} - x_{97})/\tau_2^{(ww)} \tag{126}$$

where $\tau_1 = \tau_2 = \tau^{(ww)}/2$, hrs.

$x_{94} = X_{Na_2CO_3}^{(wwl)}$, concentration of Na_2CO_3 in weak wash liquor

$$x_{95} = X_{NaOH}^{(wwl)}$$

$$x_{96} = X_{Na_2S}^{(wwl)}$$

$$x_{97} = X_{Na_2SO_4}^{(wwl)}$$

PROPOSED CONTROL SYSTEM FOR THE LIQUOR PREPARATION SYSTEM

The basic control objectives for the liquor preparation system are

1. To provide a clear white liquor, with a high, uniform strength, to the digester.

2. To control mud particle size so that (1) the clarity in the first objective may be attained, and (2) the lime mud may be adequately washed and dewatered prior to calcining.

Figure 19 shows the results of a 40-hour simulation run starting at steady state using the dynamic model described in this section. As Figure 19 indicates, the two control objectives listed above are somewhat contradictory. At a very high liquor strength (TTA $\cong$ 9.0), the overflow of the white liquor clarifier was very "cloudy" (suspended solids $\cong$ 13000 PPM). At hour zero of the run, the density control set point at smelt dissolving was changed from a specific gravity of 1.195 to 1.18. (The smelt production rate remained constant.) The TTA at causticizing dropped to 8.3. The overloaded white liquor clarifier became underloaded because mud particle size increased as the green liquor strength entering causticizing decreased. At 24 hours, the clarity had improved to less than 100 PPM. The soda content of the lime mud going to the kiln held at about 2.3% for 24 hours after the change was made, but then dropped to 1.95% at 40 hours and was continuing to drop.

The sharp dip in the clarity at three hours was caused by the sudden increase in green liquor flow rate which decreased the causticizing time and increased the particle size. However, high strength green liquor still in storage caused an increase in the active lime flow rate at slaking because of the increased green liquor flow rate. This increased

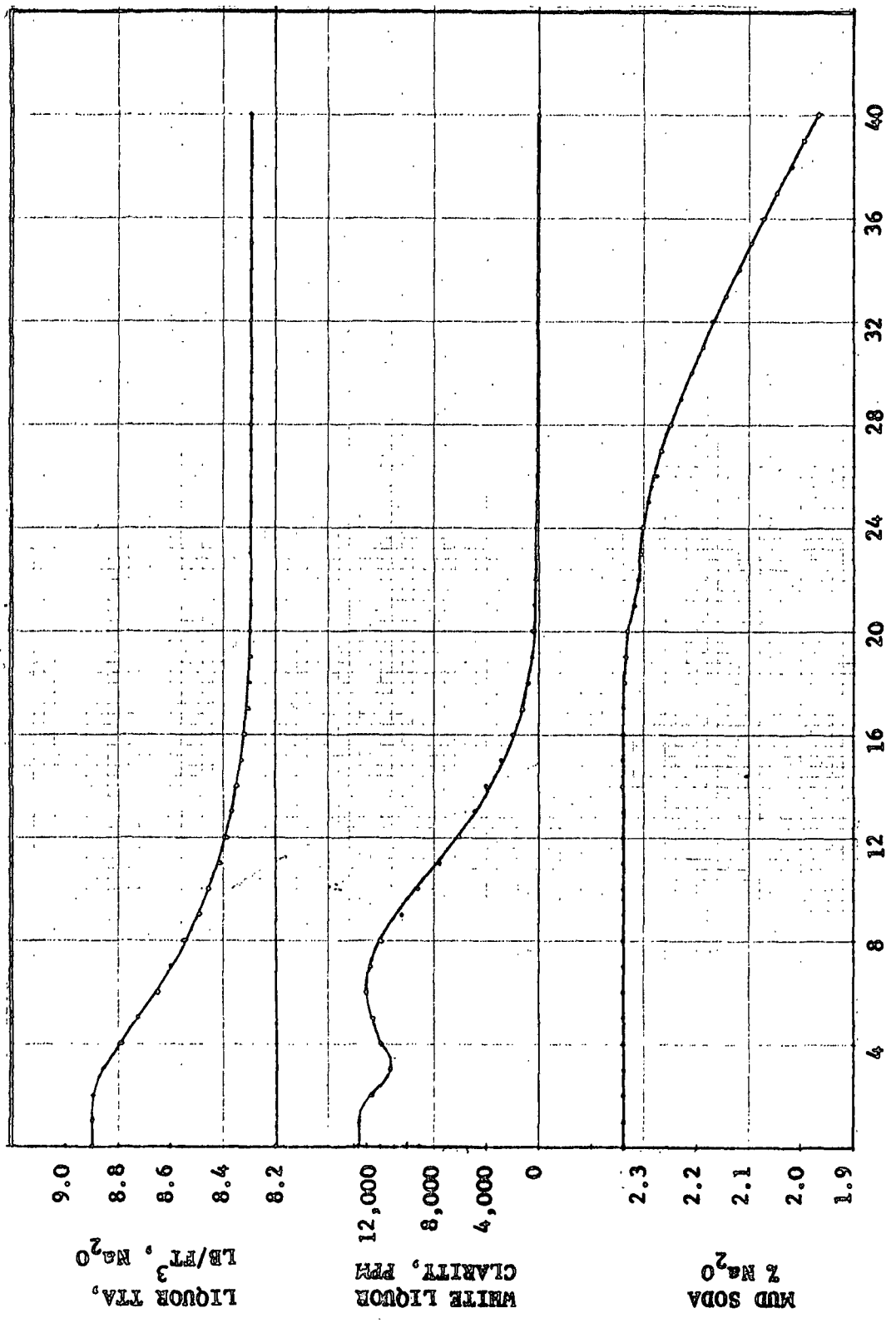

FIGURE 19

MODEL PERFORMANCE FOR STEP DECREASE IN GREEN LIQUOR DENSITY

the total solids flux entering the clarifier, and the clarity became worse between hours 3 and 6. After the stronger liquor passed from storage and from causticizing, the active lime addition dropped, as did the mud influx, while the mud particle size increased (by about 15%).

The 2.3% soda loss in the mud cake amounts to a loss of about 15 lb. $Na_2O/(T/D)$. This is about a factor of three times above what it should be. (Normal soda losses in the mud cake range from 0.5 to 1.0%.) However, as the green liquor strength decreases, the soda loss at the mud filter decreases, because the larger mud particles decrease the specific surface area and thus decrease the filtration resistance.

These results point out the need for a "trade-off" type of control system which will keep the white liquor strength high, but not too high, so that clarity, mud moisture content, and mud soda content can be maintained within reasonable limits.

Figure 20 shows the results of some simulation runs using the steady state causticizer model. The results help to explain why increasing the white liquor strength by adding excess lime will decrease the settleability of the resulting lime mud. First of all, as expected, the white liquor strength does increase, as does the causticizing efficiency. However, as the bottom curve shows, there is also a significant increase in the equilibrium concentration of $Ca(OH)_2$ (about a 50% increase at 12% excess lime over that at 0% excess). The resulting mud solids concentration in the liquor to the white liquor clarifier will be higher at 12% excess lime by about 8%. Furthermore, the $Ca(OH)_2$ particles are quite small compared to $CaCO_3$ particles. Thus, the average settling velocity of the mud will also decrease. Both of these conditions will contribute to overloading of the settlers and the mud filter.

NOTE: TTA HELD AT 7.5 LB Na_2O/FT^3

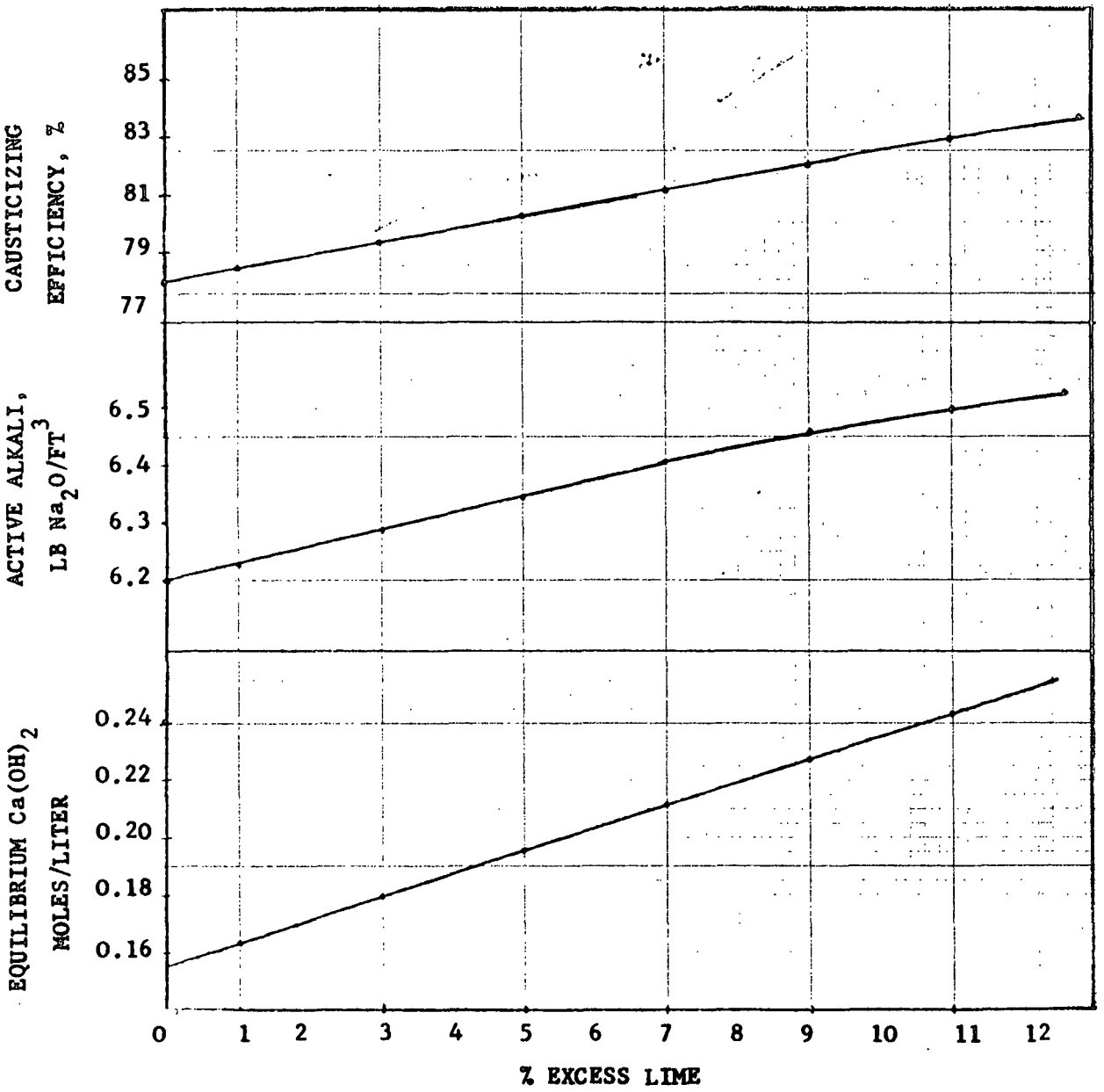

FIGURE 20

EFFECT OF EXCESS LIME ON UNPOLISHED WHITE LIQUOR CHARACTERISTICS

Most pulp mill operators understand the need to control mud particle size. They also understand that there must be some trade-off made between the desire for a high strength white liquor in terms of active alkali or effective alkali, and the settleability and washability of the lime mud. Usually, a sample of causticized liquor is taken manually every hour to determine the strength. The sample is titrated using the A, B, and C titration tests. (For a description of these tests, see Reference (4, pp. 672-678)) The results of these three tests yield the concentrations of Na_2CO_3, NaOH, and Na_2S. Based on the results of these tests the operator will often adjust the lime feed rate to improve the causticizing conversion. In some pulp mills the operator will also take a sample of causticized liquor to perform a settling rate test. For example, the operator fills a 500 cc. graduate with liquor from the first causticizer. After it has stood for five minutes, the percentage of clear liquor is recorded as settling rate. Operating experience has shown that 35 to 45% clear liquor in five minutes is indicative of a good mud settling rate. The main thrust behind this test is to let the operator know that he may have "over-limed" the liquor fed to the slaker.

However, as Figures 4 through 8 show, there are several other factors besides overliming which will cause poor mud settleability. Thus, the liquor uniformity and mud uniformity depend upon the operators and their skill in correlating various items of information made available to them by recorders, meters, and mechanical and chemical tests. This is a monumental task for one or two operators who usually have other tasks to perform.

Figure 21 shows a control scheme that should relieve the operator of considerable guesswork. These control functions would be implemented in the direct digital controller. The causticizing and mud particle size controller loop receives the following measurements:

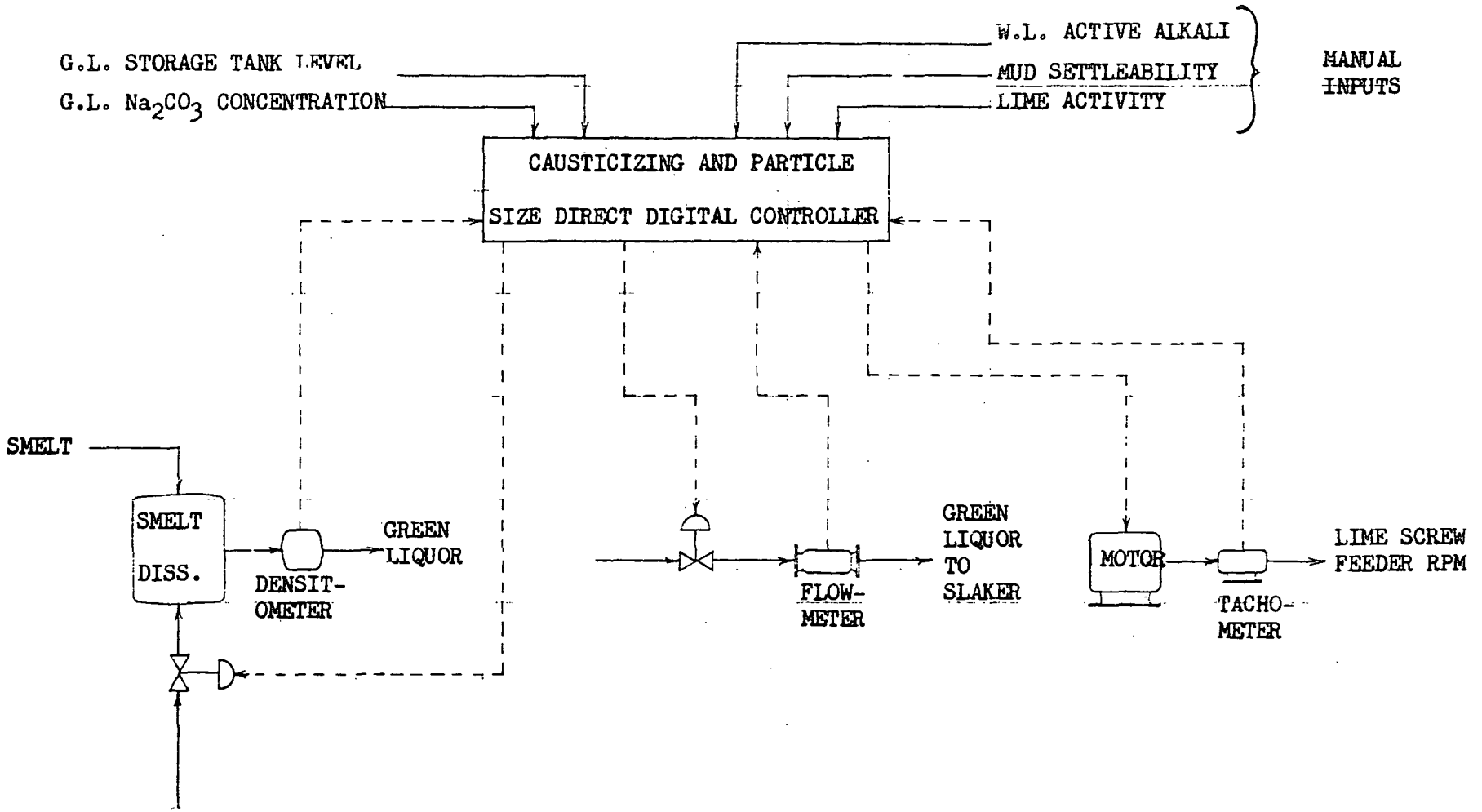

FIGURE 21. PROPOSED CAUSTICIZING AND MUD PARTICLE SIZE CONTROLLER

1. Lime activity (manual entry)
2. Green liquor Na_2CO_3 concentration (automatic titrator)
3. Mud settleability (manual entry)
4. White liquor active alkali (manual entry)
5. Green liquor storage tank level (level sensor)
6. Green liquor flow rate (magnetic flowmeter)

The controller uses these measurements to compute setpoints for:

1. Green liquor density
2. Green liquor flow rate
3. The lime feed rate

The setpoints which the operator enters are

1. Initial AA target
2. Initial excess lime target (usually 0%)
3. Green liquor storage tank level

The limits which the operator enters are

1. AA (high and low)
2. U_{si} (low)
3. Green liquor density (high and low)
4. Excess lime (high and low)
5. Green liquor tank level (high and low)

The general philosophy behind this control scheme is to maximize the AA content of the white liquor within the AA high and low limits while maintaining at least a minimum mud free settling velocity (particle size).

The settling velocity parameter is updated about once an hour using the equation:

$$U_{si}^{(c)} = B_o - 0.1155t_c - 0.00833L - .03629G_c \qquad (127)$$

where

B_o is a "constant" parameter

t_c, L, G_c are as defined in Equation (20)

Note that Equation (127) is similar to Equation (21) except that the initial constant, the per cent of green liquor to slaking (G), the causticizing temperature (T_c), the calcining temperature (T_K), and the calcining time (t_K) are all considered as constants. Their nominal values along with their appropriate slope factors are lumped into the "constant" parameter B_o. Under normal circumstances G, T_c, T_K, and t_K do not change significantly.*

However, to make sure the B_o parameter is updated periodically, a simple identification scheme is included in the particle size controller. The basic block diagram for the identification of B_o is shown in Figure 22 in FORTRAN symbols. The controller monitors the green liquor density, the green liquor flow rate, and the lime feed setpoint for a period of six hours. Simultaneously, the operator takes settleability samples from the first causticizer every hour. The free settling rate is entered manually for each sample. If the density, flow rate, and feed rate have not changed significantly for the past six hours, the system is considered to be at steady state, and B_o is updated as shown in the compute block. If the system is not at steady state, an indicator is set so that the main program will return to the identification program every half-hour or so until a steady state is reached and a new B_o is computed. The values of

*There are other disturbance conditions which affect B_o, such as the silica content of the make-up lime and the silica content of the smelt coming from the furnace.

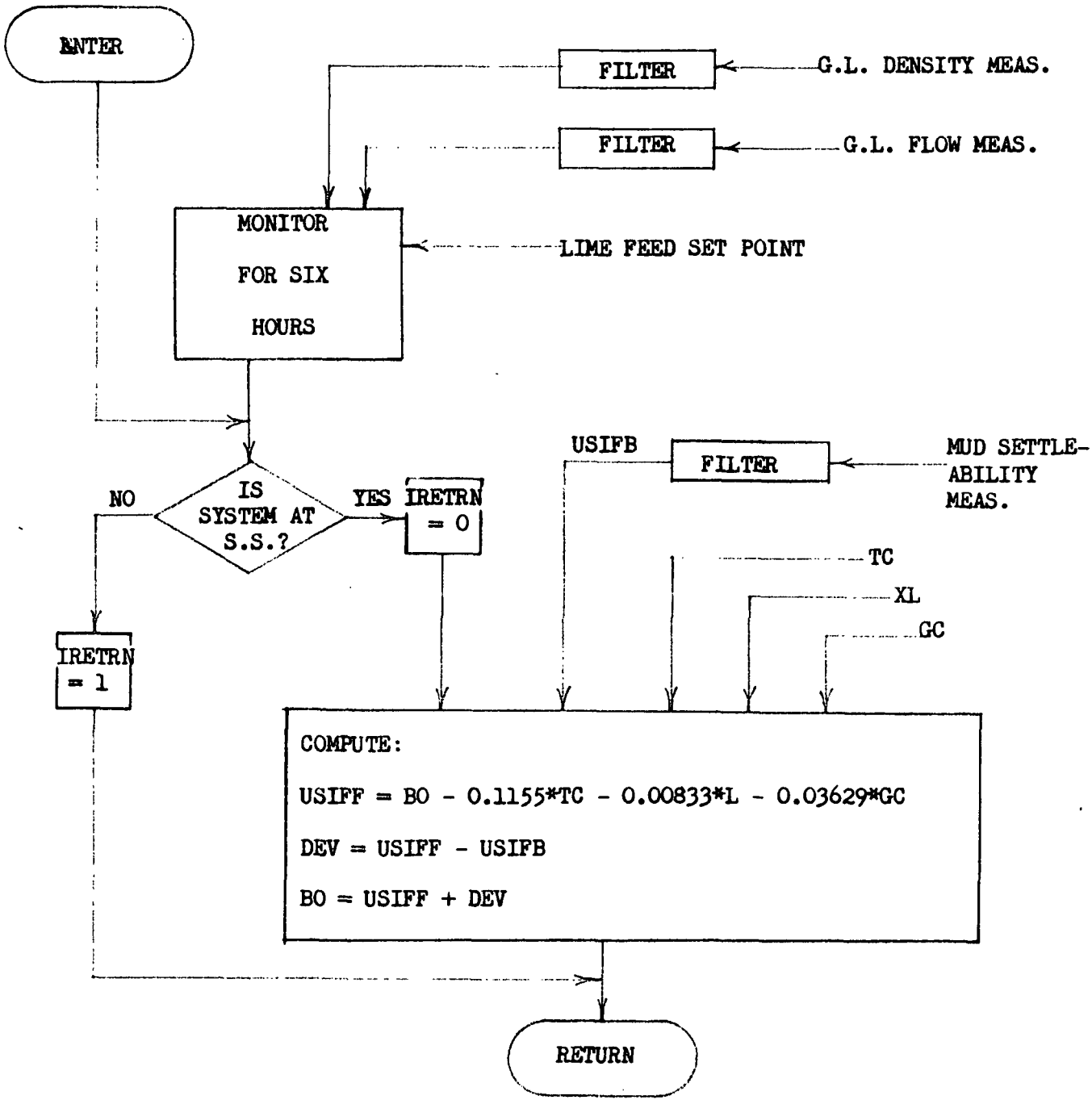

FIGURE 22. IDENTIFICATION OF B_o

t_c, L, and G_c are computed in the main program using exponentially filtered values for $Q_{gl}^{(c)}$, $X_{Na_2CO_3}^{(glc)}$, and lime causticizing power (A_{CaO}). The equations are

$$t_c = V^{(c)}/Q_{gl}^{(c)}$$

$$G_c = X_{Na_2CO_3}^{(wlc)}, \text{ (gr/liter)}$$

$$D_{CaO}^{(A)} = A_{CaO} D_{CaO}$$

$$W_{CaO}^{(A)} = S_{CaO} D_{CaO}^{(A)} F_{CaO}$$

$$L = W_{CaO}^{(A)} / \left[G_c Q_{gl}^{(c)} (56/454) \right] \qquad (128)$$

where

$D_{CaO}^{(A)}$ = density of active lime, lb/ft^3

D_{CaO} = total density of lime, lb/ft^3

$W_{CaO}^{(A)}$ = actual active lime flow, lb/hr

S_{CaO} = set point for turning rate of lime screw conveyor, RPM

F_{CaO} = volumetric flow of lime per revolution of the conveyor, ft^3/Rev

The minimum particle size control algorithm serves as the "master" control. Figure 23 illustrates the idea. If the computed free settling velocity, U_{siff}, exceeds the minimum value, the AA setpoint is "bumped" by 0.05 lb. Na_2O/ft^3, unless the AA is already at the upper control limit. If AA is at the upper limit, an alarm message is given. If the U_{siff} is less than U_{simin}, by less than 0.1 ft/hr in absolute value, nothing is done. This

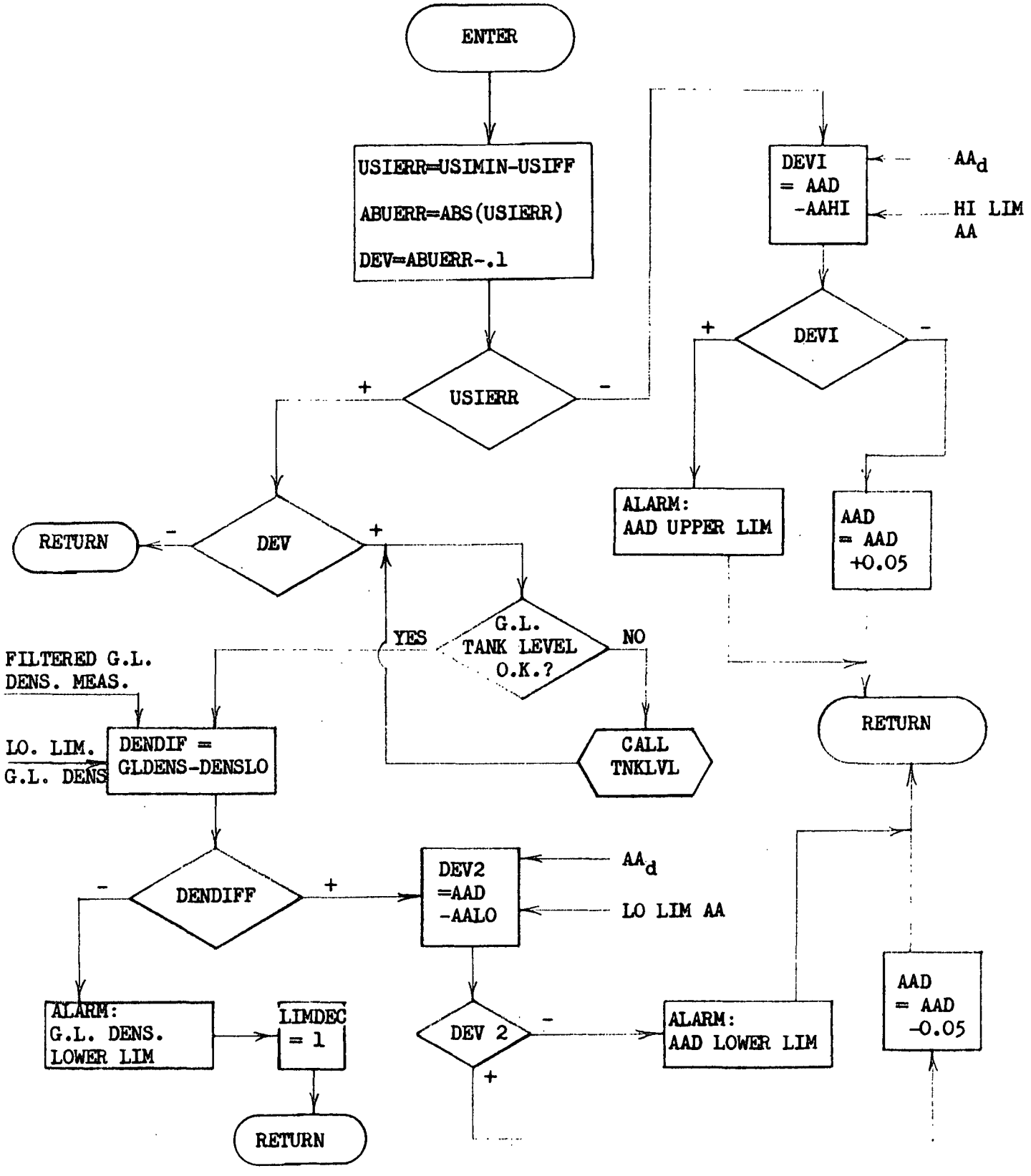

FIGURE 23. PROGRAM FOR PARTICLE SIZE CONTROL

deadband is provided so that oscillations will not occur when AA is near the upper limit and U_{siff} is near the lower limit. Next the program checks to see if the green liquor tank level is within the control band. If the tank level is not satisfactory, the tank level control program is called, which adjusts the green liquor flow rate appropriately to bring the level into the control band. (See Figure 24.) Once the tank level is in control, the program checks to see if the green liquor density is above the lower limit.

The tank level and density are checked because the control method intends to decrease the density and thus increase the green liquor flow rate. Both of these actions should improve the particle size (decreases density and decreases causticizing time). If the density is below the lower limit, an indicator is set to tell the excess lime control program (XLIME) to decrease the excess active lime. Simultaneously, an alarm is given to inform the operator that the green liquor density is at the lower limit. Under this condition, the control computer will decrease the excess lime in an effort to increase the mud particle size rather than decrease the green liquor density and increase the flow rate. If the green liquor density is satisfactory, the AA setpoint is bumped down by 0.05 lb. Na_2O/ft^3 unless the AA is already at the lower limit, in which case an alarm message is given; and no change is made to the AA set point.

Reducing (or increasing) the AA setpoint will ultimately result in a reduction (or an increase) in the green liquor density set point, as Figure 25 shows. An automatic instrument or the process operator takes samples of white liquor at the first causticizer at least once every hour. The measured AA is entered into the computer controller by the instrument or by manual entry. These numbers are filtered and stored.

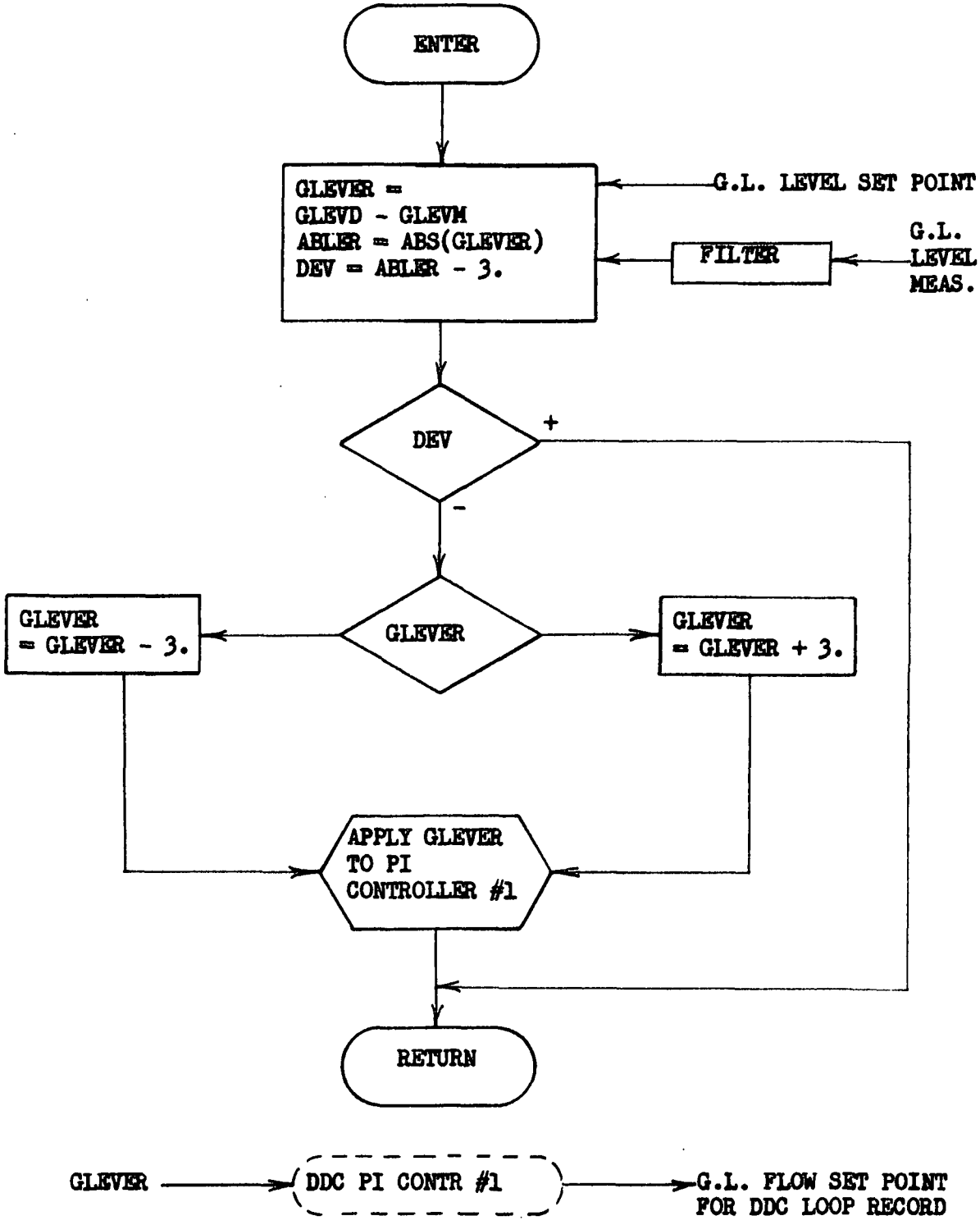

FIGURE 24. GREEN LIQUOR STORAGE TANK LEVEL CONTROL

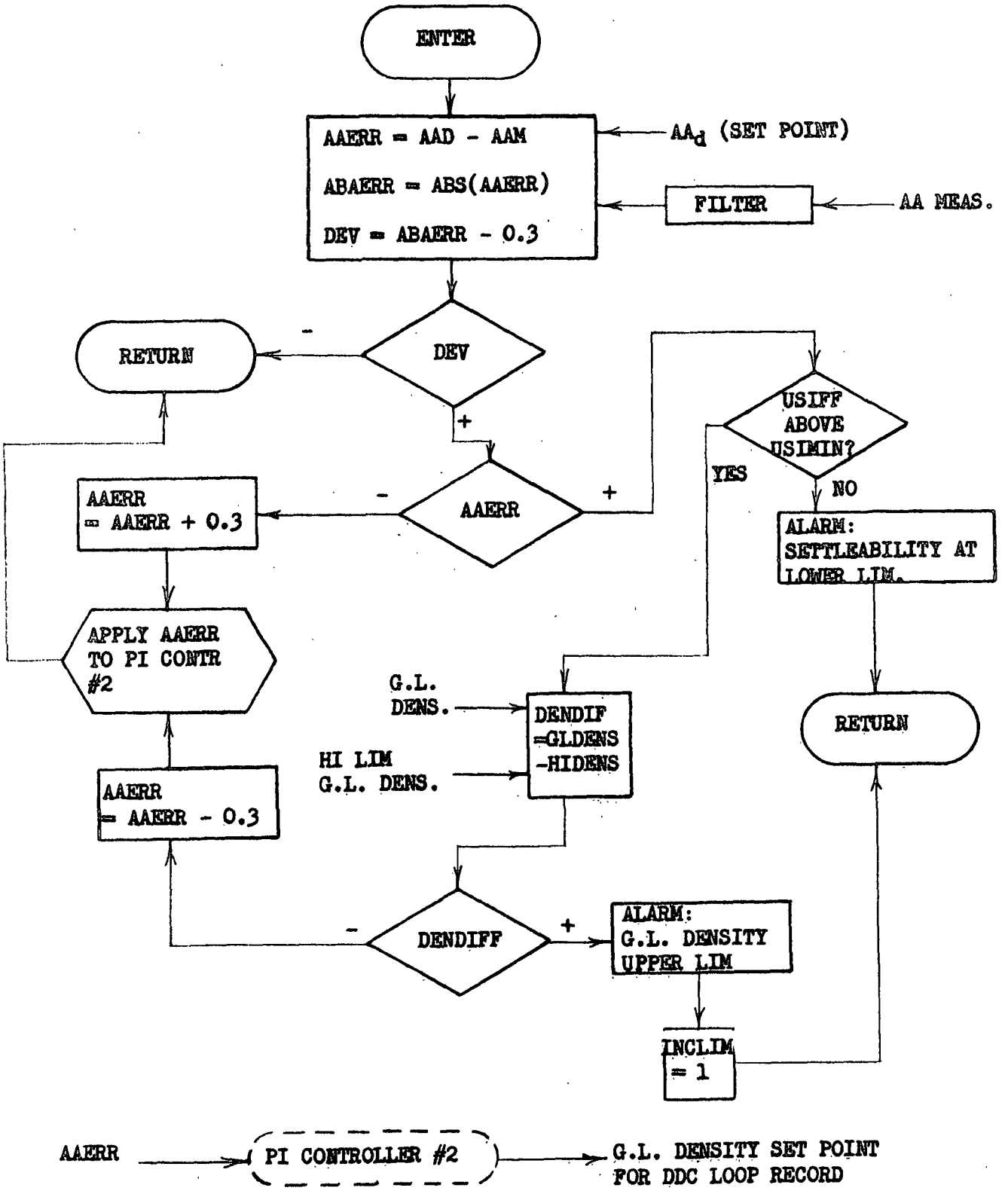

FIGURE 25. ACTIVE ALKALI (AA) CONTROL

When the AA control program is entered, a check is made to see if the AA error is within a predetermined deadband. If it is, no changes are made. If the measured AA is above the desired AA by too much, the appropriate error is applied at the input to a cascade digital PI control algorithm which adjusts the green liquor density setpoint. If the measured AA is below the desired by too much, the program first checks to see if the free settling velocity of the mud is below the lower limit. If it is, an alarm message is given, and a recommendation is made to lower the AA target. If U_{siff} is satisfactory, the green liquor density is checked to see if it is at the high limit. If it is, the green liquor density is not increased, but excess lime is increased in order to increase the AA. Otherwise, the modified error signal is applied to the digital PI density control algorithm. Note that a continued decrease (or increase) in the AA setpoint by the particle size control program will ultimately decrease (or increase) the green liquor density.

Because of the relatively long delay between the smelt dissolving tank and the first causticizer, control actions for the AA control loop will have to be delayed appropriately. The delay time can be identified approximately, because the storage and piping dimensions are known, the green liquor storage tank level is known from measurement, and the green liquor flow rate is known from measurement.

Figure 26 shows the control scheme for increasing or decreasing the excess lime (above or below the theoretical lime required). The inputs to the program include

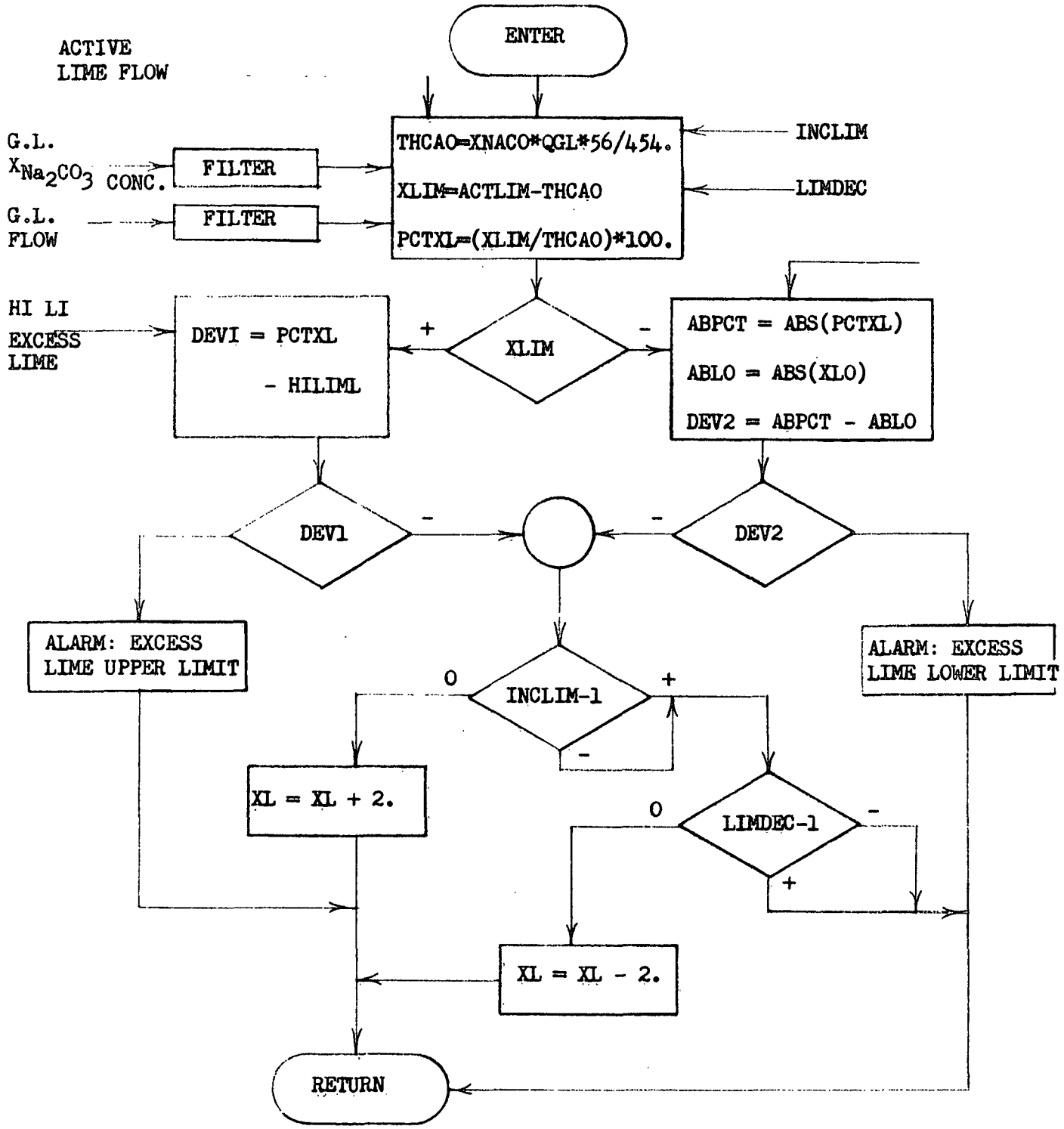

FIGURE 26. EXCESS LIME CONTROL

1. Active lime flow
2. Na_2CO_3 concentration
3. Green liquor flow rate.

The active lime flow rate is computed in the main program based on periodic manual entries of the lime causticizing power. The Na_2CO_3 concentration is obtained from an automatic titrator. Green liquor flow rate is obtained from the magnetic flowmeter.

The XLIME program first computes the present level of excess lime and compares this with the high and low limits for excess lime. If either limit has been reached, an alarm is given and no further changes are made. Based on which of the INCLIM or LIMDEC indicators are on, the excess lime parameter (%XL) will be appropriately bumped up or bumped down by 2%.

Figure 27 shows the program for lime flow control. The inputs are

1. Lime causticizing power (filtered manual entry measurement)
2. Na_2CO_3 concentration (filtered titrator measurement)
3. Green liquor flow rate (filtered flowmeter measurement)
4. Nominal lime density (DENOM)
5. Excess lime setpoint from XLIME program.

The active lime flow needed is given by:

$$W_{CaO}^{(A)} = \left[(100 + XL)/100\right] X_{Na_2CO_3}^{(wlc)} Q_{gl}^{(c)} (56/454)$$

$$D_{CaO}^{(A)} = A_{CaO} D_{CaO}$$

$$S_{CaO} = W_{CaO}^{(A)} / (D_{CaO}^{(A)} F_{CaO}) \qquad (129)$$

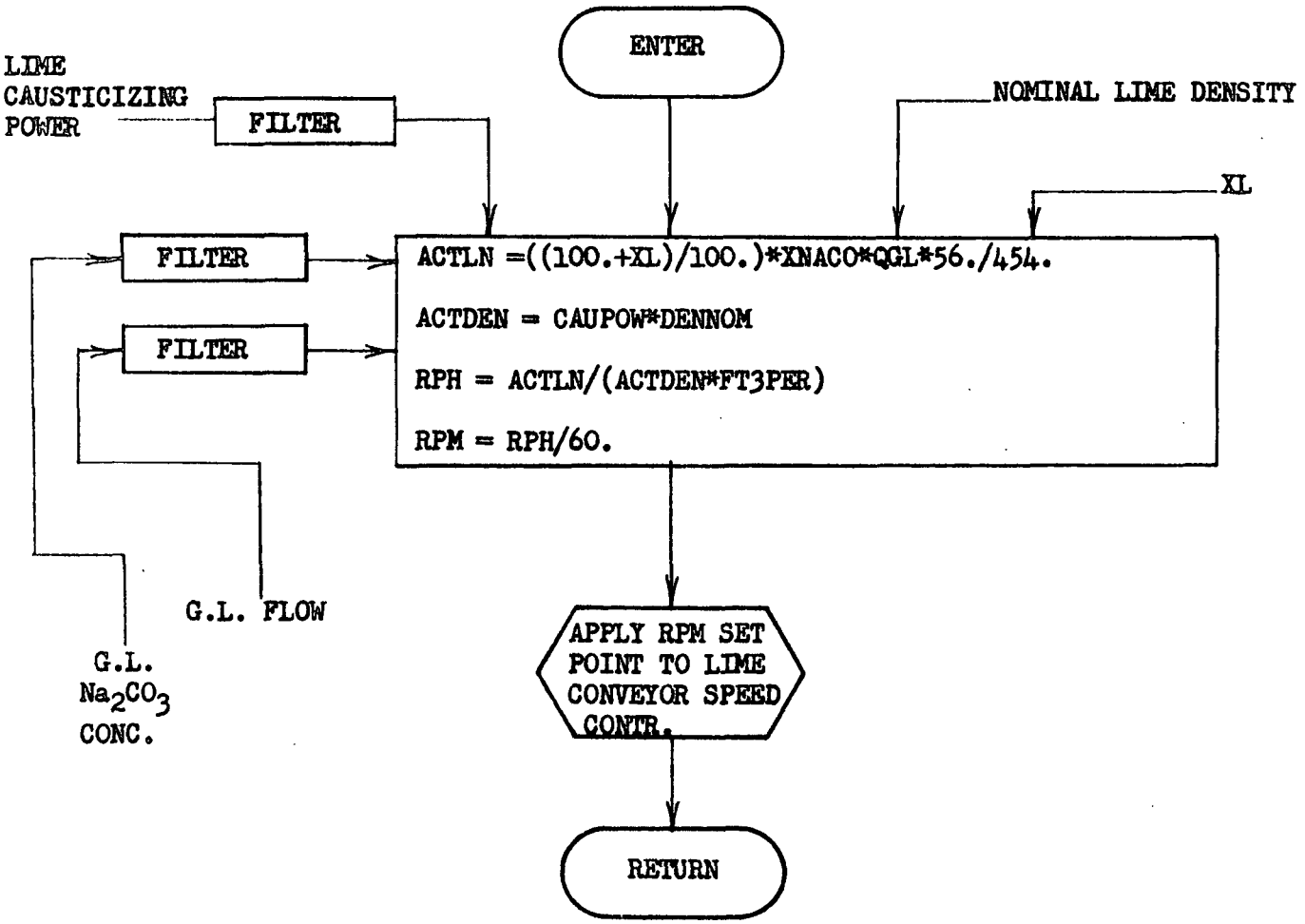

FIGURE 27. LIME FLOW CONTROL

Note that the only new instrumentation required for this controller is an automatic titrator for the Na_2CO_3 concentration of green liquor. An automatic instrument is needed here because of the frequency and regularity of measurement which is required for the lime flow rate control loop. The green liquor flowmeter, densitometer, tank level indicator, and the lime screw conveyor tachometer are already standard instruments in typical pulp mills. The green liquor density controller, flow controller, and lime screw feed controller are standard analog controllers. The operators are required to make only the standard tests they already make in most mills. Figure 28 illustrates schematically where the instruments would be located with respect to the various unit operations.

Figure 29 shows an actual one-month history for the variability of white liquor active alkali (AA) at a typical pulp mill. The data were taken at Owens-Illinois, Orange, Texas. Samples of white liquor were taken from the first causticizer every hour. A, B, and C titration tests were run manually. The resulting 2 σ limits are about $\pm 9\%$ of the mean value. With the present controller, the upper and lower limits on the AA could be set at $\pm 6\%$. Assuming that the top limit for AA for the particular pulping conditions at the digester is about at the upper 2 σ limit, we can expect to make an upward target shift of 3% for AA with the new controller.

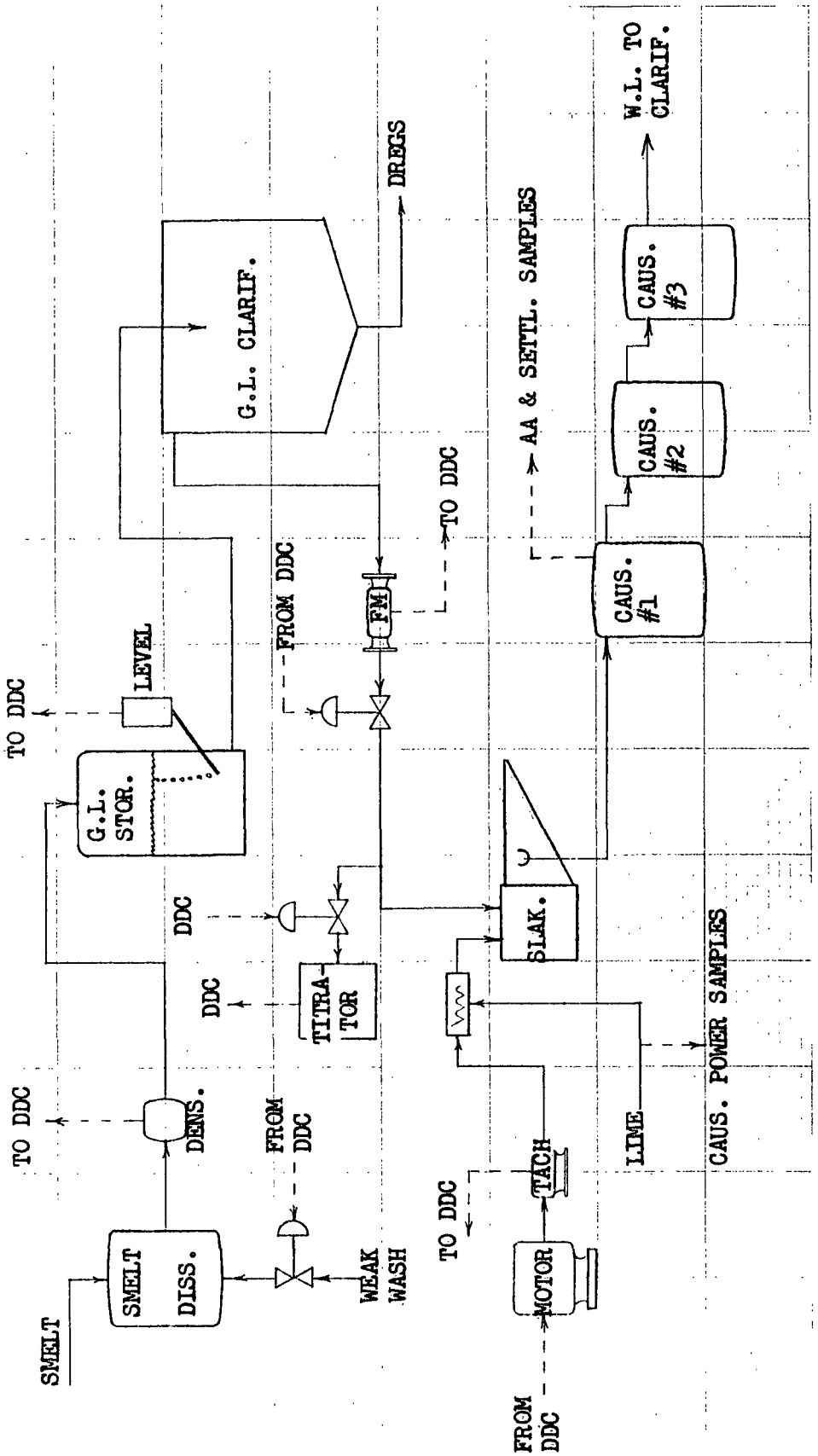

FIGURE 28. INSTRUMENTATION AND SAMPLING SCHEMATIC

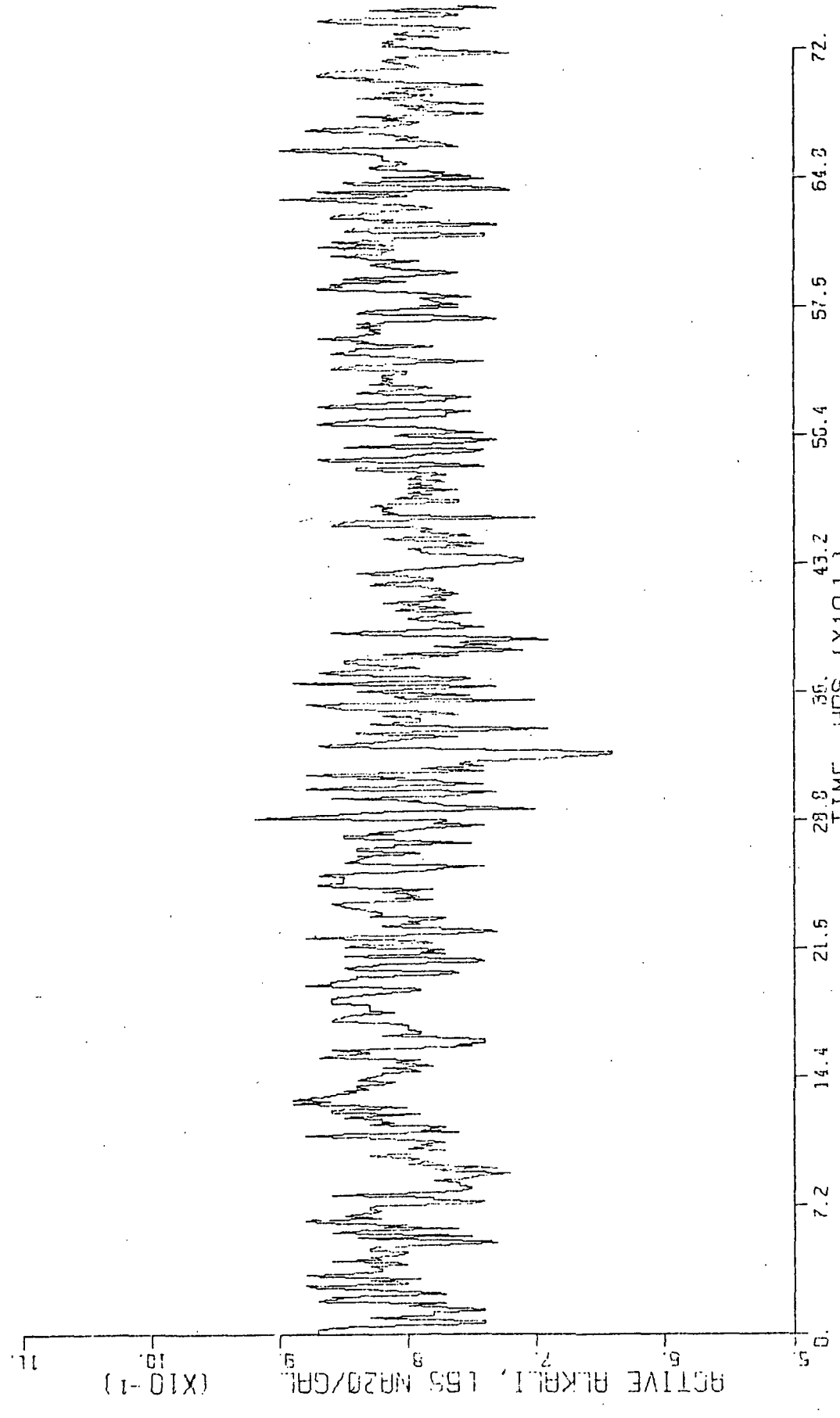

FIGURE 29. OPERATING DATA FOR ACTIVE ALKALI

(OWENS-ILLINOIS, ORANGE, TEXAS; JAN. '72)

REFERENCES CITED

1. Galtung, F.L., and Williams, T.J., A Survey of the Status of the Mathematical Modeling of the Chemical Recovery Section of a Kraft Paper Mill, Report No. 23, Purdue Laboratory for Applied Industrial Control, Purdue University, Lafayette, Indiana (July 1969).

2. Glazunov, A.I., "Approximate Mathematical Model of the Causticization Unit," Tr. Vses. Nauch.-Issled. Inst. Tsellyul.-Bumazh. Prom., no. 52, 192-200 (1967) (Russ.)

3. Kobe, K.A., and Wilkinson, J.A., "Effect of Sulfur Compounds in the Causticizing Equilibrium," Industrial and Engineering Chemistry, 45, (February 1953).

4. Stephenson, J.N., Pulp and Paper Manufacture. Vol. 1: Preparation and Treatment of Wood Pulp, McGraw-Hill Book Co., New York, New York (1950).

5. Kuehl, J. F., "Basic Process Features of Recausticizing and Lime Burning," Private Memorandum, Kimberly-Clark Corp. (1971).

6. Kinzner, Klaus, "Investigations of the Causticizing of Green Liquors," Proceedings of the Symposium on Recovery of Pulping Chemicals, Helsinki, Finland (1968).

7. Hank, F.W., "Settling Rate of Calcium Carbonate in the Caustic Department Operation," Private Correspondence, Tennessee River Pulp and Paper Company, (1968).

8. Olson, J.C., and Direnga, O.G., "Settling Rate of Calcium Carbonate in the Causticizing of Soda Ash," Industrial and Engineering Chemistry, 33, (February 1941).

9. Dorr, J.V.N., and Bull, A.W., "Some Variables Affecting the Behavior of Limes Used in Causticizing," Industrial and Engineering Chemistry, 19, No. 5 (May 1927).

10. Knowles, C.L., "Continuous Recausticizing in Pulp and Paper," Paper Trade Journal, 84, TAPPI Section (April 1927).

11. Jacobi, E.F., "Mathematical Model of Slaking/Causticizing and Solids Settling," Section VII of Systems Analysis of Chemicals and Energy Recovery in Sulfate Pulping, Final Report for Project Period, PLAIC, Purdue University, Lafayette, Indiana (September 14, 1971).

12. Jernqvist, A.S.-H., "Experimental and Theoretical Studies of Thickeners, Part 1," Svensk-Papperstidning, 68, No. 15, 506-511 (1965).

13. Ibid, Svensk Papperstidning, 68, No. 16, 545-548 (1965).

14. Ibid., Svensk Papperstidning, 68, No. 17, 578-582, (1965).

15. Ibid., Svensk Papperstidning, 69, No. 11, 395-398 (1966).

16. Coulson, J.M., and Richardson, J.F., Chemical Engineering, II, 387-453, Pergamon Press (1959).

17. Brown, G.G., Unit Operations, 210-255, John Wiley and Sons (1950).

18. Tiller, F.M., "Filtration Theory Today," Chemical Engineering, (June 20, 1966).

19. Perry, J.F., "Preliminary Mathematical Model of a Vacuum Drum Washer," IPC Progress Report for Project 2893, 11-12 (December 4, 1970).

20. Whitney, R.P., Chemical Recovery in Alkaline Pulping Processes, TAPPI Monograph No. 32, Mack Printing Co., Easton, Pa. (1968).

21. TAPPI Technical Information Sheets, No. 102.02, TAPPI, Augusta, Ga., (1965).

22. Knowles, C.L., "How to Control the Continuous Recausticizing System," Paper Trade Journal, TAPPI Papers, 21, 289-294 (June 1938).

23. McCabe, W.L., and Smith, J.C., Unit Operations of Chemical Engineering, 885-900, McGraw-Hill Book Co., New York, New York (1967).

24. Adler, L.S., "Steady State Model of the Kraft Recovery Cycle," Section III of Systems Analysis of Chemical and Energy Recovery in Sulfate Pulping, Final Report for the Project Period, PLAIC, Purdue University, Lafayette, Indiana (September 14, 1971).

SECTION V

FURTHER RESULTS IN THE OPTIMIZATION AND CONTROL OF THE ROTARY LIME KILN

INTRODUCTION

This report is an extension of the work on the control of the rotary lime kiln described in the previous report (1). It contains a mathematical formulation for the steady state optimal control problem for the kiln, a method for its numerical solution, and the results obtained from its application to the kiln studied in this research. A discussion of the design of the dynamical controllers for the kiln is also included.

The optimal steady state operating conditions are such that the value of the output (free lime) produced per hour is maximized and, simultaneously, the cost of the fuel consumed per hour is minimized.

Mathematically, the problem is to compute the minimal value of a quadratic cost functional, which is specified by the fuel rate, the product output rate, and their attendant commercial costs. Besides providing economical operating conditions, it may be expected that such an optimal mode of operation will also reduce kiln maintenance and improve the uniformity of the product.

MATHEMATICAL FORMULATION OF THE STEADY STATE EQUATIONS

PLANT EQUATIONS

The time-invariant steady state equations for the process are obtained by setting the partial derivatives of the rotary lime kiln variables in Equation 60 (1) to zero. The time-invariance follows from the assumptions that: (a) the control variables are constant; (b) the parameter values (i.e., heat transfer coefficients, etc.) do not change with time; and (c) the spatial boundary conditions are constant with respect to time (i.e., the gas and burden mass variables associated with the rotary lime kiln are constant at the point at which they enter the kiln). Thus, the following equations describe the system:

$$\frac{d}{d\ell}\left[q(\ell)\right] = f(q,u,\ell), \quad \ell \varepsilon [\ell_o, \ell_f] \tag{1}$$

$$q_i(\ell_o) = a_i \qquad i = 1,2,3 \text{ and } 7 \tag{2}$$

$$q_i(\ell_f) = b_i \qquad i = 4,5,6 \text{ and } 8 \tag{3}$$

where $q(\ell) = \text{col}\left[X_{CaCO_3}, X_{CaO}, X_W, Y_{O_2}, Y_W, Y_{CO_2}, T_s, T_g\right]$ is an 8^{th} order column vector defined on the interval $[\ell_o, \ell_f]$; the argument, ℓ, represents the axial position on the interval specified by the cold end ($\ell = \ell_o$) and hot end ($\ell = \ell_f$) of the rotary lime kiln. The function $f(\cdot)$ is derived from Equation 60 (1) by setting $\partial q/\partial t$ equal to zero. The function $f(\cdot)$ is vector-valued and of dimension 8*; it is piecewise continuous and differentiable with respect to the arguments q, u and ℓ. The vectors col $[a_1, a_2, a_3, a_7]$ and col $[b_4, b_5, b_6, b_8]$ are the values

*In the steady state, $q_9(\ell)$, is constant for all ℓ.

of the burden states and gas states, respectively, as they enter the kiln. The control u is a column vector of dimension 2 given by

$$u = \begin{bmatrix} u_1 \\ u_2 \end{bmatrix} = \begin{bmatrix} \text{fuel flow rate (lb/hr)} \\ \text{nitrogen flow rate (lb/hr)} \end{bmatrix} \tag{4}$$

OPTIMIZATION OF STEADY STATE KILN BEHAVIOR AS A MINIMIZATION PROBLEM

To evaluate the operation of a lime kiln, a measure of the performance, or a cost functional, is defined by the following considerations: The value of the free lime output, $u_3 q_2(\ell_f)$, of the rotary lime kiln is to be maximized. Also, the cost of the fuel, u, should be minimized with respect to the control variables. The output of free lime from the kiln, $u_3 q_2(\ell_f)$, is the (mathematical) product of u_3, the calcinable mass flow rate entering the kiln, and $q_2(\ell_f)$, the pounds of free lime per pound of calcinable mass at the hot end of the kiln. The controls which are to be determined in order to optimize the chosen performance criterion are: u_1, the fuel flow rate; and u_2, the nitrogen gas flow rate.

On the basis of these considerations, a performance criterion for the evaluation of the operation of the rotary lime kiln is chosen as follows:

$$J(u_1,u_2) = \frac{1}{2} w_f[u_1]^2 - \frac{1}{2} w_p[q_2(\ell_f)u_3]^2 \tag{5}$$

The first term on the right-hand side of Equation 5 represents the dollar cost of the fuel per hour. The second term is the negative of the

dollar cost, on the open market, of the lime output of the rotary lime kiln per hour. The negative sign has been chosen because the minimization of the negative dollar cost of lime is equivalent to the maximization of the positive dollar value of lime. In the second term, $q_2(\ell_f)$, is the pounds of lime per pound of calcinable mass at the hot end of the rotary lime kiln, and u_3 is the specified calcinable mass flow rate into the rotary lime kiln. The selected cost coefficients in Equation 5, w_p and w_f, have units of \$ - hr/(lb)^2. If desired, the cost coefficients can be chosen to give the measure of performance of the rotary lime kiln in units of dollars per ton of air dryed pulp (\$/t.a.d.p.) instead of in units of dollars per hour (\$/hr.).

The problem is to find the optimal controls, $u_1 = u_1^*$, and, $u_2 = u_2^*$, which simultaneously minimize the performance index given by Equation 5 and satisfy the process equations, Equations 1, 2, and 3.

METHOD OF SOLUTION

In order to find the optimal values of u_1 and u_2 which minimize the measure of performance, $J(u_1,u_2)$ given by Equation 5, a grid search in the u_1u_2 - space was performed. It is noted that optimal values of u_1^* and u_2^* are constants, and not time-functions. To perform this grid search, two algorithms are needed. One algorithm systematically generates values of u_1 and u_2 in a specified region of u_1u_2 - space. Then, the other algorithm solves the rotary lime kiln steady state equations, Equations 1, 2, and 3 (which constitute a two-point boundary value problem), for the specified values of u_1 and u_2. This latter algorithm will now be described in detail.

CONSTRUCTION OF AN ALGORITHM FOR SOLVING A TWO-POINT BOUNDARY VALUE PROBLEM

It should be observed that the plant Equations 1, 2, and 3, by themselves, constitute a two-point boundary value problem (TPBVP). Indeed, the temperature of the gas and the composition of the gas are given at the firing end of the rotary lime kiln by Equation 3, whereas the temperature of the burden mass and the composition of the burden mass are specified at the feed end of the kiln by Equation 2. Therefore, the first step in construction of the algorithm which performs a grid search in the u_1u_2 - space on the performance measure $J(u_1,u_2)$, given by Equation 5 is to have available an efficient computational scheme to solve the TPBVP. Such a scheme has been derived in this research. In the interests of space in this report, it will be presented in the thesis report to follow (4). The algorithm is shown to approximate quasi-linearization by using a first-order approximation to the state transition matrix of the linearized state equations (4).

When a complete combustion of the fuel and a complete evaporation of the water from the burden mass are assumed, the efficiency of the algorithm for solving the TPBVP can be enhanced. From the assumption that the combustion of the fuel is complete, the quantity, $q_4(\ell_o)$, the pounds of oxygen per pound of nitrogen leaving the rotary lime kiln can be calculated from the following equation:

$$q_4(\ell_o) = 0.316 - 4.0(u_1/u_2) \tag{6}$$

where 0.316 is the ratio (by weight) of oxygen to nitrogen in air, which enters the hot end of the kiln; the factor 4.0 is the ratio of the weight of oxygen consumed by the complete combustion of a unit weight of fuel (methane). This quantity (u_1/u_2) has units of pounds of fuel per pound of nitrogen.

From the additional assumption that all of the water evaporates from the burden mass on its way down the kiln, the value of $q_5(\ell_o)$ (the pounds of water vapor per pound of nitrogen leaving from the cold end of the rotary lime kiln) is given by:

$$q_5(\ell_o) = q_3(\ell_o)\ (u_3/u_2) + 2.25(u_1/u_2) \tag{7}$$

where $q_3(\ell_o)$ is the weight of water per pound of calcinable mass entering the rotary lime kiln; u_3 is the specified flow rate of calcinable mass into the kiln; the factor 2.25 equals the pounds of water vapor formed due to the complete combustion of one pound of fuel (methane); and the division by u_2 normalizes the variables u_3 and u_1 to pounds per pound of nitrogen,

Therefore, by use of Equations 6 and 7, only the values of $q_6(\ell_o)$, the pounds of carbon dioxide per pound of nitrogen leaving the kiln, and $q_8(\ell_o)$, the temperature of the gas leaving the rotary lime kiln, are unknown at the cold end of the kiln. Thus, given values for the controls u_1 and u_2, the algorithm which solves the TPBVP is as follows:

(i) Guess values for $q_6(\ell_o)$ and $q_8(\ell_o)$.

(ii) Integrate Equation 1.

(iii) Perturb $q_6^n(\ell_o)$, the value of $q_6(\ell_o)$ in the n^{th} iteration, and integrate Equation 1 to determine $\frac{\Delta q_6(\ell_f)}{\Delta q_6(\ell_o)}$ and $\frac{\Delta q_8(\ell_f)}{\Delta q_6(\ell_o)}$.

(iv) Perturb $q_8^n(\ell_o)$, the value of $q_8(\ell_o)$ in the n^{th} iteration, and integrate Equation 1 to determine $\frac{\Delta q_6(\ell_f)}{\Delta q_8(\ell_o)}$ and $\frac{\Delta q_8(\ell_f)}{\Delta q_6(\ell_o)}$.

(v) Set $\Phi_{22}(\ell_f,\ell_o) = \frac{\Delta(q_6(\ell_f),q_8(\ell_f))}{\Delta(q_6(\ell_o),q_8(\ell_o))}$ and determine $q_6^{n+1}(\ell_o)$ and $q_8^{n+1}(\ell_o)$, the values of $q_6(\ell_o)$ and $q_8(\ell_o)$ in the $n+1^{th}$ iteration.

(vi) Integrate Equation 1.

(vii) If $10^3(|q_6^{n+1}(\ell_f)-b_6|) + |q_8^{n+1}(\ell_f)-b_8| < \delta$, a small previously chosen constant, then accept $q^{n+1}(\ell)$ as the solution to Equations 1, 2, and 3. If $|q_8^{n+1}(\ell_f)-b_8| + 10^3(|q_6(\ell_f)-b_6| \geq \delta$, return to step (iii) and repeat the computational cycle.

In the actual program, δ was chosen to be 10^{-2} and the perturbations on the values of $q_6(\ell_o)$ and $q_8(\ell_o)$ were 10^{-4} and 0.1, respectively. A

flowchart of the subroutine, called QUASI, which solves the TPBVP associated with the rotary lime kiln is displayed in Figure 1.

The subroutine found a solution in 4 or 5 iterations using an average of 1.5 seconds per iteration on a CDC 6500 computer. The convergence appears to be quadratic (which is also a trait of quasi-linearization) and occurs for initial guesses of $q_8(\ell_o)$ "reasonably close" ($\pm$ 200°F) to the true value of $q_8(\ell_o)$.

GRID SEARCH FOR BEST OPERATING POINT

With the use of this algorithm for the solution of the TPBVP, a grid search can be performed. First, a range of values for the nitrogen gas flow rate, u_2, is chosen. As the source of the nitrogen being inducted into the kiln is air, the rate of flow of oxygen into the kiln is determined by u_2. Thus, the maximum flow rate of the fuel, u_1, which will undergo complete combustion in the kiln can be determined. Then, a range of values for the fuel flow rate between zero and the maximum flow rate of the fuel must be specified. The algorithm which performs a grid search can now be summarized:

(i) Choose a maximum and minimum value of u_2, umax_2 and umin_2, respectively.

(ii) Choose a maximum and minimum value of u_1, $\text{umax}_1(u_2)$ and $\text{umin}_2(u_2)$, respectively.

(iii) Choose a number of values of u_2, N_2, according to

$$u_2^j = \text{umin}_2 + \left\{\frac{(\text{umax}_2 - \text{umin}_2)}{N_2 - 1}\right\} j, \quad j=0,1,\ldots,N_2-1$$

Q = Initial Guess of $q(\ell_o)$

DELTA = The δ Used in Stopping Rule of Algorithm

N = Order of the System of Differential Equations

QD = $\text{col}[a_1, a_2, a_3, b_4, b_5, b_6, a_7, b_8]$

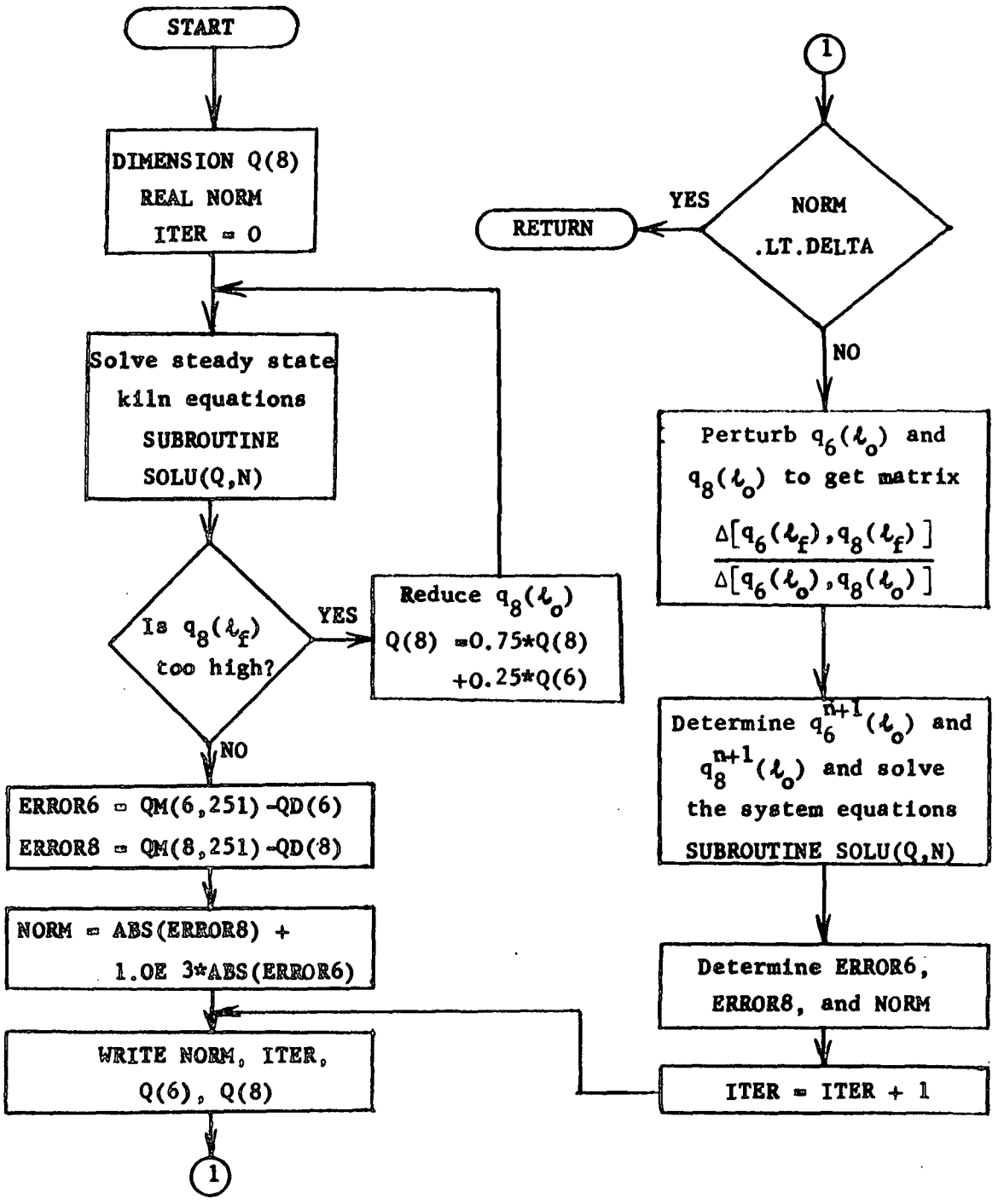

FIGURE 1

FLOWCHART OF SUBROUTINE QUASI(Q,DELTA,N)

This generates N_2 values of u_2 equally spaced between $umin_2$ and $umax_2$ as shown

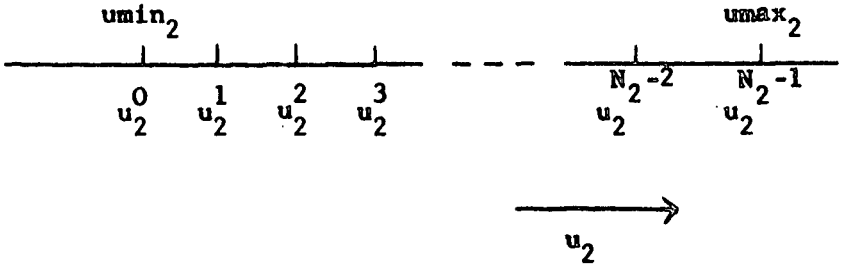

(iv) Choose a number of values of u_1, N_1, according to

$$u_1^i = umin_1 + \frac{(umax_1 - umin_1)}{N_1 - 1} \; i, \; i = 0,1,2,\ldots,N_1-1$$

The N_1 values of u_1 generated by this scheme are shown graphically as follows

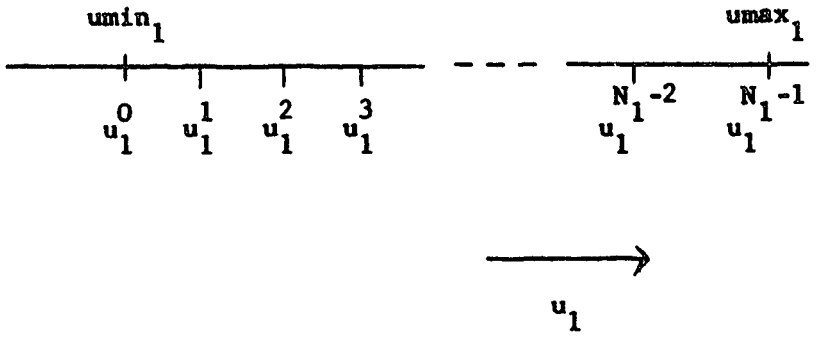

(v) Solve the plant Equations 1, 2 and 3 and determine $J(u_1^i, u_2^j)$ in Equation 5, $i = 0, 1, \ldots, N_1-1$ and $j = 0, 1, \ldots, N_2-1$.

(vi) Plot the value of the performance index, $J(u_1, u_2)$, over the region of interest and choose the values of u_1 and u_2 which yield the "best" value of $J(u_1, u_2)$.

SIMULATION RESULTS OF THE GRID SEARCH TECHNIQUE

The results of the grid search in u_1u_2 - space are shown in Figure 2 for the quadratic performance index defined by Equation 5. The ordinate is scaled both in dollars per hour ($/hr) and in dollars per ton of air-dried pulp ($/t.a.d.p.). The abscissa is normalized with respect to the maximum amount of fuel that theoretically could be completely combusted, $umax_1$. The value of $umax_1$ is a function of the nitrogen gas flow rate, u_2, in pounds per hour. The specific formula for $umax_1$ is

$$umax_1 = (0.316)\ (u_2)/4 \qquad (8)$$

where (as before) 0.316 is the pounds of oxygen per pound of nitrogen in air and the factor 4 is due to four pounds of oxygen being necessary for the complete combustion of one pound of the fuel, here methane gas.

From Figure 2, it can be seen that for a given value of u_2 there is a definite local minimum. For values of u_2 less than approximately 13,500 pounds of nitrogen gas per hour, the point of minimum cost will occur to the right of the line $u_1/umax_1 = 1.0$.

Comparison of Figure 3 and Figure 2 shows that the shape of the linear cost curves in u_1u_2 - space are quite similar to the shape of the quadratic cost curves. In particular, the minima of the cost function for a given value of u_2 occur at the same value of $u_1/umax_1$. This coincidence of minimum points takes place for two reasons - the judicious choice of constants w_p and w_f in Equation 5, and the narrow range (1100-1500 lbs/hr) of u_1 over which these minima occur.

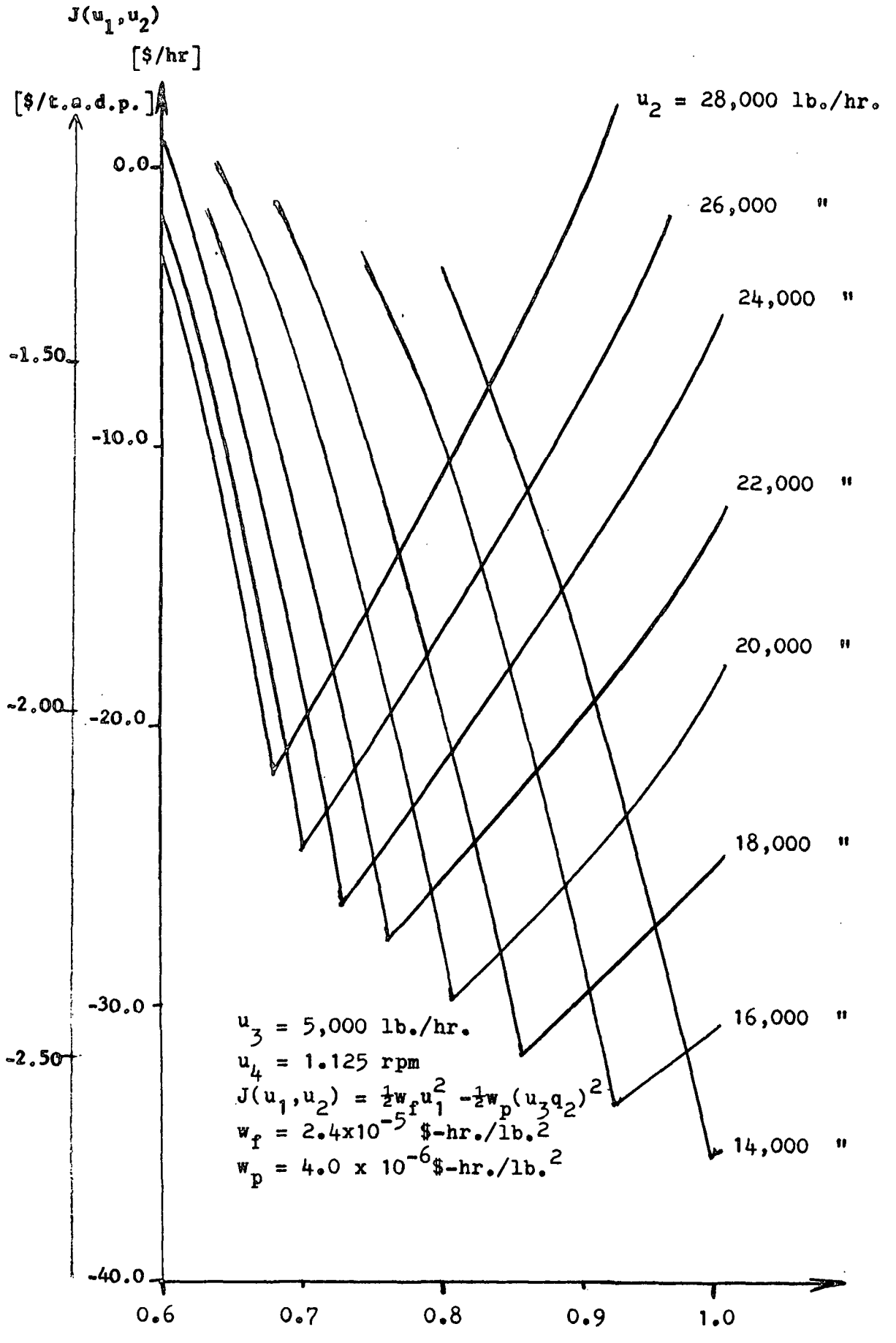

FIGURE 2

QUADRATIC PERFORMANCE MEASURE CURVES IN u_1-u_2 SPACE

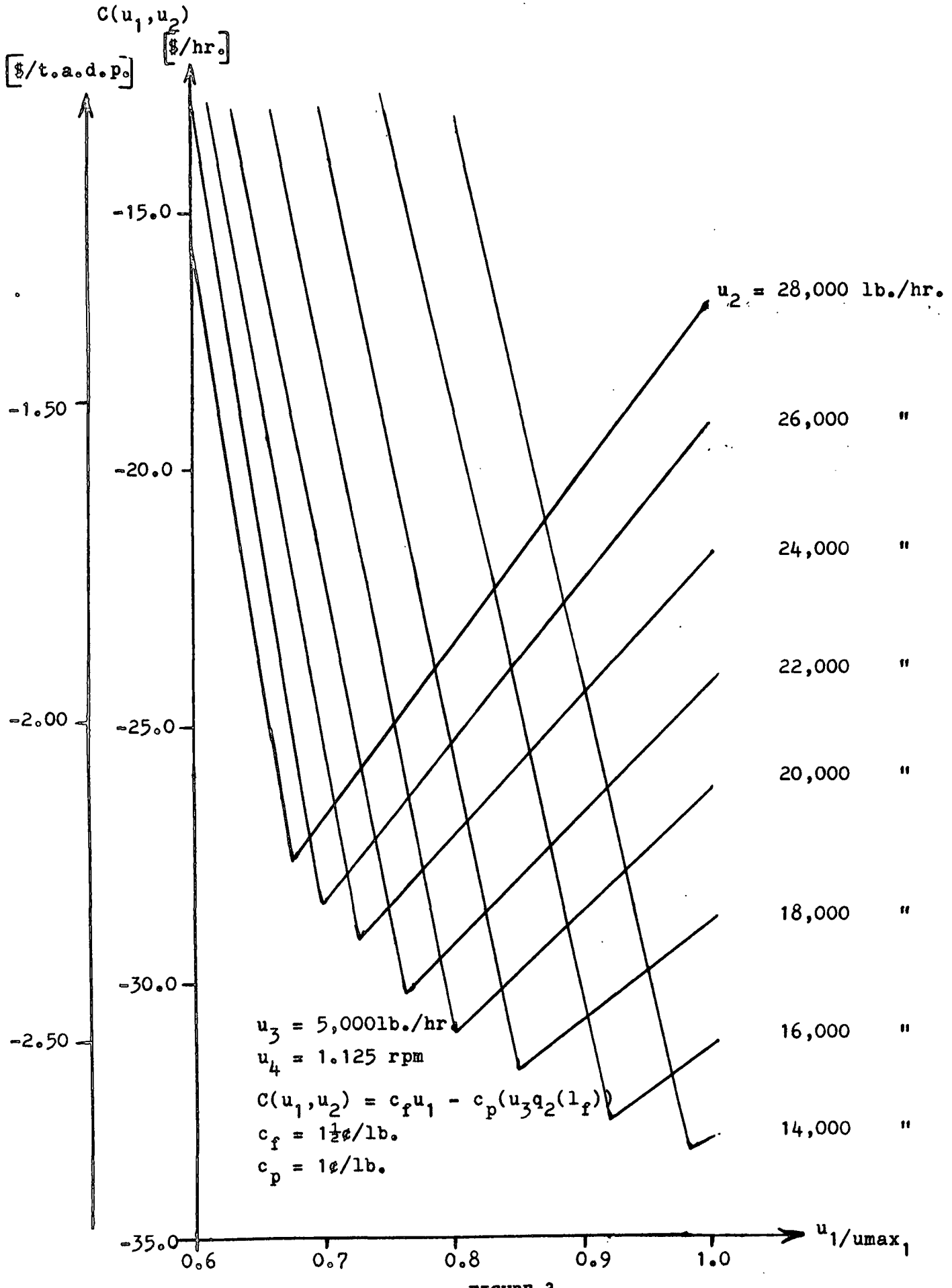

FIGURE 3
GRAPH OF LINEAR COST IN THE u_1-u_2 SPACE

The actual costs of operating a rotary lime kiln in dollars per hour are given by an expression of the form

$$C(u_1,u_2) = c_f u_1 - c_p(u_3 q_2(\ell_f)) \tag{9}$$

where c_p is the purchase price of lime in dollars per pound, and c_f is the cost of the fuel in dollars per pound. Consequently, the constants w_f and w_p for Equation 5 are chosen as follows:

$$w_f = \frac{2\ c_f}{est(u_1^*)} \tag{10}$$

$$w_p = \frac{2\ c_p}{est(u_3 q_2^*(\ell_f))} \tag{11}$$

where $est(u_1^*)$ is the estimate of the rate of fuel consumption and $est(u_3 q_2^*(\ell_f))$ is the estimate of the free lime produced by the kiln during optimal steady state operation.

The estimates used to determine the values of w_f and w_p were 1,250 pounds per hour for the fuel being combusted and 5,000 pounds per hour for the rate of free lime being produced. The actual values of fuel rate, nitrogen gas flow rate, calcination rate and costs per hour determined at the minima of Figures 2 and 3 are given in Table I.

The numerical values which are obtained with the quadratic cost are close to the values obtained with a linear cost. More importantly, an operating point which yields a lower quadratic cost than another operating point also yields a lower linear cost than the other operating point.

TABLE I

RESULTS OF THE OPTIMIZATION OF

THE ROTARY LIME KILN

N_2 Flow Rate (lbs/hr)	CH_4 Flow Rate (lbs/hr)	Calcination Rate (lbs/hr)	Quadratic Cost ($/hr)	Linear Cost ($/hr)
28,000	1,490	5,000	-23.35	-27.65
26,000	1,430	5,000	-25.40	-28.55
24,000	1,375	5,000	-27.30	-29.43
22,000	1,320	5,000	-29.00	-30.20
20,000	1,265	5,000	-30.80	-31.03
18,000	1,210	5,000	-32.75	-31.85
16,000	1,165	5,000	-33.70	-32.53
14,000	1,100	5,000	-35.50	-33.50

$w_p = 4.0 \times 10^{-6}$ \$-hr/lb^2; $c_p = 1.0 \times 10^{-2}$ \$/lb

$w_f = 2.4 \times 10^{-5}$ \$-hr/lb^2; $c_f = 1.5 \times 10^{-2}$ \$/lb

u_4 = 1-1/8 rpm

For the given constant values of u_2, the minima shown in Figures 2 and 3 are obtained at values of u_1 over the range 1,490 to 1,100 pounds per hour. The closer the estimates of the values of u_1^* and $u_3 q_2^*(\ell_f)$, in Equations 10 and 11 are to the actual values at any operating point of the rotary lime kiln, the closer to each other are the values of the linear and quadratic cost functions with respect to each other. Moreover, if the estimates of u_1^* and $u_3^* q_2(\ell_f)$ are equal to the actual values of u_1^* and $u_3 q_2^*(\ell_f)$, then Equations 10 and 11 imply that the linear and quadratic cost functions are equal.

To facilitate a discussion of the sensitivity of the cost curves of Figure 3 with respect to fuel costs and lime costs, three features are defined for each of the cost curves obtained for a constant value of u_2. The minimum is defined as the point on the cost curve for a constant value of u_2 at which the cost is lowest. The region of overburning is the region to the right of the minimum, where more fuel is being combusted in the rotary lime kiln than is necessary for the complete calcination of $CaCO_3$. The region of incomplete calcination is the region to the left of the minimum which corresponds to insufficient fuel being combusted in the kiln to cause complete calcination.

The linear cost in the neighborhood of a minimum is sensitive to changes in both the cost of fuel and the cost of lime; however, the values of $u_1/umax_1$ and u_2 at which a minimum occurs are quite insensitive to changes in fuel and lime costs. For example, the highest minimum in Figure 3 is at $u_1/umax_1 = 0.676$ and $u_2 = 28{,}000$ lb/hr. At this point, the net linear cost, given by Equation 9 with $c_p = 1.0¢/lb$ and $c_f = 1.5¢/lb$, is -$27.65/hr. The quantity -$27.65/hr is the sum of -$50.00/hr for the

5,000 pounds per hour product of the kiln and $22.35/hr for 1,490 pounds of fuel per hour (see Table I) being combusted in the kiln. The linear cost at these values of $u_1/umax_1$ and u_2 will be less than the linear cost in the region of overburning (i.e., the points on the curve u_2 = 28,000 lb/hr for which $u_1/umax_1 \geq 0.676$) for all positive values of fuel cost.

The linear cost at $u_1/umax_1 = 0.676$ and u_2 = 28,000 lb/hr will be less than the linear cost in the region of incomplete calcination (i.e., u_2 = 28,000 lb/hr and $u_1/umax_1 < 0.676$) for all ratios of c_f to c_p less than u_3 to u_1 (which equals 5000/1490 = 3.35/1). If the ratio of c_f to c_p is greater than the ratio of u_3 to u_1, then it would be less expensive to purchase free lime than to expend fuel to calcine the calcium carbonate in this rotary lime kiln. This conjecture and the conjecture of the preceding paragraph are graphically displayed in Figures 4 and 5.

At the other minima of the curves of Figure 3, the sensitivity of the minima with respect to the cost coefficients c_p and c_f will be less than the sensitivity at the minimum specified by the point $u_1/umax_1 = 0.676$ and u_2 = 28,000 lb/hr. This lessening of sensitivity with respect to cost coefficient occurs because less fuel is consumed at these other minima as shown by Table I. For example, at the point u_2 = 16,000 lb/hr and $u_1/umax_1 = 0.92$, the ratio of u_3(5,000 lb/hr) to u_1 (1,165 lb/hr) is 4.27. Therefore, the ratio of c_f to c_p must be greater than 4.27 or the value of $u_1/umax_1$ which gives a minimum will remain the same.

In addition to a low cost of operation, other desirable characteristics for the operation of a kiln are a high product quality and a low rate of pollution. The operation of a rotary lime kiln generates pollutants in five major forms: carbon monoxide, sulfur dioxide, dust particles in

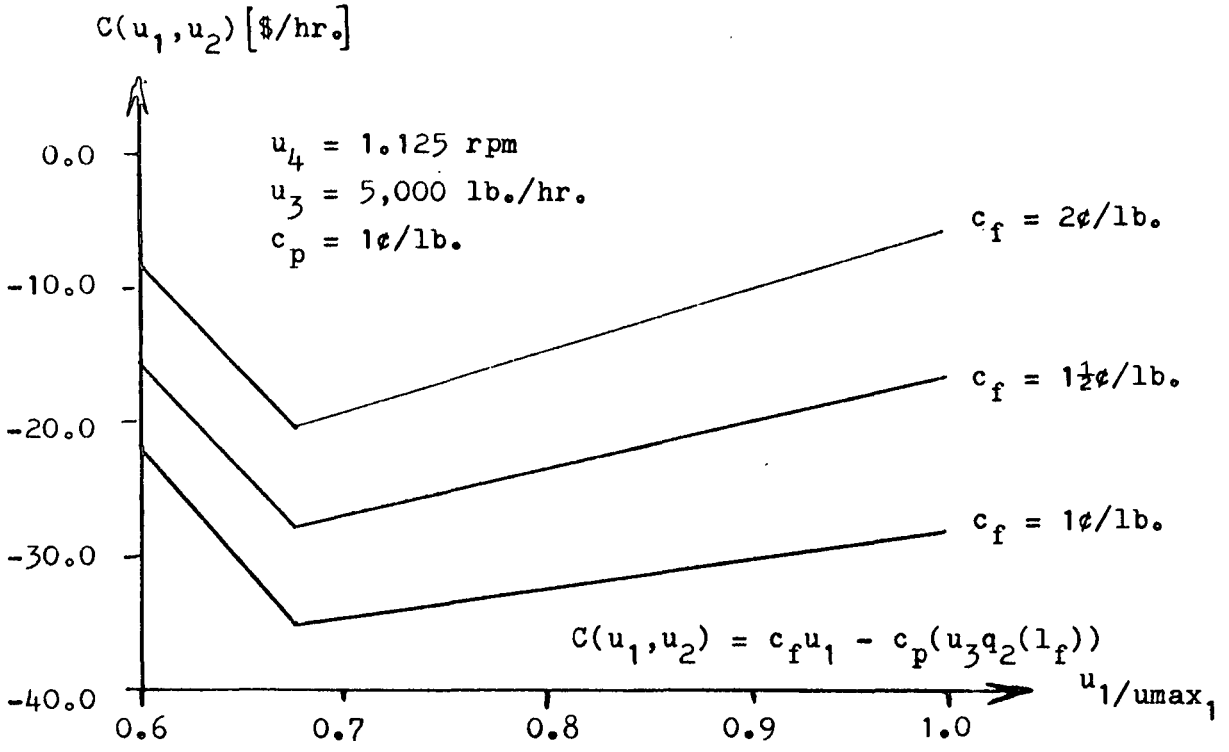

FIGURE 4

EFFECT OF FUEL COST ON LINEAR COST CURVE (u_2 = 28,000)

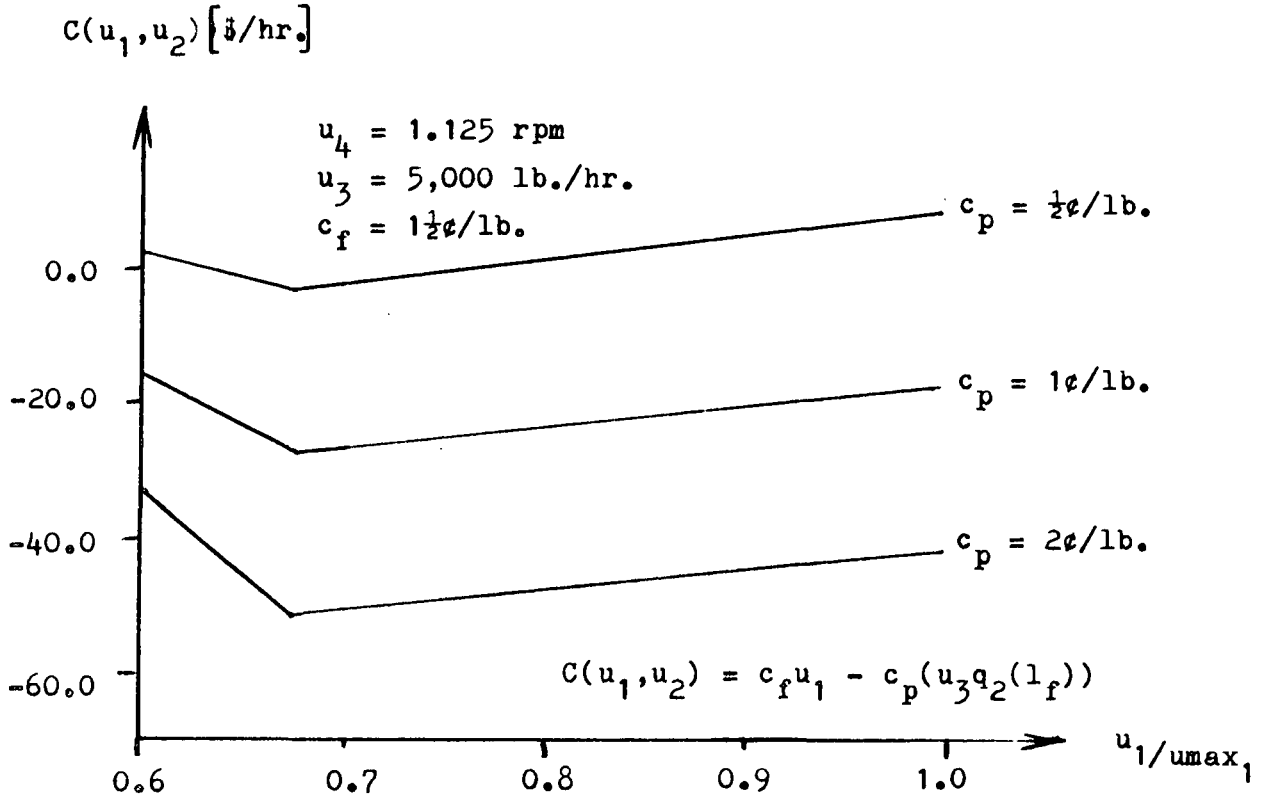

FIGURE 5

EFFECT OF COST OF LIME ON LINEAR COST CURVE (u_2 = 28,000)

the exhaust gases, overburnt lime and uncalcined lime.

The product quality is increased and the last three forms are lessened in the course of finding a minimum to the cost function as defined by Equation 5. Namely, at the minimum, only enough fuel is combusted to completely calcine all of the calcium carbonate flowing through the kiln and the total gas flow through the kiln (and hence the gas velocity) is as low as possible. It has been found (2) that dust particles are picked up by a gas stream from a solid at a rate proportional to the cube of the gas velocity.

The problem of production of sulfur dioxide is dependent upon the efficiency of the washing of the lime mud in the lime mud washer. It has been the author's experience that the sulfur dioxide (measured by titration) produced in the rotary lime kiln increases drastically when the flow of lime mud to the washer exceeds a certain limit. In the particular kiln for which data was available, this limit was u_3 equal to 7,000 pounds of calcinable mass per hour. Therefore, the problem is primarily one of specifying a lime mud washer of sufficient capacity. This problem could be further aggravated if large fluctuations of the flow of lime mud to the washer occur.

The production of carbon monoxide can be relieved by allowing a slight excess of nitrogen gas flow into the rotary kiln. This will guarantee enough oxygen to allow complete combustion to take place in the kiln. For example, if the ratio u_1 to $umax_1$ equals 0.9, then the excess of oxygen in the combustion zone of the kiln is 2.3%, which should be sufficient to eliminate most carbon monoxide.

The rotational speed of the kiln, u_4, is not varied in this optimizing procedure because the rotational speed of the kiln on which the data was collected could only assume one or the other of two discrete values. Therefore, by assigning to u_4 the possible discrete values, the optimal one could be obtained. The calcinable mass flow rate, u_3, was not varied, either, because the lime mud ($CaCO_3$) generated in the kraft chemical recovery cycle must either be calcined at the rate at which it is generated in the recausticizing process, be stored, or be rejected from the kraft mill as a potential pollutant to the water treatment system of the mill. Examination of Figures 3 and 6 indicates that the $CaCO_3$ can be calcined in the rotary lime kiln to yield lime (CaO) much more cheaply than to purchase lime commercially. Thus, lime mud should not be ejected from the recovery cycle as an effluent. It will not have to be stored in any greater quantity than that needed to have a sufficient inventory on hand to enable the kiln to be transferred from one optimal steady state operating point to another optimal steady state operating point.

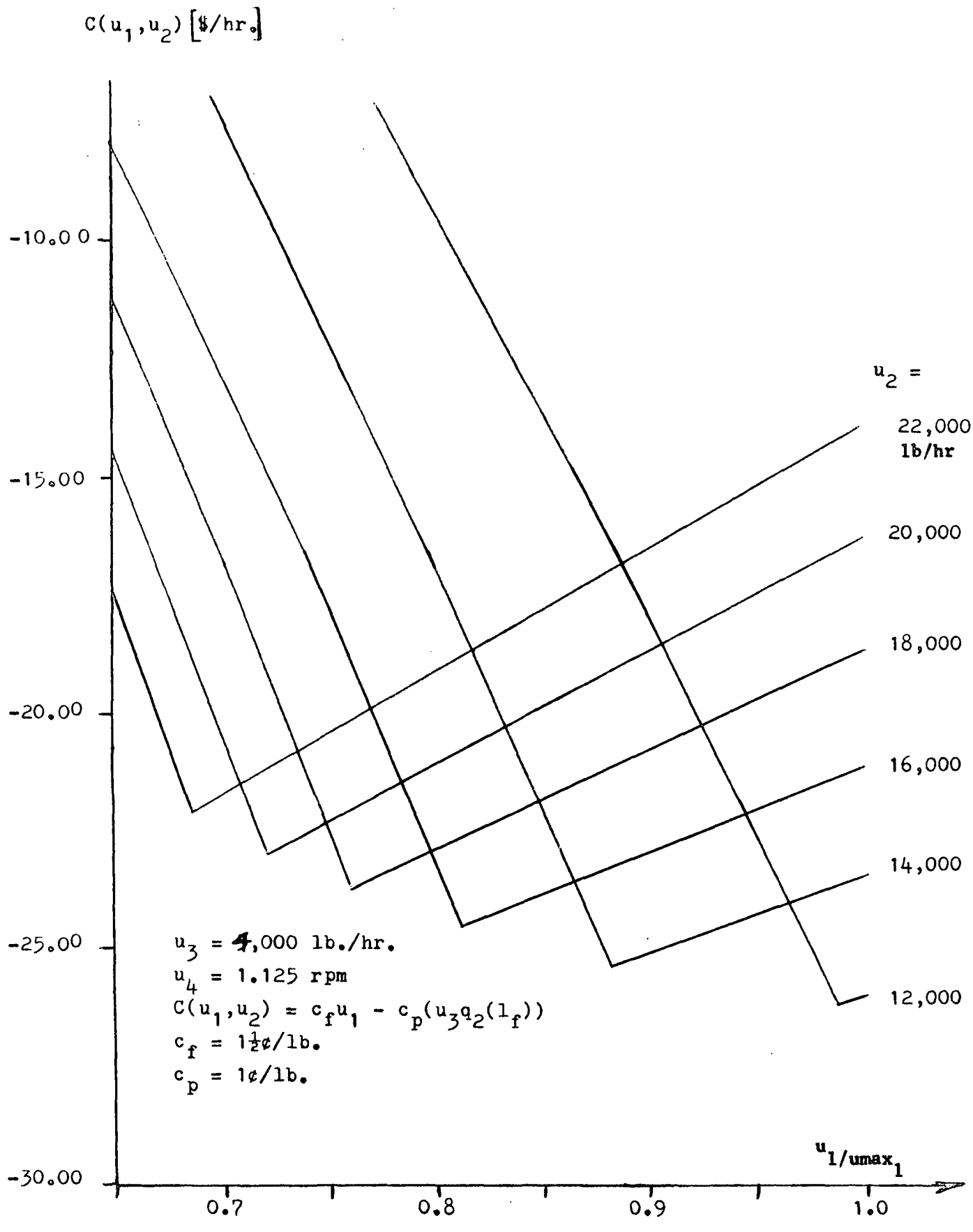

FIGURE 6

GRAPH OF LINEAR COST IN THE u_1-u_2 SPACE

DESIGN OF DYNAMIC OPTIMAL CONTROLLERS FOR THE ROTARY LIME KILN

The controllers for the rotary lime kiln will be designed for two typical situations: (1) to voluntarily change the operating point of the lime kiln from one set-point to another; and (2) to keep the values of the system variables as close as possible to the desired values specified by this set-point in order to optimize its optimization as described above.

The mathematical model (plant equations) to be used in the design of the controllers is governed for case (i) by Equations 60 through 65 of Reference (1) and for case (ii) by the linearized equations which result from the linearization of these same equations about an operating point. The controller for case (i) is called a primary controller and that for case (ii), a secondary controller. The following variables have been chosen as the basic controls: fuel rate, nitrogen gas rate, and burden mass feed rate.

Due to the absence of more complete instrumentation on the kiln, an open loop optimal control is first determined for both cases (i) and (ii). In case (i), this open loop optimal control is approximated by an "optimal control generator" as shown in Figure 7. This "optimal control generator" uses the present set-point and the specified (future) set-point in order to generate the optimal control-input function. The "optimal control generator" also produces the simulated values of the available measurements, $\hat{z}(\ell_1, t)$, as a function of time. These simulated values of measurements are compared to the actual values of the available measurements. An alarm condition is indicated when the differences between expected and actual measurements become too great.

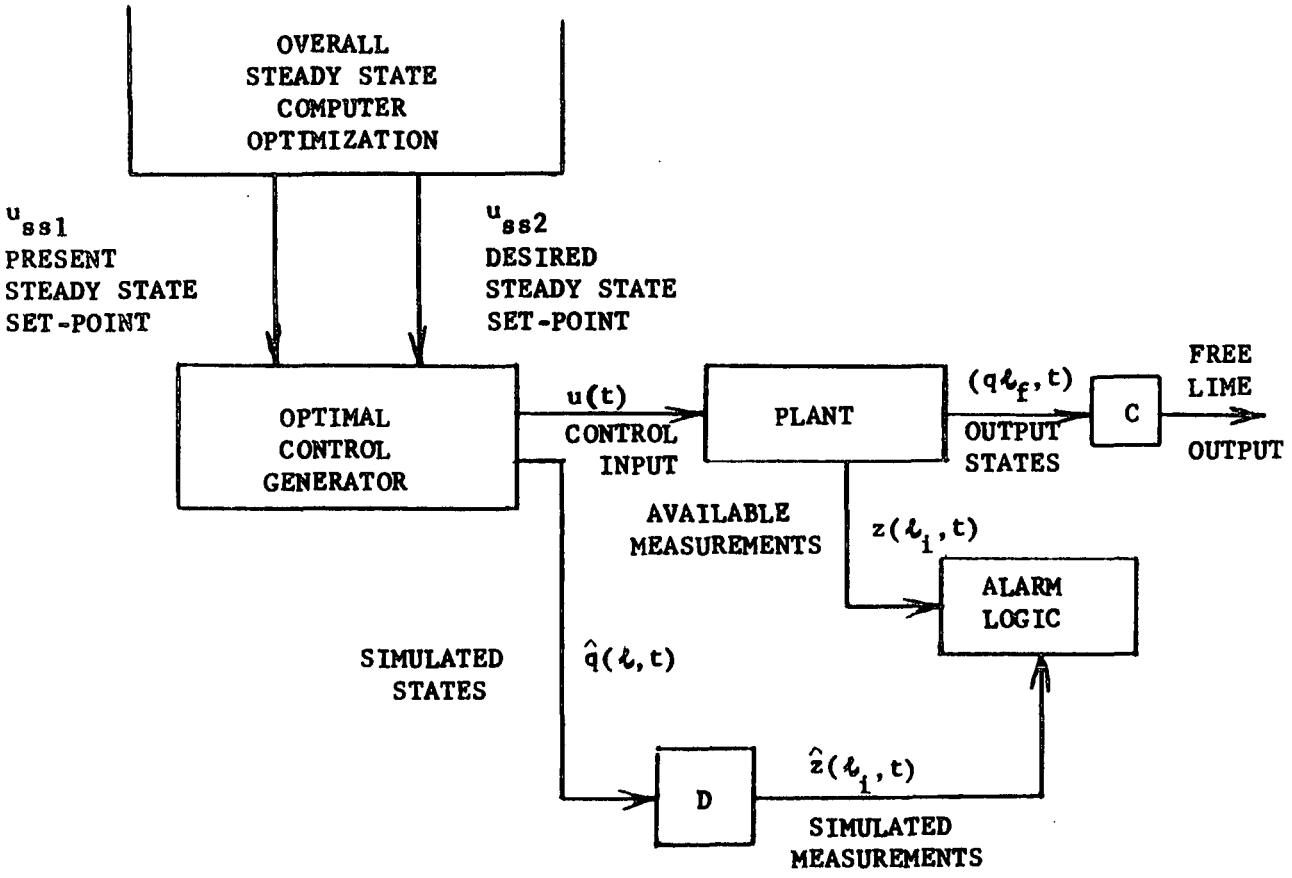

FIGURE 7

BLOCK DIAGRAM OF OPTIMAL PRIMARY CONTROLLER

In case (ii), the secondary controller is a feedback controller as shown in Figure 8. The present set points for the operation of the kiln are used to determine steady state profiles of the kiln variables versus length. The simulated values of the available measurements on the kiln, $\hat{z}(\ell_i)$, are also computed. The difference between these simulated values, $\hat{z}(\ell_i)$, and their respective actual values of measurements, $z(\ell_i)$, is the input to the secondary controller. The parameter values of the secondary controller are adjusted according to an off-line computer optimization based on the set-points and the steady state profiles of the rotary lime kiln. The output of the secondary controller is a correction, $\tilde{u}(t)$ to the value of the set-point of the kiln, $\hat{u}$. The resultant of this correction, $u(t)$, is a physically realizable control-input function which uses the performance of the open-loop control as a reference in the design.

The determination of the optimal open-loop control is performed by solving the necessary conditions for the optimal solution of both cases (i) and (ii).

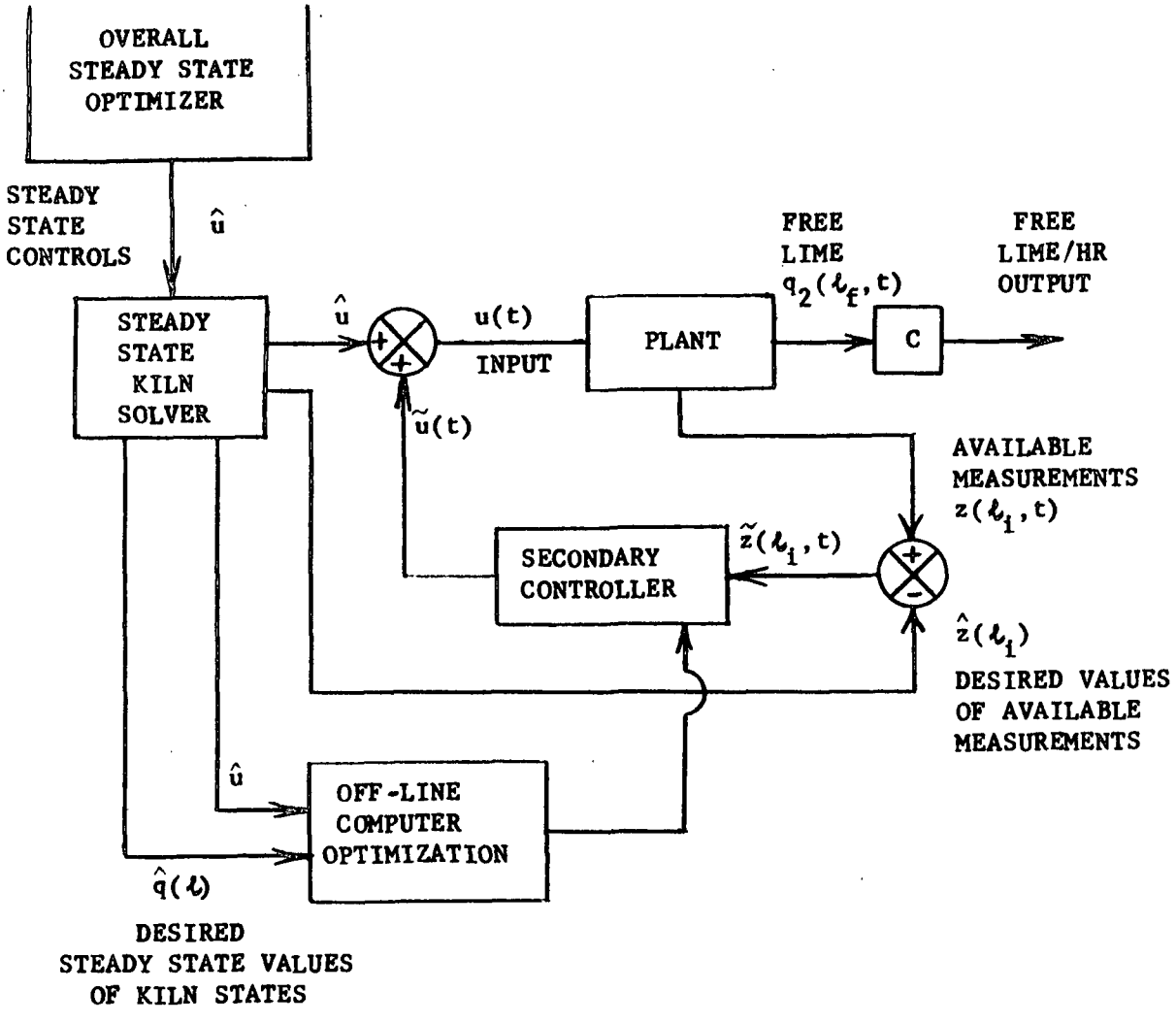

FIGURE 8

BLOCK DIAGRAM OF OPTIMAL SECONDARY CONTROLLER

REFERENCES CITED

1. Project Staff, "A Design of an Optimal Controller for the Rotary Lime Kiln and Related Units," pp. 102-115 in Systems Analysis of Chemicals and Energy Recovery in Sulfate Pulping, IPC Report No. 3, PLAIC Report No. 45, September 1971.

2. Pysiak, J., "Quantity of Powdered-Like Material Carried Away with the Gases in the Rotary Kiln," Przemysl Chemiozny, 44, No. 4, 1965.

3. Galtung, F.L., and Williams, T.J., A Mathematical Model and Digital Computer Based Advanced Control System for a Kraft Mill Recovery Unit, Report No. 43, Purdue Laboratory for Applied Industrial Control, Purdue University, West Lafayette, Indiana (November 1971).

4. Chase, P.M., and Koivo, A.J., Optimization and Control of a Rotary Lime Kiln, Report of the Purdue Laboratory for Applied Industrial Control, Purdue University, Lafayette, Indiana (to be published in January 1973).